PROCESSES AT THE MINERAL-WATER INTERFACE IN THE ACID SOILS OF THE SUDBURY AREA

by

Sonia Lanteigne

A thesis submitted in partial fulfillment
of the requirements for the degree of
Master of Science (MSc) in Geology

The School of Graduate Studies
Laurentian University
Sudbury, Ontario, Canada

THESIS DEFENCE COMMITTEE/COMITÉ DE SOUTENANCE DE THÈSE

Laurentian Université/Université Laurentienne

School of Graduate Studies/École des études supérieures

Title of Thesis PROCESSES AT THE MINERAL-WATER INTERFACE IN THE ACID SOILS OF THE SUDBURY AREA

Name of Candidate Lanteigne, Sonia M.L.

Nom du candidat

Degree Master of Science

Department/Program Geology Date of Defence September 27, 2013

APPROVED/APPROUVÉ

Thesis Examiners/Examinateurs de thèse:

Dr. Michael Schindler

(Co-supervisor/Co-directeur de thèse)

Dr. Andrew M. McDonald

(Co-supervisor/Co-directeur de thèse)

Dr. Graeme Spiers

(Committee member/Membre du comité)

Dr. Heather E. Jamieson

(External Examiner/Examinatrice externe)

Approved for the School of Graduate Studies

Dr. David Lesbarrères

Director, School of Graduate Studies

M. David Lesbarrères

ACCESSIBILITY CLAUSE AND PERMISSION TO USE

ABSTRACT

Over a century of mining activities and smelting in the area of Sudbury, Ontario, Canada have resulted in the contamination of the local soils with metal(loid) bearing particulates. Minor and trace elements associated with these phases are released during their weathering. This release is therefore strongly dependent on the mineralogical and chemical character of the metal(loid) bearing phases. The metal(loid)s are then subject to transport before being attenuated through their incorporation into secondary phases. Elevated concentrations of metal(loid)s in silica rich alteration layers has recently been described for altered surfaces at the solid-water and solid-atmospheric interfaces in tailings, and in the vicinity of smelters, respectively. To determine if similar coatings occur in soils, samples were taken from areas around three major smelting centers in the area. Coated grains were extracted from these samples and individually mounted to be analysed. Particulate matter (representing primary metal(loid)-bearing phases) and coatings (secondary metal(loid)-bearing phases) were analysed using scanning electron microscopy, Raman spectroscopy, Laser-Ablation Inductively-coupled plasma mass spectroscopy, Micro-X-ray fluorescence, and X-ray photoelectron spectroscopy. The particulates were divided into three main groups: smelter-derived particles, sulfides, and nickel-oxides. Smelter derived particles contained the most elevated concentrations of metal(loid)s in their sulfide inclusions and metal(loid)-rich rims. The mobility of metal(loid)s in the identified mineral phases found within particulates mirrored the transport observed in the soil column; Zn>Cu>Ni>Pb. Once mobilized, these elements are subject to transport before being attenuated by secondary phases. Micro-coatings were found to be composed of hematite, schwertmannite, ferrihydrite, silica, and jarosite group minerals. Coatings are distinguished on the basis of their atomic Si:Fe ratios: FeOx coatings have Si:Fe <1, Si–FeOx coatings have Si:Fe between 1-10, and SiOx coatings

have Si:Fe>10. Iron-rich coatings (FeOx) and silica-rich coatings (SiOx) have lower trace-metal concentrations than Fe-SiOx coatings. Micrometer-thick coatings are predominantly composed of hematite, schwertmannite, ferrihydrite and (amorphous) silica and contain elevated metal(loid) concentrations in the form of metal(loid)-rich phosphate minerals (mainly minerals of the jarosite group). A general model is developed that describes the formation of mineral coatings in acid soils and their important role in the uptake and retention of metal(loids). Here, micrometer-thick Fe-silica coatings form through adsorption, co-precipitation and dehydration processes involving amorphous silica and iron hydroxides. Metal(loid)-bearing phases nucleate within a gel-type matrix and are subsequently preserved during dehydration and solidification. Aluminum-rich surfaces form on mineral grains once the pH has been raised sufficiently high (pH~5-6) so as to lead to the complete removal of sulfate-bearing phases. The implications of this model are widespread in terms of the attenuation of metal(loid)s in acid soils and their retention or subsequent remobilization in recovered soils with near neutral pH.

Acknowledgements

I would like to begin by acknowledging my supervisors, Michael Schindler and Andrew McDonald, for providing me the opportunity to grow not only as an academic but also as a person, and encouraging my scientific curiosity. Their guidance, patience and constructive criticism provided enormous support, and resulted in numerous opportunities to learn. Many thanks and appreciation is extended Dr. G. Courtin for his encouragement to pursue further studies. In addition, I would like to thank Dr. G. Spiers for his wealth of knowledge and excellent recommendations on various aspects of my project.

In the next section I acknowledge the time, assistance and the use of facilities provided by numerous professors, technicians and university departments. From Laurentian university I would like to thank Dr. W. Zhe, and W. Desjardin for their help and training and the use of their equipment, and Joe Petrus for his guidance and help with LA ICP-MS; Dr. T. Kotzer for beamtime at the Canadian Light Source and Jennifer Durocher for all her help with the μXRF. I would also like to thank Dr. Frank C. Hawthorne for the use of his facilities for XPS.

Great thanks is extended to fellow undergraduate and graduate students, notably Jennifer Durocher, Nathalie Mantha, and Jaime Capelette for their help with data treatment, moral support and friendship during this process. And to all others who have no doubt encouraged and helped me along the way.

Thank You.

TABLE OF CONTENTS

THESIS INTRODUCTION

This thesis is presented as two separate papers, with the breakdown of the organisation of each paper shown in the Table of Contents (p.1-2). The first paper, Distribution of Metals and Metalloids in Particulate Matter in Soils has been submitted for publication and is pending review. The second paper, Attenuation of Metal and Metalloids by Mineral Surface Coatings in Smelter-Affected Acid Soils, will soon be submitted for publication. These papers address the objectives set out at the onset of the thesis, mainly:

I. What is the mineralogical composition of the primary phases in the soils;

II. What type of weathering products are associated with these phases;

III. What is the distribution of Cu, Co, Ni, Zn, Pb, As, and Se in the particulate matter and associated weathering products.

These questions are addressed in the first paper. The second paper addresses the following:

I. Once released from the source (e.g. particulate matter; mineral weathering) what is the fate of metal(loid)s?

II. What possible sinks could be sequestering these metal(loid)s?

III. What is the potential for attenuating free and toxic Al?

IV. In which secondary phases are metal(loid)s being held?

V. What is the role of nanometer thick coatings?

VI. What are the implications for their possible transport in the future?

Therefore the combination of these two papers should provide a complimentary insight into the distribution and behaviour of metals and metalloids in the contaminated soils of the Sudbury area, with wider implications for acidic and contaminated soils worldwide.

Distribution of Metals and Metalloids in Particulate Matter in Soils

Sonia Lanteigne, Michael Schindler*, Andrew McDonald

1. Department of Earth Sciences, Laurentian University, Sudbury, ON, P3E 2C6 Canada.

*corresponding author: mschindler@laurentian.ca

ABSTRACT

Over ten thousand tons of particulate matter has been emitted over the last 100 years as a result of mining activities in Sudbury, Ontario, Canada. Many of these particulates have been deposited in the local soils causing elevated concentrations of Cu, Ni, Zn, Se, As and Pb. The distribution of these metal(loid)s in particular matter and associated secondary phases is studied in order to draw conclusions about the solubility of metal(loid) bearing phases and the mobility of these elements in the soils. The particular matter is characterized using Optical Microscopy, SEM, Micro-Raman Spectroscopy, and Laser Ablation Inductively Coupled Plasma Mass Spectrometry. Particular matter can be classified intro three groups: spherical particulates and angular sulfides and NiO particulates. The spherical particulates form during the rapid cooling of hot gasses and are predominantly composed of Cu- and Ni-bearing spinels, silicates and sulfide inclusions. The collision of precursors of spherical particulate matter with finer particular matter and droplets of residual matte and slag results in the formation of metal(loid)-enriched outer rims on each sphere. These rims as well as Fe-silicates and spinels in the silicate-oxide matrix weather to hematite during a dissolution-precipitation process. Metal(loids) are released during this process in non-stoichiometric proportions relative to their initial concentration in the spinel as they have different affinities to sorb on surface sites during their diffusion through the hematite precipitate. The mobility of metal(loid)s in the soil column increases in the sequence Zn > Cu > Ni > Pb and is the result of the differences in the metal(loid)'s adsorption affinities, and the solubility differences of the metal(loid) bearing phases

INTRODUCTION

Contaminated soils are a widespread environmental risk worldwide (Weber, 2001, Nriagu and Pacnya, 1988). Elevated concentrations of metal(loid)s in soils and lakes around industrial facilities such as smelters are common and the presence of these metal(loid)s may have a negative impact on the environment (Nei et al, 2009, Weber, 2001). Many soil contaminations are caused by the emission and deposition of particular matter from various anthropogenic

processes such as mining, pyrometallurgy, refining and combustion. Particular matter is often enriched in metals (Cu, Pb, Zn) and metalloids (As, Se) which can be released into the environment through alteration processes (Weber, 2001). However this is dependent on the nature of the metal(loid)-bearing phase and it's susceptibility to weathering. Hence, understanding the mineralogical nature of these metal(loid)s is critical for predicting their residency in soils and their long term impact on the environment.

Numerous mineralogical studies of deposited particulate matter have been conducted for locations worldwide. For example, Gregurek et al (1999, 1998) conducted a mineralogical study of smelter-derived particulate matter in snow, which represents the most recent generation of smelter-derived particulates. Their studies identified a wide variety of sulfides (Ni-Cu-Fe-Co), oxides (Fe-Ni-Cu), metallic phases and alloys (Ni-Cu-Fe-Co), as well as slag particulates (Gregurek et al, 1999, 1998). Ettler et al (2005) studied the solubility of Pb-bearing particulate matter from the Příbram smelter in the Czech Republic. Using chemical modelling the authors identified Pb-bearing chlorides as the major source for the release of Pb into the soil environment after deposition. In a later study, Ettler et al (2009) studied smelter-derived particulate matter in a region of Namibia contaminated by the Tsumeb smelter, and identified spinels, metal-rich oxides, sulfide inclusions, and silicates (slag) and Pb rich arsenates as major components. Subsequent chemical modelling indicated that many metal(loid) bearing phases present in the soil could be readily dissolved in the presence of high humidity (e.g., during rain season), mobilizing and releasing significant amounts of Cu, As and Pb into the environment (Ettler et al, 2005). Studies on particulate matter deposited on filters and lichens around the Ampellum S.A. copper smelter (Zlatna, Romania) showed that particles with diameters of <1 µm were primarily composed of anglesite ($PbSO_4$) and that those with diameters of <5-100 µm included Fe-rich spherules with Pb and S rich encrustations (Williamson et al, 2003).

Mining-related activities in the Sudbury area, including the emission of particulate matter, have been on-going for over a century. Studies on the total concentrations of metals in soils and

plants have been well documented by Dudka et al (1995), and the Sudbury soil study (Wren, 2012). However, neither of these provided any predictive insights on the bioavailability, mobility and fate of the metal(loid) contaminants (D'Amore et al, 2005). To assess these aspects, numerous studies focused on determining the chemical composition, mineralogy or weathering of metal-bearing phases in the Sudbury area have been conducted (Lanteigne et al, 2012; Adamo, 1996; Hutchinson et al, 1974). In the study by Lanteigne *et al.* (2012), a detailed chemical and mineralogical characterization of smelter-derived spherical particulates and their weathering features was presented. However it did not include data pertaining to the distribution of trace elements in these particulates, nor did it identify non-smelter-derived metal(loid)-bearing particulate matter in the soil. Knowledge regarding the distribution of metal(loid)s and the mineralogical characteristics of the various metal-bearing phases is, however, required to achieve a holistic understanding of the behaviour of metal(loid)s in soils as particulate matter and associated secondary phases control the long-term release of potentially hazardous elements. Hence, the objectives of this study are to examine unaltered and weathered metal(loid)-bearing particulate matter in the Sudbury soils in order to understand:

I. the mineralogical composition of the primary phases;
II. the type of weathering products associated with these phases;
III. the distribution of Cu, Co, Ni, Zn, Pb, As, and Se in the particulate matter and associated weathering products.

2.0 METHODS

2.1 Background information on the Sudbury area and soils

In the early 19th century development began in the Sudbury area with the establishment of a fur-trading post and the logging industry (Wallace and Thomson, 1993). In the course of developing infrastructure, large Ni-Cu deposits were discovered in 1883 and open roast beds and smelters with short emission stacks were erected to process local ore in 1888. In 1928, the use of open-roast beds was discontinued and smelting became more prolific. Three major

smelting centers were established in the Greater Sudbury area from 1913-1972: Copper Cliff, Falconbridge and Coniston (Whitby *et al.,* 1976). These smelters released SO_2 and metal-particulate matter containing Fe, Ni, Cu, Co, Pb, As and Zn into the surrounding environment (Hutchinson and Whitby, 1974). As a consequence of the SO_2 emissions, local rainfall had extremely low pH with values commonly between 2.85 and 4.43 (Hutchinson and Whitby, 1974)

In 1972, the Coniston smelter was closed and the "Super Stack" at the Copper Cliff site was constructed at a height of 381 meters (Potvin and Negusanti, 1995). Total emissions of SO_2 declined by 50% of the highest yearly recorded emissions (2.56 million tonnes in 1960) following the Countdown Acid Rain program legal limit of 365 000 tonnes per year (Potvin and Negusanti, 1995) after 1972 and by 1994, SO_2 emissions were reduced to 14% of the initial emissions.

2.1.1 Physical, Chemical and Mineralogical characteristics of the Sudbury soils

Elevated concentrations of Ni, Cu, Zn, Co, As, Pb and Se are known to occur in the soils of the Sudbury area (Wren 2012). Soils with similar elevated contents have also been documented in other smelting-impacted areas in Canada and Russia (Chopin and Alloway, 2007; Johnson and Hale, 2004; Knight and Henderson, 2006, 2005; Ratkin et al, 2001; Selim and Sparks, 2001; Adamo et al, 1996; Niskavaara et al, 1996; Alloway, 1995; Buznikov et al, 1995; Dudka et al, 1995; Whitby et al, 1976; Hutchinson et al, 1974). In Sudbury, the highest metal(loid) concentrations are observed in the topsoil (top 5 cm), consistent with atmospheric deposition of particulate matter (Wren, 2012; Lanteigne et al. 2012).

Smelter-derived particulate matter deposited in the Sudbury soils consists of spherical particulates in the nano- to millimeter-sized range that exhibit characteristic textures consistent with quenching from high temperatures (Lanteigne et al, 2012, Mantha et al. 2012a,b). The spherical particulates (the technical term is prills) can be classified into one of two categories: oxide/silicate, and sulfide-bearing particulates. Oxide/silicate particulates (equivalent to slag) are principally composed of magnetite (Fe_3O_4), hematite (Fe_2O_3), Fe-silicates (olivines, pyroxenes)

and Fe-spinels with varying Cu and Ni concentrations (<10 wt%). This group of spherical particulates includes delafossite ($CuFeO_2$), trevorite ($NiFe_2O_4$), cuprospinel ($(Cu,Mg)Fe_2O_4$), tenorite (CuO) and cuprite (Cu_2O) (Lanteigne et al, 2012, Mantha et al. 2012a, b). Sulfide-bearing particulates are composed of sulfide inclusions encapsulated by a rim of relatively insoluble Fe-oxides and Fe-silicates. The sulfide inclusions are composed of intergrowths of three main phases: heazlewoodite (Ni_3S_2), bornite (Cu_5FeS_4) and pyrrhotite ($Fe_{(1-x)}S$) (Lanteigne et al, 2012).

2.2 Experimental

Soil samples of the upper 0-5 cm were collected and taken in duplicate at three locations in proximity to the smelter in Copper Cliff, Ontario (Figure 1). Coordinates for sample locations along with images of sample sites and sampled soil are provided in appendix A. These sites were chosen to represent un-limed soils contaminated predominantly by anthropogenic activities in the area, and it was ensured that representative samples were taken by avoiding sites in proximity to railways, roadways, waterways, slopes, and tailings areas. Sub-samples were not sieved, but instead were separated with a magnet to produce bulk soil, magnetic, and non-magnetic separates which were then embedded in one inch epoxy mounts and polished.

2.2.1 Bulk Chemical Analysis

Samples from each location were ground with a mortar and pestle and sent to two different labs for chemical analysis. At the GEOLABS laboratory (Ontario Geological Survey, Sudbury, ON), 0.5 grams of each sample were dissolved in an open vessel with a multi-acid digest composed of hydrofluoric, nitric and perchloric acids at T = 140°C until dry. The dried samples were completely dissolved in a mixture of HCl and HNO_3 and spiked with 1.0 mL of a 5 ppm Ru+Re internal standard solution. Element concentrations were measured with ICP-OES and represent the total concentrations of the elements in the sample. The metal(loid)-concentrations in the more “soluble fraction” of the soil samples (*e.g.,* secondary phases,

nanoparticles) were measured at a commercial lab (AGAT labs, Sudbury, Ontario) with a less-intensive digest. Here, one gram of each sample was digested with Aqua Regia (hydrochloric acid and nitric acid) for one hour at 90 ºC. The digests were diluted to 50 mL with de-ionized water and subsequently analysed with ICP-MS. Blanks, sample replicates, duplicates and internal reference materials, both aqueous and geochemical standards are routinely used in both laboratories as part of the quality assurance.

2.2.2 Scanning Electron Microscopy

Polished epoxy discs which produced cross sections of the particulate materials were examined by Scanning Electron Microscopy (SEM) with a JEOL 6400 instrument equipped with both back scattered (BSE) and secondary (SE) electron detectors and an Energy-Dispersive X-ray Spectrometer (EDS). It was operated at 20 kV with an estimated beam current of 1 nA.

2.2.3 Laser Ablation Inductively Coupled Plasma Spectroscopy

Trace-element distributions and concentrations in particulates were measured with a laser-ablation-inductively-coupled-plasma spectrometer (LA-ICP-MS) consisting of a New Wave Nd:YAG 213 nm laser coupled to a quadrupole Thermo X II series. Areas of interest were analysed using both line scans and composites of line scans producing maps. Ablation was done in a He atmosphere and Ar was mixed to the carrier gas before it entered the ICP-MS. For traverses, spot sizes of 3, 5 and 10 µm were used. For maps, a beam size of 3 µm was used. The spot size was chosen based on the size of the area of interest, and was utilized at a repetition rate of 10 Hz. The energy density was kept constant at 11 Jcm^{-2}. Both NIST610 and NIST 612 synthetic glass and MASS (sulfide) were used as external standards. These contain nominal trace element abundances of about 500 mg kg-1, 50 mg kg-1, and 300 mg kg-1, respectively. Standards were analyzed at the beginning, intermittently, and at the end of each data acquisition under the same conditions. Detection limits for elements varied as a function of the experimental setting of the laser scan. Line scans were designed to traverse the cross-section of particulates, beginning with the outer epoxy (labeled A in Figure 2) and cutting

through various zones of the particulate interior. Integration areas were selected on the basis of chemical differences identified in the line scans and in EDS maps. Laser-Ablation-ICP-MS data are often quantified by calibrating the counts per second (CPS) with respect to an internal standard as well as an external standard (*e.g*. NIST glasses). However, the samples analyzed in this study are heterogeneous, so no single element was suitable as an internal standard and therefore, only the external standards were used. Molar ratios of the elements were calculated from the counts and the known concentrations in the NIST glasses and MASS standard and element concentrations then being calculated by normalizing the sum of the moles to 100% and assuming that oxides are dominated by O, Fe, S, Ni, Cu, Si, Al, Ca, Na, and K and sulfides by S, Fe, Cu, Ni, Co and Zn (observed by SEM-EDS) This procedure resulted in a semi-quantitative data set (Tables 1 and 2) with an estimated error of <5% for the concentration of trace elements in an individual measurement.

2.2.4 *Micro-Raman spectroscopy*

Raman spectroscopy was performed on cross-sections of particulates with a thickness of at least 10 µm. Spectra were obtained over the range of 100 to 4000 cm^{-1} and collected with a HORIBA Jobin Yvon XPLORA spectrometer interfaced with an Olympus BX 41 microscope, 100x magnification (estimated spot size of 2 µm), a 1200 grating and an excitation radiation of λ=532 nm. Calibration was made using the 521 cm^{-1} line of a silicon wafer.

3.0 RESULTS

The trace-element composition and distribution within unaltered spherical particulate matter will be presented first, and changes in their trace-element composition during weathering will be subsequently addressed. The trace-element composition of angular sulfide and oxide particulate matter and associated secondary alteration phases will be also described.

3.1 Trace-element composition and distribution within spherical particulates

Figure 2 shows an SEM backscattered electron image of a smelter-derived spherical particulate that has an inclusion of heazlewoodite, (Ni_3S_2), bornite, Cu_5FeS_4, and pyrrohotite,

$Fe_{1-x}S$, within a Fe-silicate/oxide matrix. Laser-ablation line scans indicate a higher abundance of metal(loid)s in the sulfide inclusion, and the presence of a rim enriched in Pb (Figure 2b). Similarly, laser-ablation ICP-MS element distribution maps of a spherical particulate with a heazlewoodite-pyrrhotite inclusion (Fig.3b-j) indicate an enrichment of the metal(loid)s Co, As, Se, Ni and Cu in the sulfide inclusion and a distinct rim containing elevated concentrations of Pb, As and Zn (Table 1). The element distribution maps also indicate that the latter element is enriched in the Fe-oxide matrix relative to the sulfide core. The association of Zn with the particulate matrix can also be observed in Figure 4, where Zn, Ni, Cu and Co are associated with the Fe-silicate matrix and dendritic spinel crystals of an oxide/silicate particle. Once again, this particle has a distinct rim containing elevated concentrations of Pb, As and Zn (Table 1).

These observations indicate that the unaltered rims occur on all spherical particulates, independent of their mineralogical composition, are enriched in Pb and Zn with respect to the sulfide inclusions and are enriched in Ni, Zn, As and Pb with respect to the silicate-oxide matrix (Table 1).

3.2 Trace-element composition and distribution within weathered spherical particulates

Lanteigne et al. (2012) provided a detailed description of the weathering features in and around silicate/oxide and sulfide-bearing spherical particulates from the Sudbury area. In this study, we will report the trace-element composition of some of the weathering products observed by Lanteigne et al. (2012).

In the case of particulates with a sulfide inclusion, weathering starts with the formation of cracks allowing the infiltration of oxidizing pore water and the subsequent oxidation of sulfides to sulfates. At high sulfur-removal rates (*e.g.*, complete dissolution of the sulfides and sulfates), the pore space of the former sulfide inclusion is often coated by a layer of secondary oxide minerals. For example, Figure 5a shows a spherical particulate with coarse subhedral crystals of magnetite in a Fe-oxide-silicate matrix. There had been two sulfide inclusions in the interior of this sphere: One inclusion that remained nearly unaltered (labelled 1) and one that was

completely removed leaving a void now rimmed by a Ni-oxide with a stoichiometry close to that of a spinel (labelled 2). Laser-ablation line scans through and along both inclusions indicate that the trace elements Cu, Se, As and Pb remain present in the relatively unaltered inclusion (labelled 1), but have been completely released from the particulate during the weathering of the second inclusion (labelled 2).

Figures 6a and b show microscopic images of a spherical particulate before and after the recording of chemical distribution maps with LA-ICP-MS. The sphere contains an inclusion of Ni-bearing pyrrhotite (Fe : Ni atomic ratio = 3: 1) and an inclusion composed of mainly Al-(hydr)oxides with minor sulfates and silicates (Al : Si : S : (Fe + Ni) = 4 : 2 : 2 : 1) which are embedded in an Fe-Al-silicate matrix (Fe : Al : Si = 1 : 1 : 1). The latter matrix is surrounded by a hematized rim with Fe : Al atomic ratio of 1 : 1. Major parts of the sulfide and sulfate-hydroxide inclusion were initially located below the surface but were exposed or completely removed during laser ablation. High intensities (CPS) in the distribution maps of Ni and S indicate the location of the sulfide inclusion (highlighted). The inclusion contains significant concentrations of Cu (10 wt%) and minor concentrations of Co and Pb (500, 2100 $mgkg^{-1}$). High intensities (CPS) in the distribution maps of Hg and K delineate the location of the sulfate-hydroxide inclusion. Chemical distribution maps and Table 1 indicate that inclusions contain elevated concentrations of Ni, Cu, Co, Hg and As (Figure 6).

Mössbauer and Raman spectroscopy demonstrated that the weathering of Fe-silicates and spinels involved their gradual transformation into hematite (Lanteigne et al. 2012). This weathering process commonly starts along the outer Fe-bearing rim of the spherical particulates. The line scans discussed above showed that these rims are enriched in metal(loids) with respect to the oxide/silicate matrix. On the basis of experimental studies by Sidhu *et al.* (1981), Lanteigne et al. (2012) argued that many metal(loids) (*e.g*. Cu, Ni) were not compatible with the structure of hematite and were thus released during the transformation process from the magnetite to hematite structure. This phenomenon can be indeed observed

when examining the element distribution maps of the spherical particulate (Figure 6c) as well as the average metal(loid) concentrations of unaltered and hematized rims (Table 1).

Although the former maps still indicate the occurrence of a Pb-enriched rim, the concentration of the latter elements decreased by a factor of ~4, and those of Cu, Ni and Zn by factors of 9, 12 and 4 , respectively. Table 1 indicates however that the concentration of metal(loid)s forming oxy-anions such as As and Se is on average higher in the hematized rim than in the unaltered rim.

3.3 Angular sulfides particulates

Sulfide particulates are less common as smelter-derived particulates in the Sudbury soils. They occur in the micrometer range and are mostly composed of chalcopyrite, $CuFeS_2$ and pentlandite, $(Fe,Ni)_9S_8$, the major ore minerals for Cu and Ni in Sudbury. Particulates of both can be found unaltered or strongly weathered. For example, Figure 7a and b show a chalcopyrite particulate with a relatively thick Fe-Al-(hydr)oxide coating. The coating itself is rimmed in certain areas by an alumino-silicate layer. Laser-ablation transects through the alteration layers and the underlying sulfides indicate that the latter minerals are depleted in trace elements such as Pb, As, and Se relative to the former layers (Figure 7c, Table 1). The abundance of trace-elements in the coatings can vary, however, with chemical composition. This is demonstrated in Fig.7 where the Fe-Al-(hydr)oxide coating contains significantly higher concentrations of As and Se than the outer alumino-silicate layer. There are also differences between the trace-element composition of chalcopyrite and pentlandite particulates. Table 1 shows the differences in trace element composition of pentlandite and chalcopyrite, namely that with the exception of Co, chalcopyrite hosts higher concentrations of all other metal(loid)s.

3.4 Nickel Oxides

Angular Ni-oxides particulates were found to be less common than other particulates in the Sudbury soils. Due to the chemistry and very angular nature of these particulates, it is

assumed that they are most likely of anthropogenic origin. They range in size from 20-80 µm and are coated in certain areas by Fe-(hydr)oxides (Figure 8). The Raman spectra of these angular grains (Fig.9) are consistent with that of NiO and no peaks were noted in the 3000-3500 cm^{-1} region which would suggest the presence of hydroxyl. Laser-ablation transects show the presence of Co, Cu and Zn in the interior of NiO and an Fe-(hydr)oxide rim enriched in Pb, As and Al (Figure 8c, d). The NiO particulates are often associated with soil agglomerates containing mixtures of rock-forming minerals, amorphous silica and Fe-Al-hydroxides (Figure 10). Laser ablation transects (Figure 10) and Table 2 indicate that higher concentrations of Co are associated with NiO and that the concentrations of Ni and Co decrease from the NiO grain towards an inner Fe-Al-(hydr)oxide coating (labelled Al-FeOX), an amorphous Fe-Al-bearing silica coating (labelled Fe-Al-SiOx) and an outer Fe-Al-(hydr)oxide coating (labelled Al-FeOX). They also demonstrate that the surrounding coatings are enriched in Pb, Cu, As and Se, which decrease in concentration in moving from the outer Fe-Al-SiOx towards NiO.

4.0 DISCUSSION

The focus of the discussion will be on the heterogeneous distribution of trace elements in unaltered and weathered spherical particulates, which can only be understood if one considers the conditions under which they developed during their formation in the smelting process, the type of secondary phases formed during weathering and differences in the mobility of the elements during dissolution of the primary high-temperature phases. The fate of trace elements during dissolution-reprecipitation on the surface of Fe-bearing sulfides will be subsequently addressed followed by a discussion of the distribution of trace elements in the NiO particulates and associated coatings.

4.1 Smelter-derived spherical particulates

Smelter-derived spherical particulates in the Sudbury area are mainly composed of silicate glasses, spinels (mainly magnetite and Cu+Ni- bearing spinels but also cuprospinel),

high temperature silicates such as olivine (fayalite) and Cu-Ni-Fe sulfides embedded in an oxide/silicate matrix. The abundance of these phases in the spherical particulates will vary as a function of the composition of the ore, matte, smelting technology and cooling history of the particulate matter.

At the Copper Cliff facility, concentrates of Ni- and Cu-sulfides are smelted at different temperatures, creating a Ni- and Cu-sulfide-rich matte and a slag composed of mainly magnetite, fayalite or SiO_2 (Pengfu and Chuanfu 1997). In the subsequent converting processes, the remaining Fe- and S are driven from the molten matte by forcing O_2-enriched air into the matte. Emissions produced during these processes commonly consist of SO_2, droplets of slag and matte, unreacted flux, condensed particulates, and finer sulfate-bearing aerosols, all of which were released in the past without any filtering (Wren, 2012). Gases containing these components commonly leave the corresponding facilities at $T > 1200°C$ and are quenched in the air within seconds to several hundred ºC. For example, Evans et al. (1991) showed that gases leaving the Horne Cu-smelter reactor at Rouyn-Noranda at 1230 °C were quench-cooled to 620 °C in 0.6 s and further cooled down to 350°C in 6 seconds.

Particulate matter in the emissions originates either from vaporization and condensation of gaseous components or through the collision of solid and liquid particulates (Samuelsson and Bjorkman 1998). These particulates can subsequently transform during the smelting, cooling and filtering processes, thus leading to a wide variation in their size, chemical and mineralogical composition, as well as in the internal and external morphologies of emitted particulate matter and finer aerosols (Knight and Henderson 2006, 2005; Kliza et al. 2000; Gregurek et al. 1999, 1998; Lastra-Quintero et al. 1998; Samuelsson and Bjorkman 1998; Adamo et al. 1996; Chan et al. 1982).

4.1.2 Metal(loid)s in the sulfide inclusions

Sulfide inclusions are composed of heazlewoodite, bornite and pyrrhotite and contain elevated concentrations of As, Se, Co and occasionally Pb (Figures 2 and 3).

The high abundance of Cu (up to 20 wt.%) in the heazlewoodite-pyrrhotite inclusion (Fig. 6) may be explained by the occurrence of chalcocite, Cu_2S, or bornite nano-inclusions, as the former mineral is commonly intergrowth with heazlewoodite in the Ni-matte and the latter mineral commonly occurs as nano-to micrometer inclusions in the heazlewoodite (Lanteigne et al. 2012). The presence of Se in the sulfide inclusions is most likely the result of their substitution for S in the observed sulfide minerals, and the high concentrations of Co, and As are likely the result of small Ni-Co pentlandite and gersdorffite (NiAsS) inclusions commonly found in heazlewoodite (Giuliani et al, 2013; Hawley and Nichol, 1959).

The enrichment in Hg in the sulfate-hydroxide inclusion (1052 $mgkg^{-1}$) is surprising, given that I. Sudbury ore contains only minor Hg in the range of 1-10 $mgkg^{-1}$ (Ames and Farrow, 2007); II. Hg-bearing spinels, sulfides or silicates were not observed in any other spherical particulate and III. Hg-bearing sulfate minerals such as schuetteite, $Hg_3(SO_4)O_2$ are rare and have not been reported from Sudbury. The source for Hg within the sulfide inclusion may have been small amounts of Hg phases as heazlewoodite and other identified sulfides have not been reported to incorporate large proportions of Hg. In the Sudbury ore for example, Hg does not occur within the base metal sulfide minerals but instead occurs in association with discrete platinum group minerals which are not in solid solution with the sulphides (reference). The source for Hg cannot be determined because the specific mineral hosts for Hg within the smelted ore have not been identified, Hg-enriched ore originating from outside of the Sudbury area may have been utilized, and Hg may have been added to the smelting process in the form of electrochemical waste-products.

4.1.3 Metal(loid)s in oxides and silicates

Slag, ore and oxidized portions of the matte are the major sources for oxides in the spherical particulates such as magnetite, Fe_3O_4, Ni- and Cu-bearing spinel [(Fe, Ni)Fe_2O_4, (Fe, Cu)Fe_2O_4], trevorite, $NiFe_2O_4$ and cuprospinel, $CuFe_2O_4$. The occurrence of secondary spinels such as trevorite around the sulfide inclusions is the result of the precipitation of Ni^{2+} hydroxides

and their transformation into the more stable crystalline spinel-type phases (Cornell et al. 1992, Lanteigne et al. 2012).

The spinel structure of magnetite, trevorite and cuprospinel can accommodate other divalent cations such as Zn^{2+} and Co^{2+}. For example, zinc-bearing spinels such as gahnite ($ZnAl_2O_4$) were identified in smelter-derived particulates and slags at numerous locations world-wide (Bril et al, 2008; Nachtegaal et al, 2005; Panfili et al, 2005). The incorporation of trace elements into the Cu^+-bearing oxides delafossite, $Cu^+Fe^{3+}O_2$, and cuprite, Cu_2O is limited as Cu^+ occurs in linear coordination. Ni^{2+} most commonly occurs in octahedral coordination with O and therefore does not replace Cu^+ in delafossite or cuprite. Nickel (II) or Zn^{2+} may replace Fe^{3+} in delafossite (in octahedral coordination), but this would require a coupled substitution where another divalent cation (M^{2+}) must replace Cu^+:

$$Cu^+ + Fe^{3+} \quad \leftrightarrow \quad M^{2+} + Ni^{2+} \qquad [1]$$

There are no divalent cations that can occur in linear coordination with O. Hence, Ni^{2+}, Zn^{2+} or Co^{2+} cannot be incorporated into the structures of delafossite or cuprite, thus explaining that these minerals are deficient in Ni, Zn and Co relative to those with the spinel structure.

Lanteigne et al. (2012) showed that minerals of the pyroxene and olivine groups as well as silicate-glasses are the dominant phases within the silicate matrix. Potential host phases for Ni and Zn could be willemite Zn_2SiO_4, various orthopyroxenes known to host Zn in conjunction with Fe, and Ni-rich olivines such as liebenbergite ($Ni_{1.5}Mg_{0.5}SiO_4$) (Le Roux et al, 2010; Annersten et al, 1982). For example willemite was identified in Zn-enriched slag from the Hegeler Zinc smelter, Illinois (USA) (Piatak and Seal 2009). The absence of large proportions of Cu in the silicate matrix (*e.g.* Figure 3) must be related to the incompatibilities of Cu^{1+} and Cu^{2+} towards many rock-forming silicates as the former often occurs in a linear two-fold coordination (Wells, 1984) and the latter in a distorted [4 + 2] or [2 + 4] coordination (Burns and Hawthorne, 1996).

4.1.4 Formation, texture and metal(loid)-composition of the outer rims

Nickel, Zn, As and Pb occur often in higher abundances in rims along the surface of the sphere rather than in the silicate-oxide matrix (Figures 2-5, Table 1).The enrichment of these metal(loid)s in the rims can be understood when one considers their formation as well as the composition of the finer material in the gas phase of the smelter and stack.

Unaltered rims on spherical particulates often display typical features of a rapid cooling process and are commonly composed of high-temperature spinel phases (Lanteigne et al. 2012). Figure 11 shows for example a spherical particulate with a porphyritic texture composed of magnetite in a Fe-silicate matrix. The sphere is rimmed by a Ni-Cu-Fe-oxide phase (most likely a spinel), which appears to have formed after the formation of the magnetite crystals. Experimental studies by Connolly and Hewins (1995) showed that similar rims can form when injected dust particulates collide with molten droplets at T~1000 °C. In this regard, Lanteigne et al. (2012) argued that the Cu- and Ni-rich rims on spherical particulate formed through trapping of finer dust particulates by droplets of lower viscosity and suggested that similar rims on spherical particulates were also formed through dust-molten-droplet collisions.

The terms *dust* and *molten droplet* may not be appropriate here as they refer exclusively to solid and liquid matter, respectively. However, there are no indications whether the material in the gas phase of the smelters and stacks occurred in a liquid or in a partially or fully solidified form. Hence, we will use the terms *particulate matter-liquid droplets* when referring to the finer material and *precursors of the spherical particulates* when referring to the larger condensed spheres.

The metal(loid) composition of the unaltered rims (Table 1) indicates that the particulate matter-liquid droplets were heterogeneous in composition and contained elevated concentrations of Ni, Cu, Pb, As and Zn. Atmospheric and experimental studies suggest that the collision between the precursors and the particulate matter-liquid droplets occurred over a large temperature range:

I. Pb- and As-bearing sulfate aerosols are common at low temperature in plumes emitted by the stacks in the Sudbury area as well as by smelters and coal power-plants worldwide (Mantha et al, 2012a, b);

II. PbS is a dominant phase in finer particulate matter emitted from Pb smelting at *T*=1115 °C, and anglesite ($PbSO_4$) occurs as smaller droplets (<10µm) at temperature of approximately 1170 °C (Ettler, 2005);

III. Crystallization temperatures of phases in the Cu-As-S, Cu-Zn-S, Cu-Pb-S and Pb-As-S and Zn-Pb-S system indicate that droplets of liquid matte and slag could have occurred in a temperature range of 550 to 1200 ºC (Tesfaye and Taskinen, 2011).

The penetration depth of the particulate matter-liquid droplets into the precursors of the spherical particulates and crystallization of phases on their surface is a function of the temperature and viscosity of the material within the precursors (Connolly and Hewins, 1995). In this regard, the texture of the outer rim may thus be an indication of whether the collision occurred at a higher or lower T or viscosity (Connolly and Hewins, 1995). For example, relatively thick porphyritic or skeletal textures (Figures 2 and 11) may indicate a higher T of collision, where a material of lower viscosity in the precursors allowed deeper penetration of particulate matter and a lower cooling-gradient (due to the fact that the collision may have occurred in the smelter and not in the stack) facilitated the nucleation of phases along the surface of the precursors (Connolly and Hewins, 1995). On the contrary, thin cryptocrystalline or glassy rims with or without a dendritic texture (Figure 3 and 4) may indicate a lower T of collision, where a higher cooling gradient forced the solidification of the exterior and where material of higher viscosity in the precursors prevented deeper penetration into the sphere (Connolly and Hewins, 1995).

4.1.5 Release of metal(loid)s from sulfide inclusions within smelter-derived particulates

The spherical particulates are the most common metal(loid)-bearing smelter-derived phases in the Sudbury soils. Hence, the weathering of the different components that constitute

the spherical particulates necessarily influences the release of meta(loid)s into the soils. Numerous studies have shown that the weathering sequence of the different components in the spherical particulates is as follows: sulfide inclusion → silicates → spinels (Lanteigne et al. 2012, Ettler et al., 2009; Seignez et al., 2007). Also, the complete dissolution of the silicates can occur simultaneously with the transformation of Fe-spinels into hematite (Lanteigne et al. 2012).

The weathering of sulfide inclusions involves their dissolution and the precipitation of sulfates at a low sulfur-removal rate or spinels at a high sulfur-removal rate within the vicinity of the former inclusion (Lanteigne et al. 2012). Hence, the fate of an element released during dissolution of the sulfide depends to a certain extent on its crystal-chemical compatibility with the sulfate and spinel structure. For example, Ni is commonly enriched in spinels relative to Cu (Figure 5) which can be explained with the observations that Ni-spinels are more stable than Cu-spinels (see below) and that Ni-spinels can form at low T through dehydration of Ni-hydroxides (Cornell et al. 1992, Lanteigne et al. 2012).

4.1.6 The release of metal(loid)s from oxides/silicates in smelter-derived particulates

The transformation of magnetite or an Fe-silicate into hematite involves the breaking of bonds and the structural re-arrangement of Fe and O. Considering that a solid-state diffusion process does not commonly occur at room temperature in contact with soil pore-water, the transformation of an Fe-spinel or Fe-silicate into hematite most likely involves the dissolution and oxidation of the former minerals, and the precipitation of the latter mineral. Porosity is important in this dissolution-precipitation process, as a pore system is required for the mass-exchange between the hematite-(spinel/silicate) interface and the hematite surface (Putnis, 2009). This mass exchange involves the diffusion of hydronium ions and dissolved O_2 from the hematite surface towards the hematite-(spinel-silicate) interface as these components are required to break Fe-O bonds and to accept electrons released by the oxidation of Fe^{2+}. It also includes the migration of divalent cations *(e.g*. Cu, Ni, Co, Zn and Pb) from the hematite-(spinel/silicate) interface towards the hematite surface as these cations are incompatible with

the hematite structure (Sidhu et al. 1981). The migration process results in a depletion profile that corresponds to a decrease in the concentration of divalent cations towards the hematite surface consistent with the observation made in previous studies relating to the transformation of magnetite to hematite (Sidhu et al. 1981 and Tang et al. 2003).

The transformation of magnetite into hematite often occurs via the formation of intermediate maghemite (which has a defect spinel structure) in which the divalent cations present in the spinel structure are also lost (Tang et al, 2003). However, neither Mössbauer nor Raman spectroscopy indicated the presence of maghemite in the spherical particulate, suggesting that most of the divalent cations were released during the breakdown of the primary magnetite and not maghemite (Lanteigne et al. 2012).

The average concentrations of divalent cations in the hematite and the spinel phases along the rim may be used to rank their relative abilities to diffuse through the hematite precipitate. On the basis of the concentrations listed in Table 1, the ability of metals to diffuse through the hematite precipitate decreases in the sequence Ni > Cu > Zn = Pb. The diffusion of a cation through a porous medium depends on, among other factors, (*e.g.* concentration gradient) on its affinity to sorb to surface sites; *i.e.* the higher the sorption affinity, the lower the ability to diffuse through the medium. Adsorption studies show that the affinity of the divalent cations to sorb on Fe-hydroxides decreases in the sequence Ni < Zn < Cu < Pb (Stumm 1992). The relatively close agreement between both rankings indicates that the release of metal(loid)s during weathering of the spinel phases is partially controlled by their affinity to sorb on surface sites of hematite.

The higher porosity of the hematite precipitate relative to the spinel structure also results in an increase in surface area and thus in a higher number of positively-charged surface sites. As the pH of the sampled soils (average ~5) is below the point of zero charge (~8.5) for hematite (Eggleston et al, 2006), one would expect higher concentrations of adsorbed anions in the hematite precipitate relative to the spinel phase. This is consistent with the observations

made in this study, *e.g.,* the hematized rims are enriched in As and Se (Table 1), which most likely would have been bound to the positively charged surface-sites as oxy-anions ($(AsO_4)^{3-}$,$(SeO_4)^{2-}$). These oxy- anions most likely originated from both: (a) the oxidation and subsequent dissolution of the sulfide inclusions and (b) from the spinel rim itself, as the rims can be enriched in As relative to the Fe-silicate-oxide matrix (Figure 5).

4.2 Weathering of angular sulfide

The angular sulfide particulates composed predominantly of pentlandite and chalcopyrite are detrital residuals of the ore processed at the various smelter centres in the area. Depending on the pH and composition of the local soils, coatings of secondary Fe-Al-hydroxides and alumino-silicates would be expected to form on the sulfide particulates.

The composition of relatively thick coatings (of Fe-Al hydroxides and Si) on chalcopyrite grains indicate the presence of elements which are either absent (*e.g.,* Si and Al; Figure 7) or occur in lower concentrations in the sulfides than in the coatings (all metal(loid)s except Cu and Zn; Table 1; Figure 7). The coatings, especially those composed of Fe-Al-hydroxides are thus not only sinks for metal(loid)s released during dissolution of chalcopyrite such as Se and Zn but also for metal(loid)s present in the soil pore-water (*e.g*. Ni, Co, Pb and As).

The Al-Fe-hydroxide coatings most likely formed *via* a dissolution-precipitation process possibly involving the incorporation of Fe^{3+} liberated from the chalcopyrite dissolution (note that Fe occurs in the trivalent state in chalcopyrite; Eissa et al, 1976) and its co-precipitation with free Fe^{3+} and Al^{3+} present in the acid soils of the Sudbury area (Lanteigne et al. 2013). The formation of the outer alumino-silicate coatings may be explained with the initial adsorption of silica species on the Fe-Al-hydroxide coatings, which, similarly to arsenate and selenate species, have a high affinity for surface sites of Al-Fe-hydroxides under acidic conditions (Sigg and Stumm, 1981). An interesting aspect of these coatings is whether they can prevent or slow down the release of metal(loid)s from the underlying sulfide grains. As indicated above, secondary phases that may have formed through dissolution-precipitation processes are

commonly nano-to microcrystalline and contain a network of pores that allow the mass transfer between underlying minerals and the solution above. Hence, the Al-Fe-hydroxide coatings depicted in Figure 7 may slow down the release of metal(loid)s but cannot prevent the complete dissolution of the underlying chalcopyrite. In this regard, a study by Huminicki and Rimstidt (2009) showed that the presence of Fe-hydroxide coatings on pyrite decreases the oxidation rate of pyrite under basic conditions by a factor of more than 5 orders of magnitude. This observation suggests that enhanced formation of Fe and Al-hydroxide coatings on sulfide particulates caused by an increase in soil pH as a result of the liming of soils, can significantly inhibit the dissolution of sulfides particulates, and therefore reduce the rate of metal(loid) release.

4.3 Weathering of angular NiO particulates

Nickel is siderophilic and forms Fe-Ni alloys during the smelting process at high temperatures, ideally above T = 1150 ºC (Barceloux and Barceloux, 1999). A by-product of this alloy-forming process is NiO (Sarkisyan, 1986).

In contrast to soluble Ni-salts (chlorides, nitrates, sulfates), Ni-oxides have a low solubility similar to that of spinels, and weather slowly under temperate weathering conditions (Barceloux and Barceloux, 1999). The latter process involves the formation of coatings composed of mainly Al-Fe-hydroxides and alumino-silicates. The formation of these coatings was not necessarily controlled by the dissolution of the underlying particulate as they only contain Ni as a trace-element. The decrease in Ni and Co and the increase of other metal(loids) (Pb, Cu, As and Se) from the inner to the outer and from the outer to the inner coatings, respectively, suggests, however slow, a mass transfer through the coatings that involved the diffusion of cations and oxy-anions from the surface of the coatings to the surface of the NiO and *vice versa*.

4.4 Patterns of metal(loid) abundance, distribution and stability in host minerals vs. the soil column

Differences in the abundance and stability of the different smelter-derived phases in conjunction with the depletion and enrichment of metal(loid)s in secondary phases can be used to explain differences in their mobility within the soil column. In the Sudbury area, metal(loid)s are mobilized through the upper 10 cm of the soil column in the order Zn > Cu > Ni > Pb with Zn experience the greatest degree of migration, and Pb the least, with three times less Pb being mobilized from the upper column than Zn (Wren, 2012). The relative mobility of these metal(loid)s is in agreement with that determined for the rate at which these metal(loid)s are being released from smelter-derived particulates. This rate of release is a function of various factors, predominantly, the solubility of the metal(loid) bearing phases. Lu and Muir (1987) showed in their dissolution study of metal-ferrites that the dissolution rate of these minerals should be ranked as follows: Fe_3O_4 >>$ZnFe_2O_4$ > $CuFe_2O_4$ > Fe_2O_3 > $NiFe_2O_4$. The higher dissolution rate of Cu-spinels than Ni spinels was thoroughly discussed by Lanteigne et al. (2012) and Cornell et al. (1992) who showed that Cu is more readily lost through the dissolution of their host phases than is Ni, which upon weathering immediately re-precipitates into trevorite. Lead is the least mobile of the metal(loid)s in Sudbury as is common in most soils. In various studies Pb has been shown to be retained by soils to the greatest extent (Manceau et al, 1996; McLean and Bledsoe,1992). In smelter-derived particulates, the Pb-bearing rim remains even after the transformation of the matrix into hematite (Figure 6) as the element has the highest affinity of all divalent cations to sorb on the surface sites of the Fe-oxide (see above). Therefore, the release of metal(loid)s from smelter-derived particulates is controlled by the dissolution rate of their host phases ($ZnFe_2O_4$ > $CuFe_2O_4$ > $NiFe_2O_4$.), their occurrence in secondary phases ($NiFe_2O_4$) and their affinity to sorb on the surface of secondary Fe-(hydr)oxides (Pb > Cu > Zn > Ni). On the basis of these observations, the release of metal(loid)s during weathering of the spherical particulates may be ranked in the order: Zn > Cu > Ni > Pb, which agrees with the mobility of the metal(loid)s in the upper 10 cm of the soil column. Hence, interfacial processes

on the nano- to micrometer-scale in spherical smelter-derived particulates exert control on the mobility of metal(loid)s in the soil column on the cm/meter scale.

4.0 CONCLUSION

Metal(loid)-bearing soil particulate matter is a chemically and mineralogically complex form of waste which represents the source of the majority of metal(loid)s in the Sudbury soils. Trace element distributions in particulate matter and associated secondary phases are equally complex and are affected by the type of phase, its formation and alteration as well as on the composition of the soil pore-solutions. This study showed in detail that

I. The weathering of sulfide inclusions within spherical particulates results in the formation of oxides (spinels) and hydroxide/sulfates where the former and latter minerals have elevated concentrations of Ni + Co and Cu + Hg, respectively;

II. Metal(loid)-rich rims form during the collision of the spherical particulate precursors, with finer particulate matter or liquid droplets from the slag or matte, and are composed of spinels which weather via dissolution-precipitation processes into hematite. Metal(loid)s released during the dissolution process diffuse at different rates through the precipitated hematite and are released in non-stoichiometric proportions relative to their initial concentration in the spinel.

III. Weathering of angular sulfides and NiO particulates results in the formation of mainly Al-Fe-hydroxide coatings with minor abundances of alumino-silicates. The coatings are sinks of metal(loid)s that are either absent or only occur in small concentration in the underlying parent minerals. Thusly, these coatings act as a control on the mobility of metal(oid)s in the soil column.

IV. The mobility of minerals in the soil column are ranked as follows: Zn > Cu > Ni > Pb which reflects the order in which they are released from particulates in the soil. Therefore the mineralogy of the host phases for these metal(loid)s is a critical factor in

controlling the release and long term mobility of these contaminants in the soil environment.

5.0 REFERENCES

Adamo P., Dudka S., Wilson M. J., McHardy W. J. (1996). *Chemical and mineralogical forms of Cu and Ni in contaminated soils from the Sudbury mining and smelting region. Canada*. Environ. Pollut. 91, 11–19.

Alloway B.J. (1990). *Soil processes and the behaviour of metals*. In B.J. Alloway (Ed.), Heavy metals in soils. New York: Wiley, 339. p.7-28.

Ames D.E., Farrow C.E.G. (2007). *Metallogeny of the Sudbury mining camp, Ontario*, Goodfellow, W.D., ed., Mineral Deposits of Canada: A Synthesis of Major Deposit-Types, District Metallogeny, the Evolution of Geological Provinces, and Exploration Methods: Geological Association of Canada, Mineral Deposits Division, Special Publication No. 5, p. 329-350.

Annersten H., Ericsson T., Filippidis A. (1982). *Cation ordering in Ni-Fe olivines,* American Mineralogist*,* 67, 1212-12171.

Barceloux D.G., Barceloux D. (1999). Nickel. Clinical toxicology, 37:2, 239-258.

Bril H., Zainoun K., Puziewicz J., Courtin-Nomade A., Vanaecker M., Bollinger J.C. (2008). *Secondary phases from the alteration of a pile of zinc-smelting slag as indicators of environmental conditions: An example from ŚWIĘTOCHŁOWICE, Upper Silesia, Poland.*

Burns P.C., Hawthorne F.C. (1996). *Static and Dynamic Jahn-Teller Effects in Cu^{2+} Oxysalt Minerals*, The Canadian Mineralogist, 34, 1089-1105.

Buznikov A. A., Payanskaya-Gvozdeva I. I., Jurkovskaya T. K., Andreeva, E. N. (1995). *Use of remote and ground methods to assess the impacts of smelter emissions in the Kola peninsula*. Science of the Total Environment, 160/161, 285–293.

Connolly H. C., Hewins R. H. (1995). *Chondrules as products of dust collisions with totally molten droplets within a dust-rich nebular environment: An experimental investigation*. Geochim. Cosmochim., 59, 3231–3246.

Cornell, R. M., Schneider, W., & Giovanoli, R. (1992). *The effect of nickel on the conversion of amorphous iron(III) hydroxide into more crystalline iron oxides in alkaline media*. J. Chem. Tech. Biot., 53, 73–79.

Chan W.H., Lusis M.A., Vet R., and Skelton B.G. (1982) *Size distribution and emission rate measurements of particulates in the Inco 381 m chimney and iron ore recovery plant stack fumes*, 1979–80. Sudbury Environmental Study, Ontario Ministry of Environment. p.101.

Chopin E.I.B., Alloway B.J. (2007). *Trace element partitioning and soil particle characterisation around mining and smelting areas at Tharsis, Ríotinto and Huelva, SW Spain*, Science of the Total Environment. 373, 488-500.

D'Amore J.J., Al-Abed S.R., Scheckel K.G., Ryan J.A. (2005). *Methods for speciation of metals in soils: a review*, J. Environ. Qual., 8, 34:5, 1707-45.

Dudka S., Ponce-Hernandez R., Hutchinson T. C. (1995). *Current level of total element concentrations in the surface layer of Sudbury's soils*. Science of the Total Environment, 162, 161–171.

Eggleston C.M., Nidhi K., Lovelace D.M. (2006). *Cytochrome* c *interaction with hematite (α-Fe2O3) surfaces,* Journal of Electron Spectroscopy and Related Phenomena, 150, 220–227.

Eissa N. A., Sallam H. A., El-Ockr M. M., Mahmoud E. A., Saleh S. A. (1976). *Mossbauer Effect Study of Natural Egyptian Chalcopyrite,* Journal de Physique, 37, C6-793.

Ettler V., Johan Z., Kribek B., Sebek O., Mihaljevic M. (2009). *Mineralogy and environmental stability of slags from the Tsumeb smelter, Namibia,* Applied Geochemistry, 24, 1–15.

Ettler V., Johan Z., Baronnet A., Jankovsky F., Gilles C., Mihaljevic M., Sebek O., Strnad L., Bezdicka P. (2005). *Mineralogy of Air-Pollution-Control Residues from a Secondary Lead Smelter: Environmental Implications,* Environ. Sci. Technol., 39, 9309-9316.

Evans J.P., Mackey P.J., and Scott J.D. (1991). *Smelter gas cleaning. Impact of gas cooling techniques on smelter dust segregation*. In T.J.A. Smith and C.J. Newman (Eds.), Smelter process gas handling and treatment (p. 135-145). Metals and Materials Society, Warrendale.

Giuliani A., Kamenetsky V.S., Kendrick M.A., Phillips D., Goemann K. (2013). *Nickel-rich metasomatism of the lithospheric mantle by pre-kimberlitic alkali-S–Cl-rich C–O–H fluids*, Contributions to mineralogy and petrology, 165:1, 155-171.

Gregurek D., Reimann C., Stumpfl E. F. (1998). *Mineralogical fingerprints of industrial emissions—an example from Ni mining and smelting on the Kola Peninsula, NW Russia*, Science Total Environ. 221, 189–200.

Gregurek D., Melcher F., Pavlov V. A., Reimann C., Stumpfl E. F. (1999). *Mineralogy and mineral chemistry of snow filter residues in the vicinity of the nickel–copper processing industry, Kola Peninsula, NW Russia*. Mineralogy and Petrology, 65, 87–111.

Hawley J.E., Nichol I. (1959). *Selenium in some Canadian sulphides*. Econ Geol,54, 608-628.

Huminicki D.M.C., Rimstidt J.D. (2009). *Iron oxyhydroxide of pyrite for acid mine drainage control,* Applied Geochemistry, 24, 1626-1634.

Hutchinson T. C., Whitby L. M. (1974). *Heavy-metal pollution in the Sudbury mining and smelting region of Canada, I. Soil and vegetation contamination by nickel, copper, and other metals*, Environmental Conservation. 1, 123–131

Johnson D., Hale B. (2004). *White birch (Petula papyrifera Marshall) foliar litter decomposition in relation to trace element atmospheric inputs at metal-contaminated and uncontaminated sites near Sudbury, Ontario and Rouyn Noranda, Quebec, Canada*. Environmental Pollution, 127, 65–72.

Kliza, D. A., Telmer, K. T., Bonham-Carter, G. F., Hall, G. E. M. (2000). *Geochemistry of snow from the Rouyn-Noranda region of western Quebec: An environmental database*. Open File, 3869.

Knight R. D., Henderson P. J. (2006). *Smelter dust in humus around Rouyn-Noranda, Quebec,* Geochem. Exploit. Environ. Analys. 6, 203–214.

Knight R.D., and Henderson P.J. (2005) *Characterization of smelter dust from the mineral fraction of humus collected around Rouyn-Noranda, Quebec*. In G. Bonham-Carter (Ed.) Metals in the environment around smelters at Rouyn-Noranda, Quebec, and Belledune, New Brunswick: Results and conclusions of the GSC-MITE Point Sources Project. Bulletin, 584. Geological Survey of Canada.

Lanteigne S., Schindler M., McDonald A.M., Skeries K., Abdu Y., Mantha M., Murayama M., Hawthorne F.C., Hochella M.F.Jr. (2012). *Mineralogy and Weathering of Smelter-Derived Spherical Particles in Soils: Implications for the Mobility of Ni and Cu in the Surficial Environment*. Journal of Water, Air and Soil Pollution, 223:7, 3619-3641.

Lastra-Quintero R. (1998). *Characterization and separation of a copper smelter dust residue*. Can. Metallurg. Quarterly, 26, 85–90.

Le Roux V., Lee C-T.A., Turner S.J. (2010). *Zn/Fe systematics in mafic and ultramafic systems: Implications for detecting major element heterogeneities in the Earth's mantle*, Geochimica and Cosmogeochimica Acta, 74, 2779–2796.

Lu Z., Muir D. M. (1987). *Dissolution of metal ferrites and iron oxides by HCl under oxidizing and reducing conditions*, Hydrometallurgy, 21, 9–21.

Manceau A., Boisset M-C., Sarret G., Hazemann J-L., Mench M., Cambier P., Prost R. (1996). *Direct Determination of Lead Speciation in Contaminated Soils by EXAFS Spectroscopy*, Environ. Sci. Technol, 30, 1540-1552.

Mantha N. M., Schindler M., Murayama M., Hochella M. F.Jr. (2012) Silica- and sulfate-bearing rock coatings in smelter areas: Products of chemical weathering and atmospheric pollution I. Formation and mineralogical composition. Geochim. Cosmochim. Acta. doi:doi:10.1016/j.gca.2012.01.033

Mantha N.M., Schindler M.,Kyser T.K. (2012b) *Silica- and sulfate-bearing rock coatings insmelter areas: Part II. Forensic tools for atmospheric metal(loid)- and sulfur-isotope compositions*, Geochimica et Cosmochimica Acta, 90:1, 221‑241.

McLean J.E., Bledsoe B.E. (1992). *Behaviour of Metals in Soils*, Groundwater Issue, United States Environmental Protection Agency, EPA/540/S-92/018.

Mironova-Ulmane N., Kuzmin A., Steins I., Grabis J., Sildos I., Pärs M. (2007). *Raman scattering in nano-sized nickel oxide NiO, Functional Materials and Nanotechnologies*, Journal of Physics: Conference Series, 93, 012039.

Nachtegaal M., Marcus M.A., Sonke J.E., Vangronsveld J., Livi K.J.T., VanDerLelie D., Sparks D.L. (2005). *Effects of* in situ *remediation on the speciation and bioavailability of zinc in a smelter contaminated soil*, Geochimica and Cosmogeochimica Acta, 69:19, 4649-4664.

Nei L., Kruusma J., Ivask M., Kuu A. (2009). *Novel Approaches to Bioindication of Heavy Metals in Soils Contaminated by Oil Shale Wastes*, Oil Shale, 26:3, pp. 424–431.

Niskavaara H., Reiman C., Chekushin V. (1996). *Distribution and pathways of heavy metals and sulphur in the vicinity of the copper-nickel smelters in Nikel and Zapoljarnij, Kola Peninsula, Russia, as revealed by different sample media*, Applied Geochemistry, 11, 25–34.

Nriagu, J.O., & Pacnya, J.M. (1988). *Quantitative Assessment of Worldwide Contamination of Air, Water and Soils by Trace Metals,* Nature. 338, 47-49.

Panfili F., Manceau A., Sarret G., Spadini L., Kirpichtchikova T., Bert V., Laboudigue A., Marcus M.A., Ahamdach N., Libert M-F. (2005). *The effect of phytostabilization on Zn speciation in a dredged contaminated sediment using scanning electron microscopy, X-ray fluorescence, EXAFS spectroscopy, and principal components analysis,* Geochimica and Cosmogeochimica Acta, 69:9, 2265-2284.

Piatak N. M., Seal, R. R. (2010). *Mineralogy and the release of trace elements from slag from the Hegeler Zinc smelter, Illinois (USA)*. Applied Geochemistry, 25, 302–320.

Pengfu T., Chuanfu Z. (1997). *Thermodynamic Analysis of Nickel Smelting Process*, J. Cent. South Univ. Technol. 4, 2.

Potvin R., Negusanti J. (1995). Declining Industrial Emissions, Improving Air Quality, and Reduced Damage to Vegetation, In: Gunn (1995), pp. 51-65.

Putnis A. (2009). *Mineral Replacement Reactions,* Reviews in Mineralogy and Geochemistry, 70, 87-124.

Ratkin N. E., Asming V. E., Koshkin V. V. (2001). *Cartographic modelling of aerotechnogenic pollution in snow cover in the landscapes of the Kola Peninsula*, Chemosphere, 42, 1–8.

Samuelsson, C., Bjorkman, B. (1998). *Dust forming mechanisms in the gas cleaning system after the copper converting process. (I) Sampling and characterization*. Scand. J. Metallurg., 27, 54–63.

Sarkisyan L.E. (1986). *Mechanism and kinetics of reduction of complex oxides of the NiO, Fe_2O_3 system,* Soviet Powder Metallurgy and Metal Ceramics, 25:10, 832-837.

Seignez N., Gauthier A., Bulteel D., Buatier M., Recourt P., Damidot D., Potdevin J.L. (2007). *Effect of Pb-rich and Fe-rich entities during alteration of a partially vitrified metallurgical waste*. J. Hazard. Mater. 149, 418–431.

Selim H. M., Sparks D. L. (2001). *Heavy metals release in soils*. Boca Raton: Lewis.

Sidhu P. S., Gilkes R. J., Posner A. M. (1981). *Oxidation and ejection of nickel and zinc from natural and synthetic magnetites*. Soil Science Society of America Journal, 45, 641–644.

Sigg L., Stumm W. (1981). *The interaction of anions and weak acids with the hydrous goethite (a-FeOOH) surface*, Colloid Surf. 2, 101–117

Stumm W. (1992). Chemistry of the solid–water interface, New York: Wiley

Tang J., Myers M., Bosnick K.A., Brus L.E. (2003). *Magnetite Fe3O4 Nanocrystals: Spectroscopic Observation of Aqueous Oxidation Kinetics*, J. Phys. Chem., 107, 7501-7506.

Tesfaye F., Taskinen P. (2011). *Phase Equilibria and thermodynamics of the System Zn-As-Cu-Pb-S at Temperatures Below 1173 K*, School of Chemcial Technology, Science and Technology 7/2011.

Wallace C.M., Thompson A. (1993). *Sudbury: Rail town to Regional Capital,* Dundurn Press, Toronto.

Weber O., Scholz R. W., Bühlmann R., Grasmück D. (2001). *Risk Perception of Heavy Metal Soil Contamination and Attitudes toward Decontamination Strategies*. Risk Analysis, 21: 967.

Wells A.F. (1984). *Structural Inorganic Chemistry*, 5th ed., Oxford University Press, Oxford, UK.

Whitby, L. M., Stokes, P. M., Hutchinson, T. C., & Myslik, G. (1976). *Ecological consequence of acidic and heavy-metal discharges from the Sudbury smelters*, The Canadian Mineralogist. 14, 47–57.

Williamson, B.J., Har, N., Purvis, W.O., & Rusu, A.M. (2003). *Preliminary Studies of Airborne Particulate Emissions from the Ampellum S.A Copper Smelter, Zlatna, Romania*, Studia UBB, Geologia. 48:1, 67-76.

Wren, C. (2012*). Risk assessment and environmental management: A case study in Sudbury, Ontario, Canada,* Progress in Environmental Science, Technology and Management. 1, 1–450.

Table 1. Average metal(loid) compositions (ppm) of spherical particulate matter, angular sulfides and associated secondary phases.

	Angular sulfides			Spherical particulates				
	coatings	**Chalco-pyrite**	**Pent-landite**	**Sulfide inclusions**	**Sulfate inclusions**	**Metal-rich rim**	**Hematite rim**	**Matrix**
n	6	6	3	12	5	9	9	21
Ni	2671	320	339402	274982	35860	125712	10294	54532
Cu	33922	216748	139	226690	32	23084	2453	37919
Cr	98	32	6	11	7^{E+02}	173	30	526
Mn	33	10	3	102	3^{E+05}	622	373	298
Co	44	5	7314	2881	4246	1904	412	1905
Zn	301	353	3	224	0.08252	837	188	138
As	2528	995	3	6678	44.5	157	354	97
Se	667	328	39	1066	121.2	4	24	16
Cd	28	16	b.d	1	0.162	6	b.d	1
Pb	687	168	2	155	57.34	650	144	77
Hg	N/A	N/A	N/A	N/A	1052	N/A	N/A	N/A

n = number of analyses

Table 2. Average metal(loid) compositions (ppm) of NiO particulates and associated secondary phases.

	Ni oxide matrix	Inner Fe coating	Al-SiO_x layer	Outer Fe coating
n	2	2	1	1
Ni	629877	289661	118718	28514
Cu	5600	6447	5721	10600
Cr	50	82	96	183
Mn	63	125	63	75
Co	3268	1532	429	236
Zn	43	107	85	112
As	273	1033	1162	1743
Se	31	131	123	274
Cd	b.d	1	1	1
Pb	47	83	205	1474

n = number of analyses

6.0 FIGURE CAPTIONS

Figure 1. Map showing for the Sudbury area demonstrating the location of the Copper Cliff smelting centre and the sampled sites.

Figure 2. SEM backscattering image (a) of a sulfide-bearing smelter-derived particulate showing the location of a laser ablation line scan (A-B), corresponding element distribution map for S (b) and laser-ablation line scan showing metal(loid) distribution the matrix, core and rim of the particulate (c).

Figure 3. SEM backscattering image (a) and laser ablation ICP-MS element maps (b-j) showing element distributions for metal(loid)s in a sulphide-bearing smelter-derived particle.

Figure 4. a,b) Optical and SEM backscatter images of a silicate/oxide particle showing the location of a laser ablation line scan (A-B) and c) laser-ablation line scans through the silicate/oxide particle showing the enrichment of Pb and As in the particle rim.

Figure 5. SEM backscattered image of an sulfide-bearing smelter-derived particle (a) showing the location of a laser ablation line scan (A-B), with corresponding element distribution maps for Fe (red), S (green), and Ni (blue), and a laser-ablation line scan showing metal(loid) distribution in the sulfide core (1), the oxide silicate matrix, and the secondary Ni rim (2).

Figure 6. Optical images of a sulfur-bearing smelter-derived particulate with a hematized rim (a,b) and laser ablation element distribution maps for Co, Pb, S, K, Hg, Ni, Cu and As (c). Shown are 1- a sulfate inclusion before ablation, 2- a hematite rim, and 3- a sulfide inclusion after ablation.

Figure 7. SEM backscattered image of an angular chalcopyrite particulate (a) showing the location of a laser ablation line scan (A-B), with corresponding element distribution maps for Cu (red), Al (green), and Si (blue), and a laser-ablation line scan showing metal(loid) distribution in the sulfide and it's alteration layers (c).

Figure 8. SEM backscattered image of a NiO particle (a) showing the location of a laser ablation line scan (A-B) with corresponding element distribution maps for Ni (b) and Fe (c), and laser-ablation line scan (d) showing the distribution of metal(loid)s within the NiO matrix as well as in the Pb+Fe rim.

Figure 9. Raman spectra of a Ni-rich particulate from the Sudbury soils (grey) and a NiO standard (black). Peaks are attributable to 1 phonon (1P), 2 phonon (2P) and 2 magnon (2M) scattering (Mironova-Ulmane et al, 2007).

Figure 10. SEM backscattering image of a NiO particle coated with an agglomerate (a) showing the location of a laser ablation line scan (A-B) , with corresponding element distribution maps for Fe (red) and Ni (green)(b), and laser-ablation line scan (c) showing the trace element distribution within the chemically different zones.

Figure 11. SEM backscattered image (a) of a smelter-derived particle with a metal-rich rim and corresponding element distribution maps for Fe, Si, Ni and Cu (b-e) respectively.

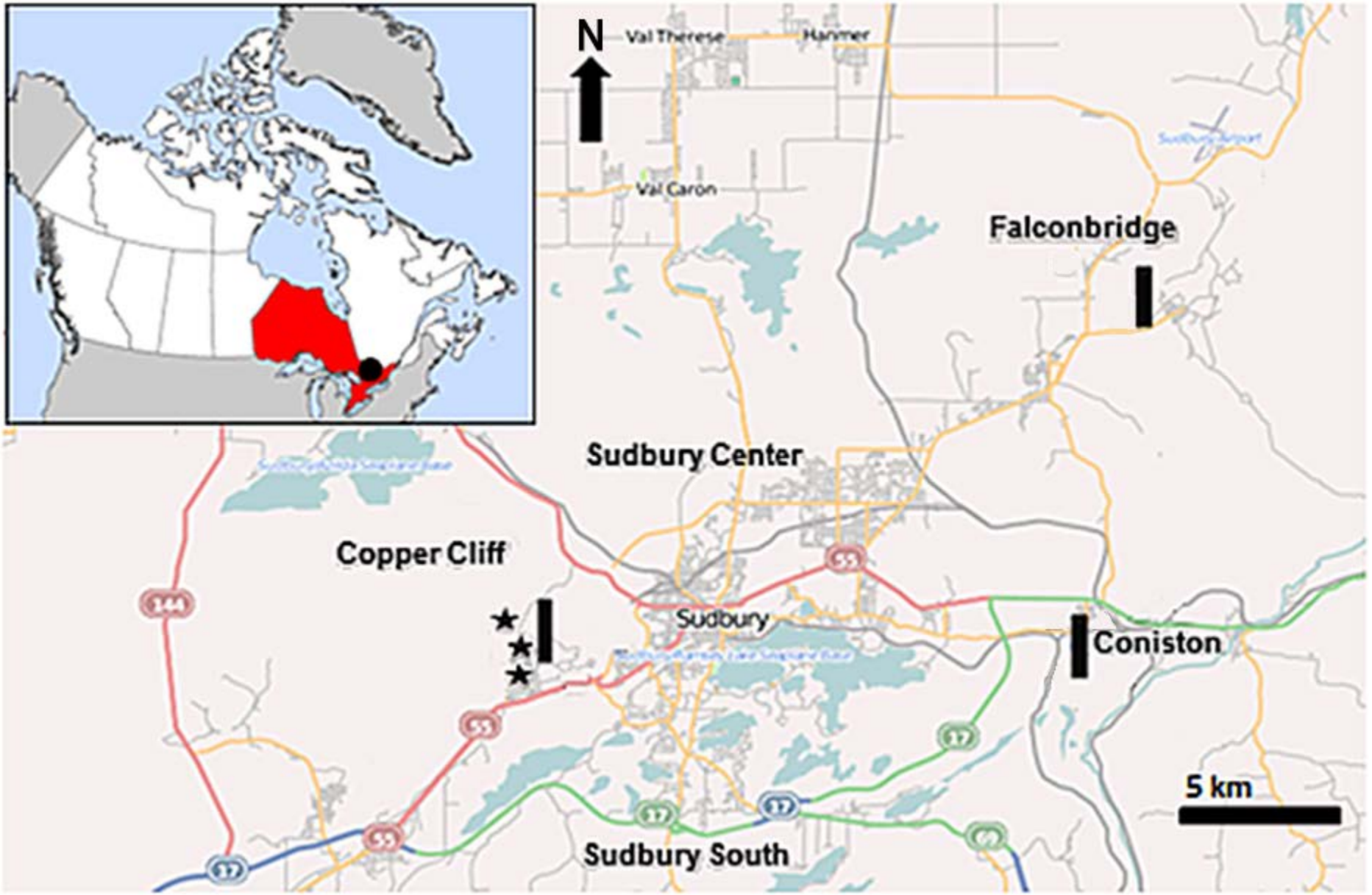
N
Val Therese
Hanmer
Val Caron
Falconbridge
Sudbury Center
Copper Cliff
Sudbury
Coniston
5 km
Sudbury South

Figure 1.

a)

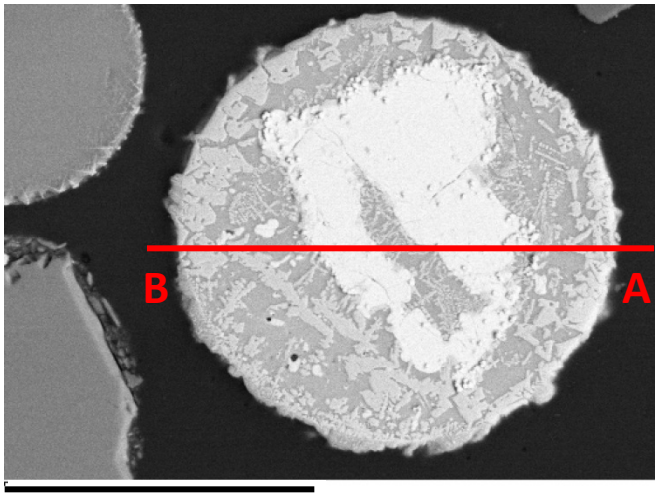

100µm

c)

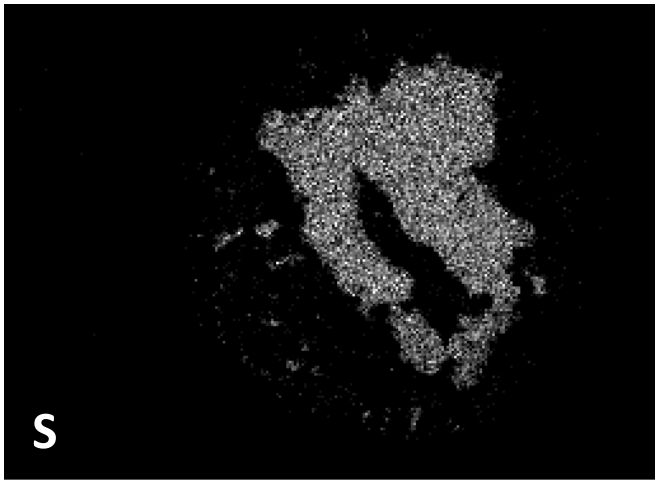

100µm

Figure 2.

c)

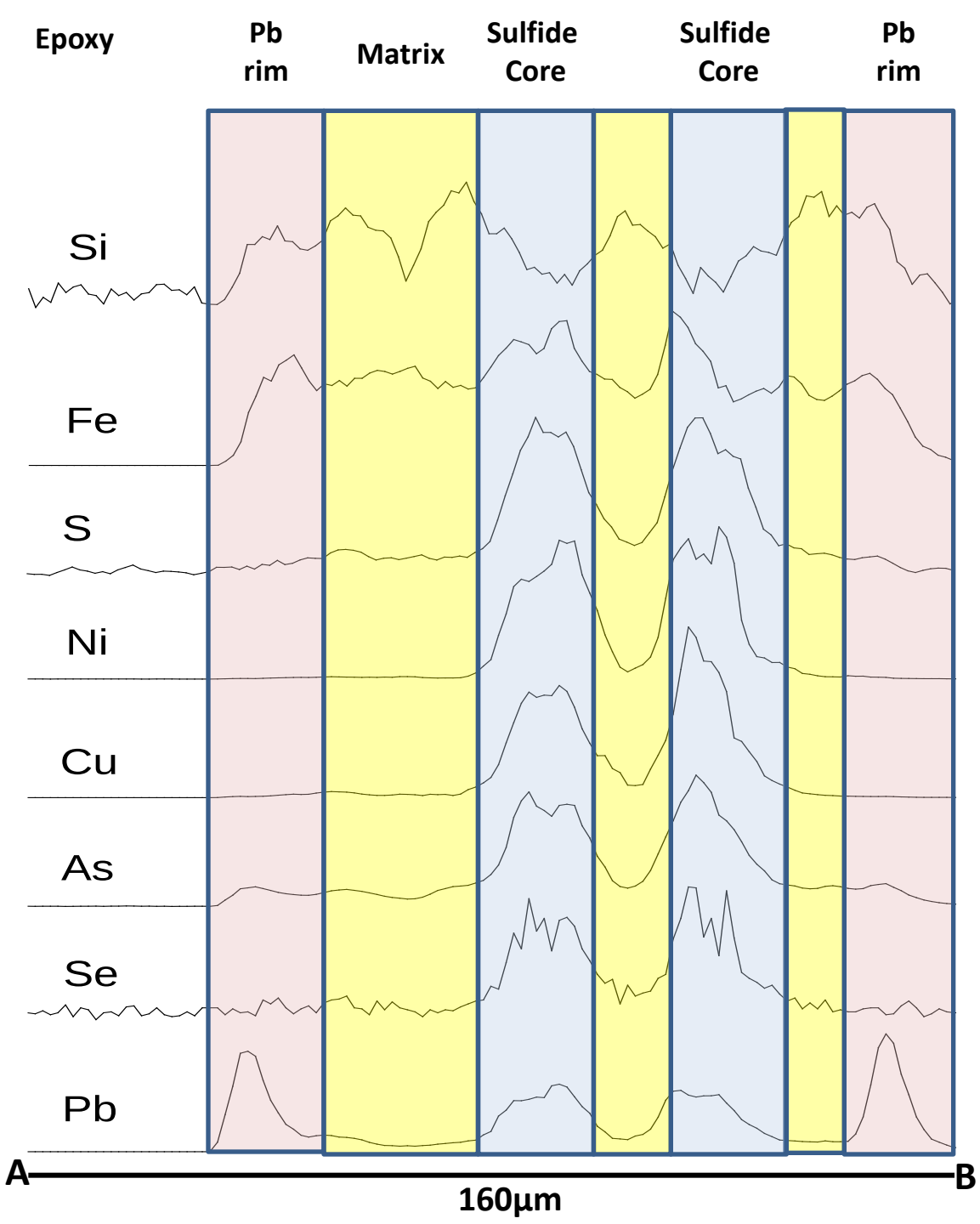

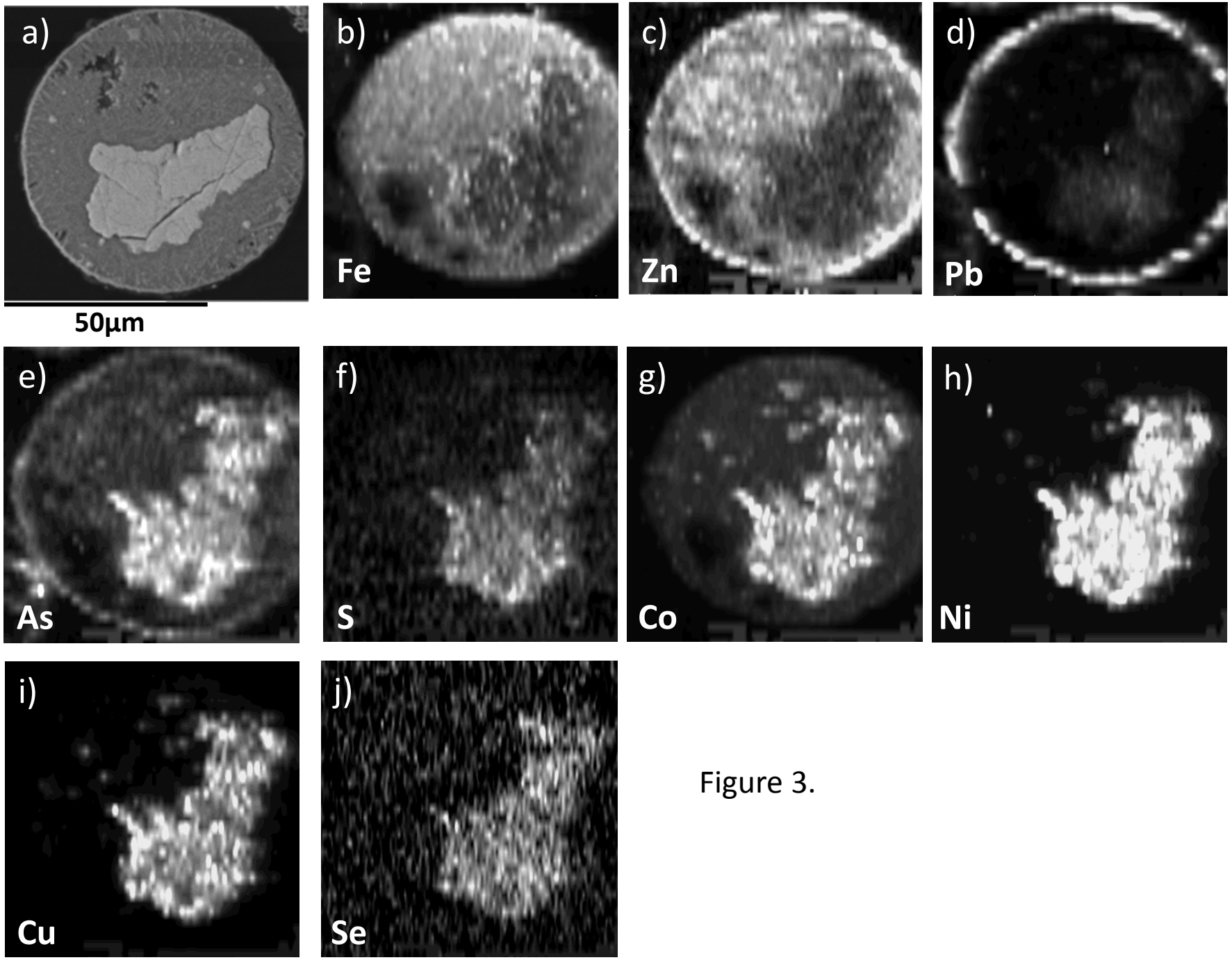

Figure 3.

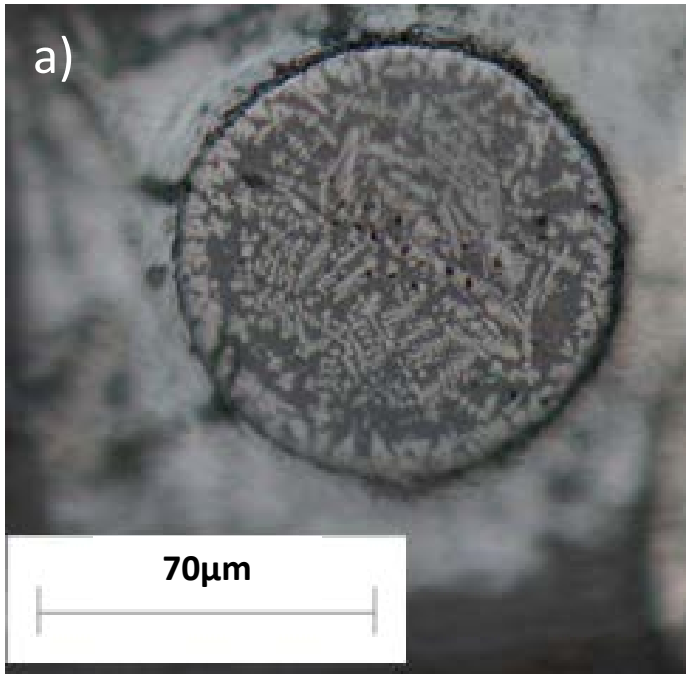
a)
70µm

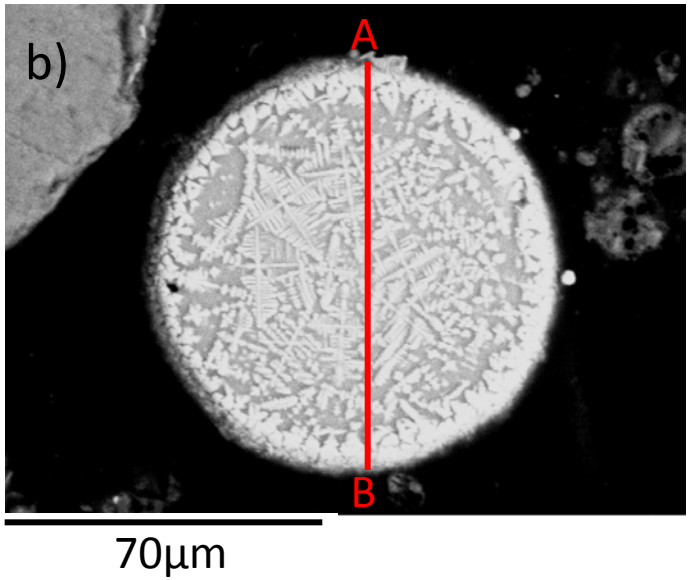
b)
A
B
70µm

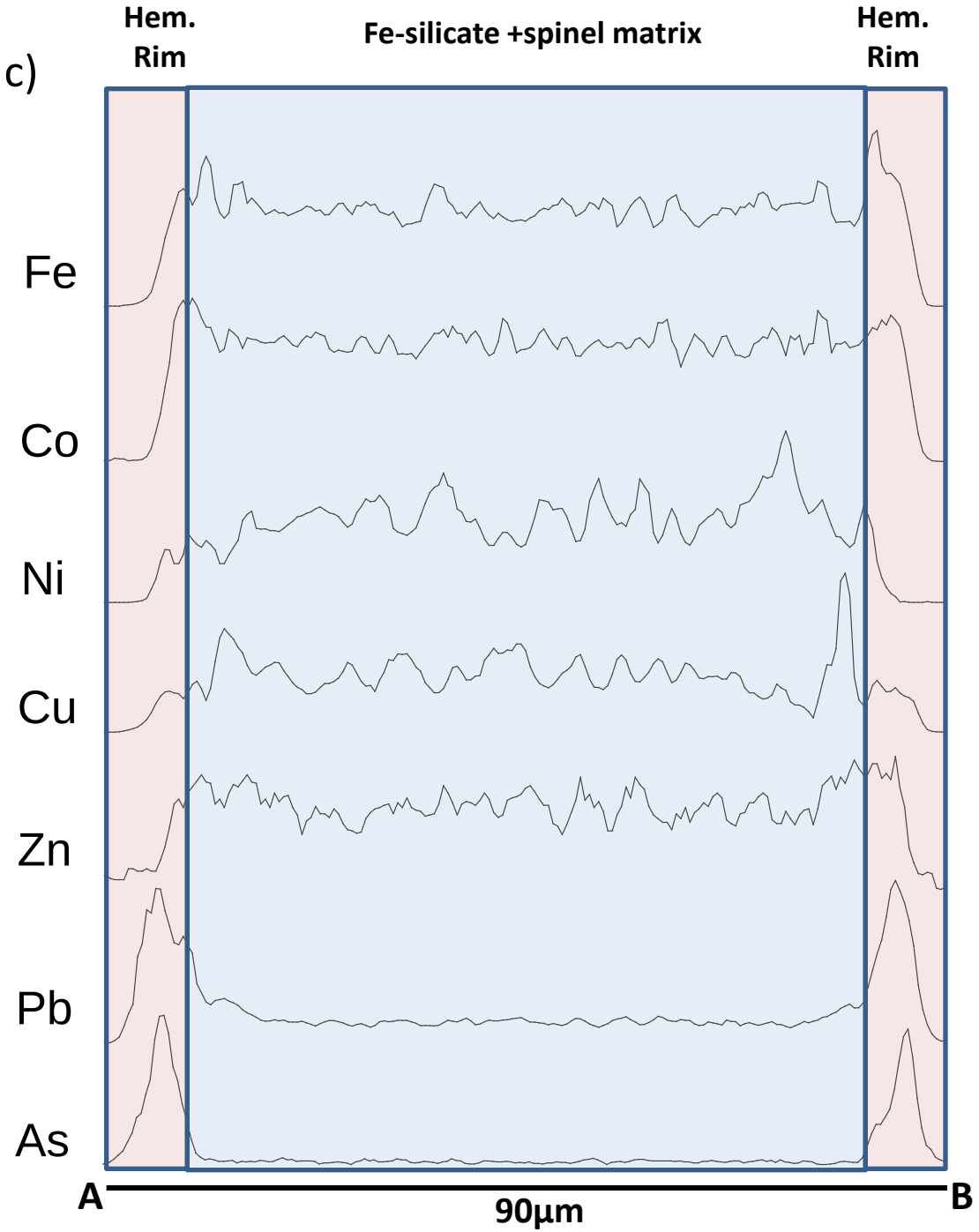
c)
Hem. Rim
Fe-silicate +spinel matrix
Hem. Rim
Fe
Co
Ni
Cu
Zn
Pb
As
A
B
90µm

Figure 4.

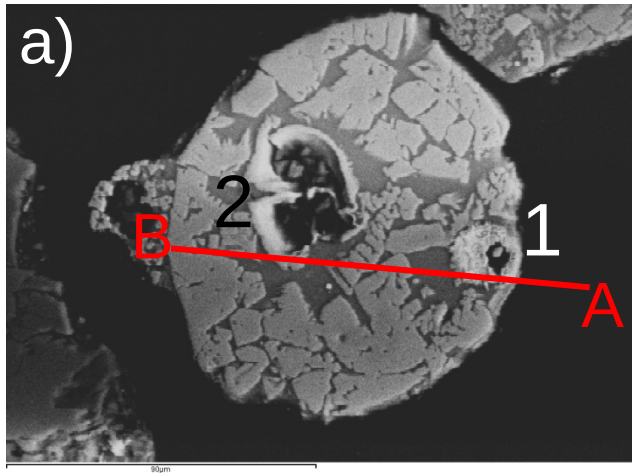
a)
2
1
B
A

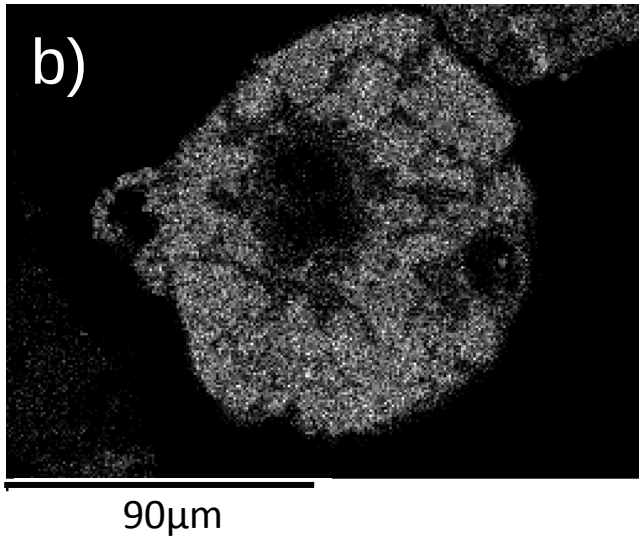
b)
90µm

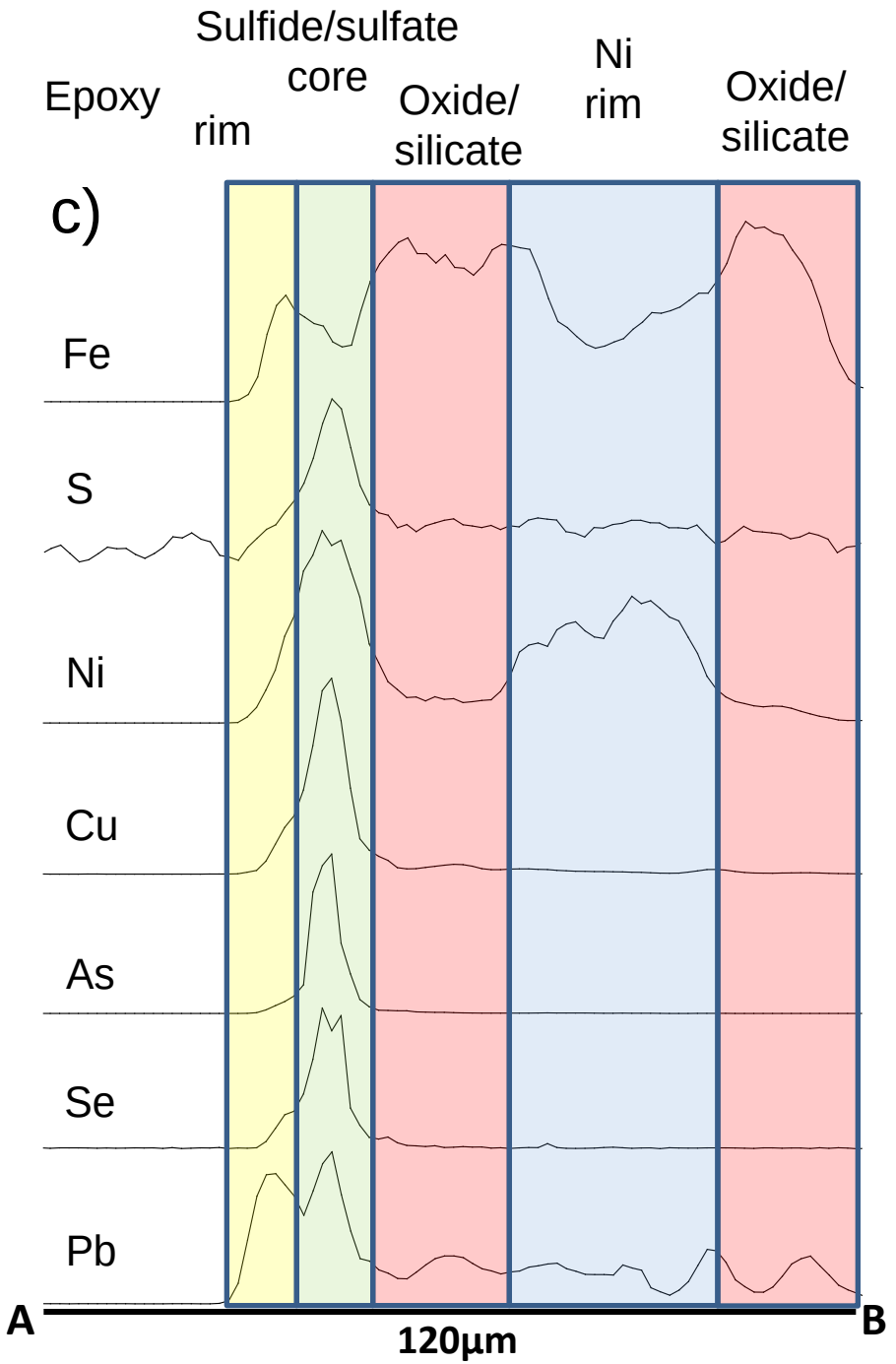
Epoxy
Sulfide/sulfate rim
core
Oxide/ silicate
Ni rim
Oxide/ silicate
c)
Fe
S
Ni
Cu
As
Se
Pb
A
B
120µm

Figure 5.

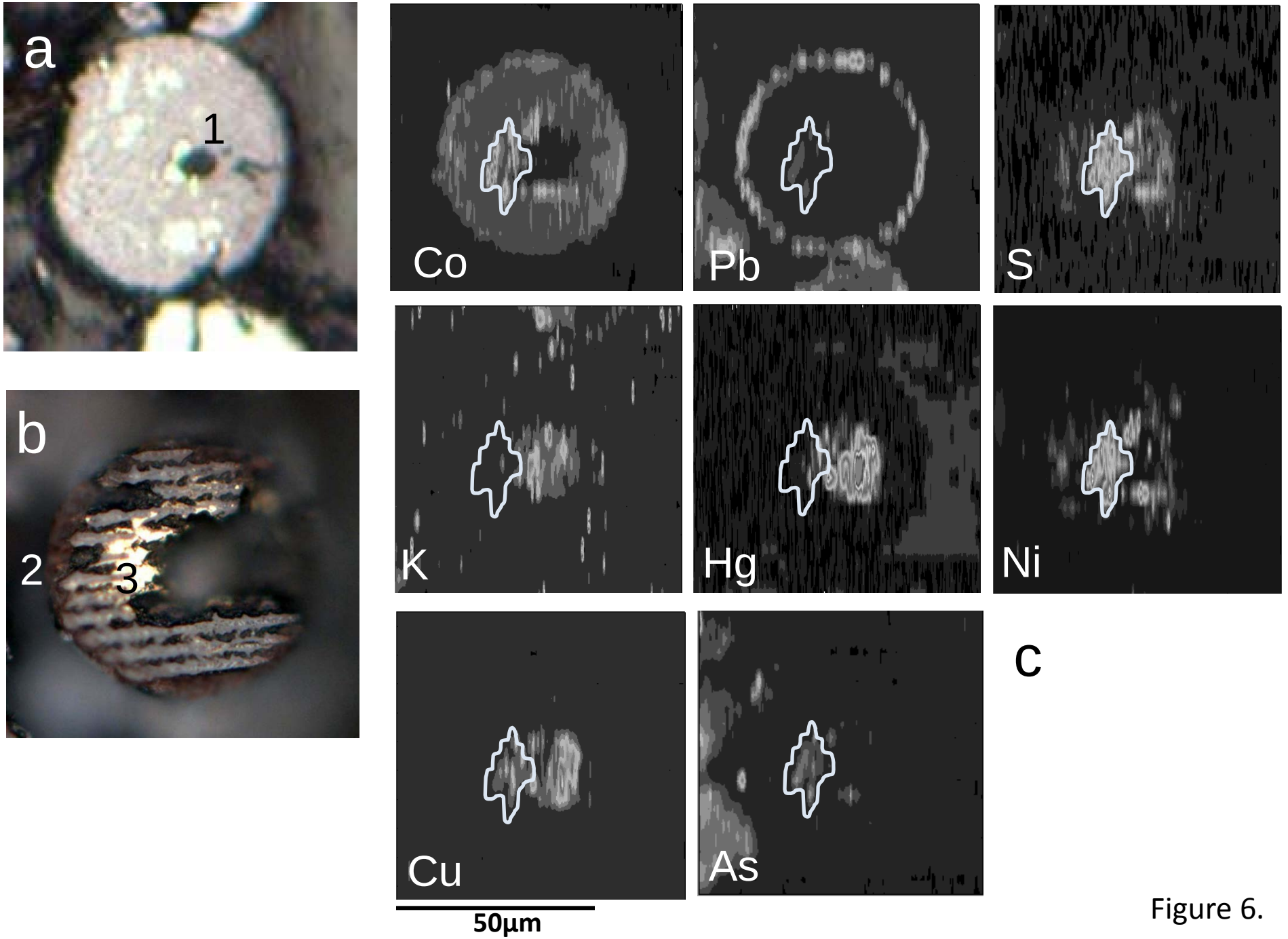

Figure 6.

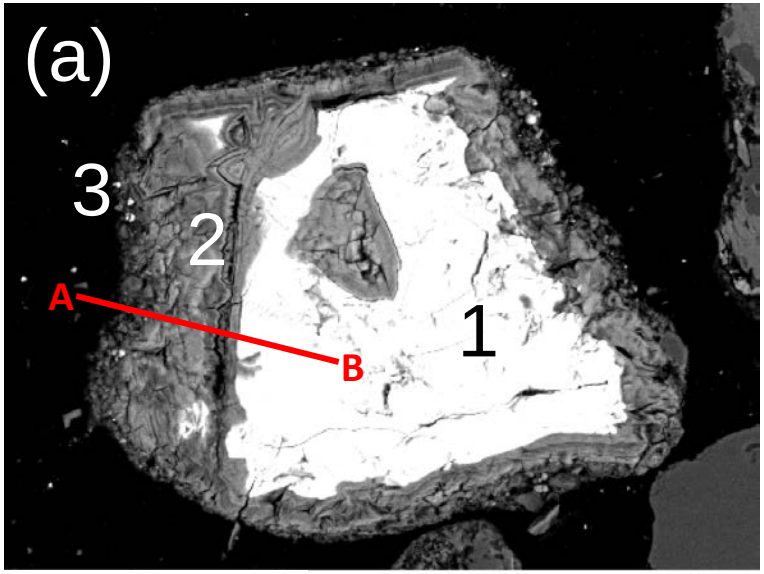
(a)
3
2
1
A
B
100µm

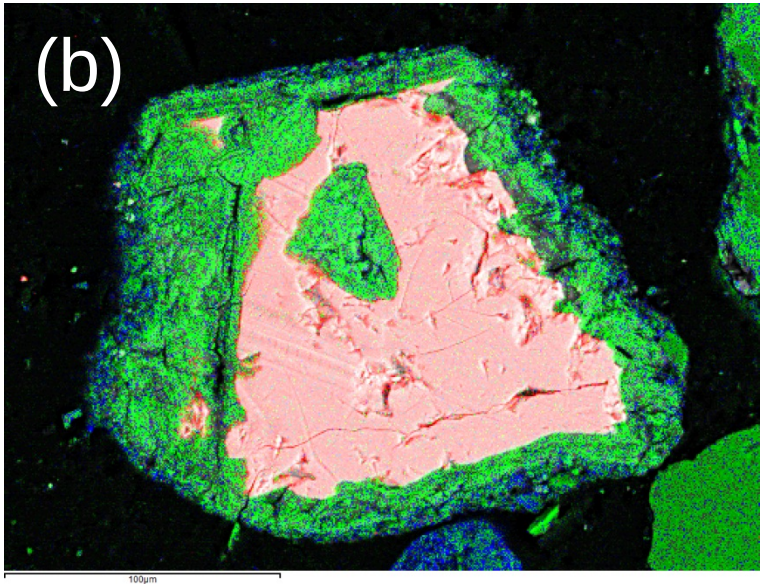
(b)

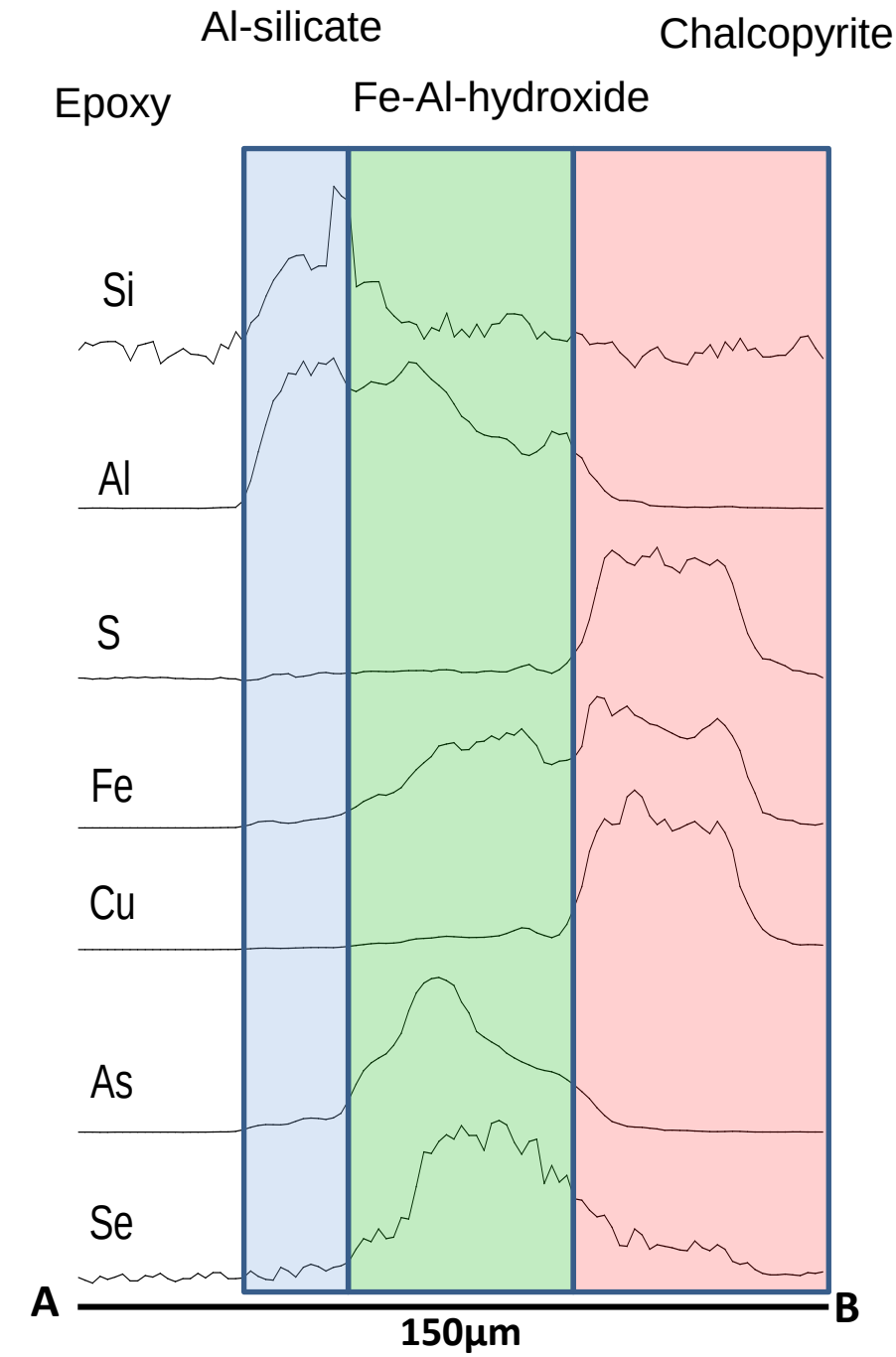
(c)
Al-silicate
Chalcopyrite
Epoxy
Fe-Al-hydroxide
Si
Al
S
Fe
Cu
As
Se
A
B
150µm

Figure 7

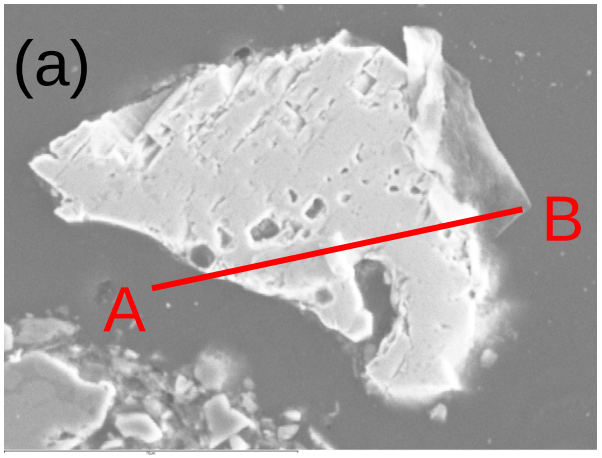

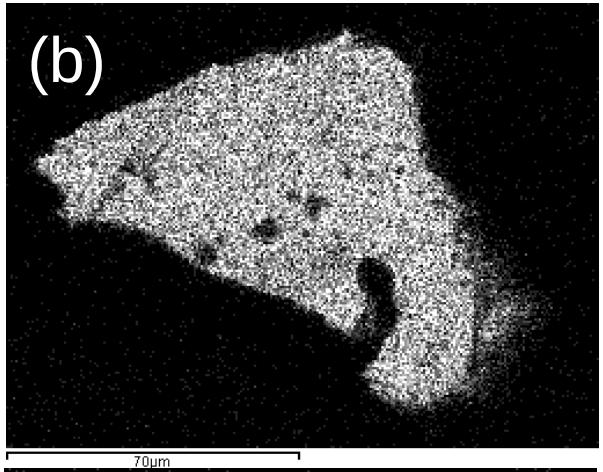

Ni

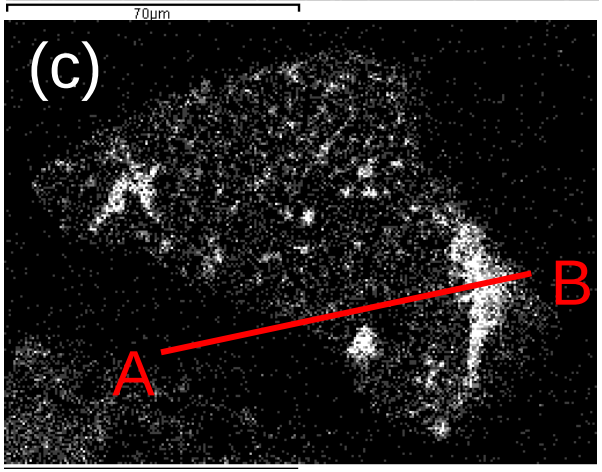

Fe

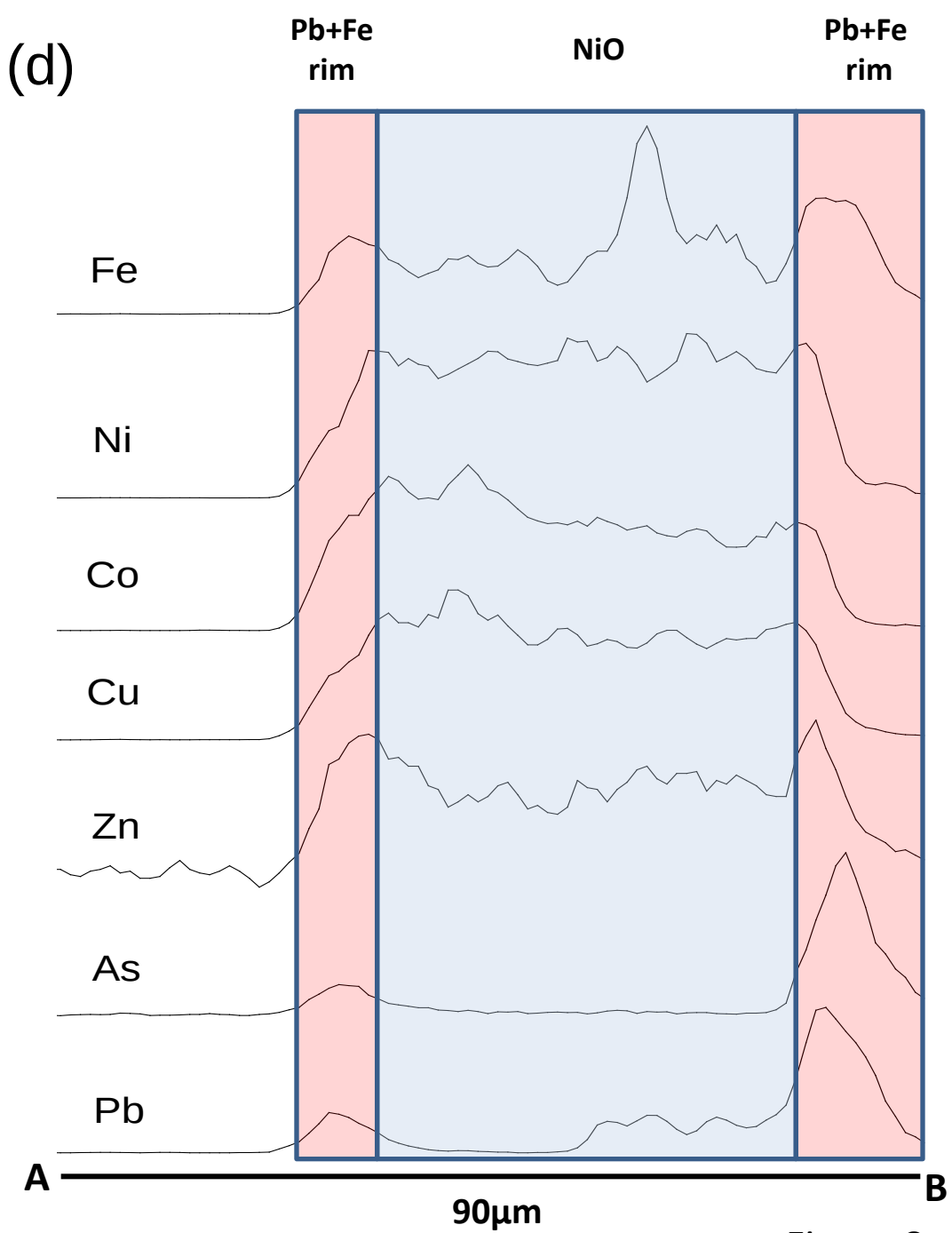

Figure 8.

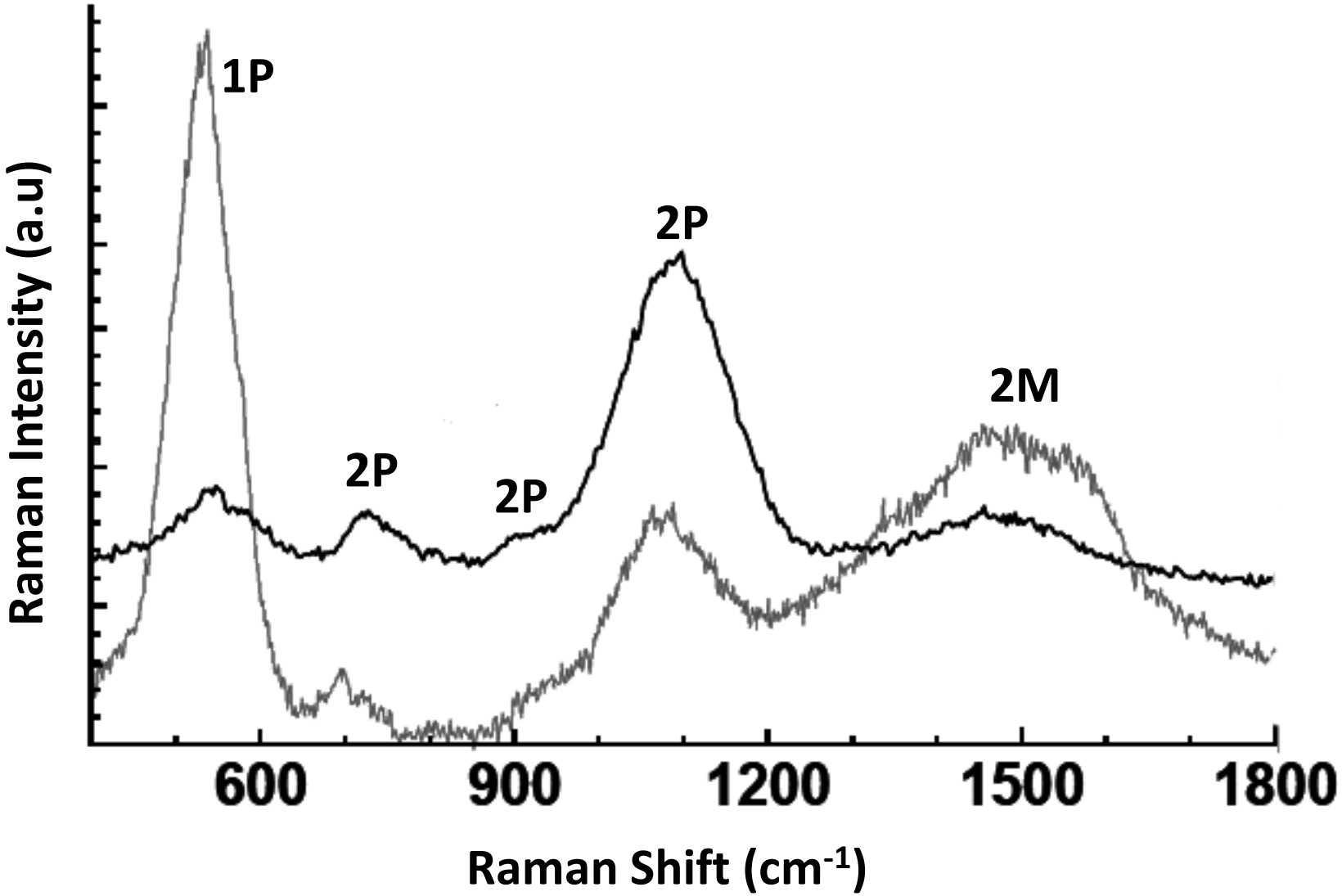
1P
2P
2P
2P
2M
Raman Intensity (a.u)
600
900
1200
1500
1800
Raman Shift (cm-1)
NiO standard
Ni-rich particulate

Figure 9.

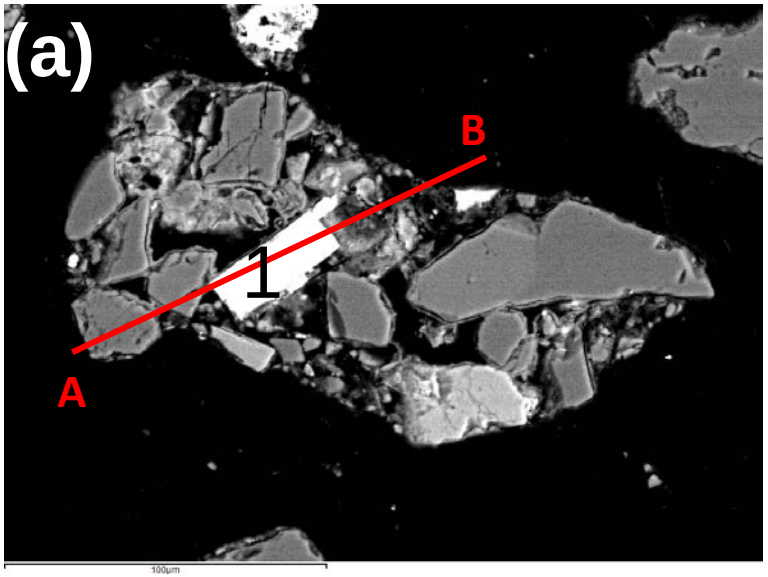
(a)
B
1
A

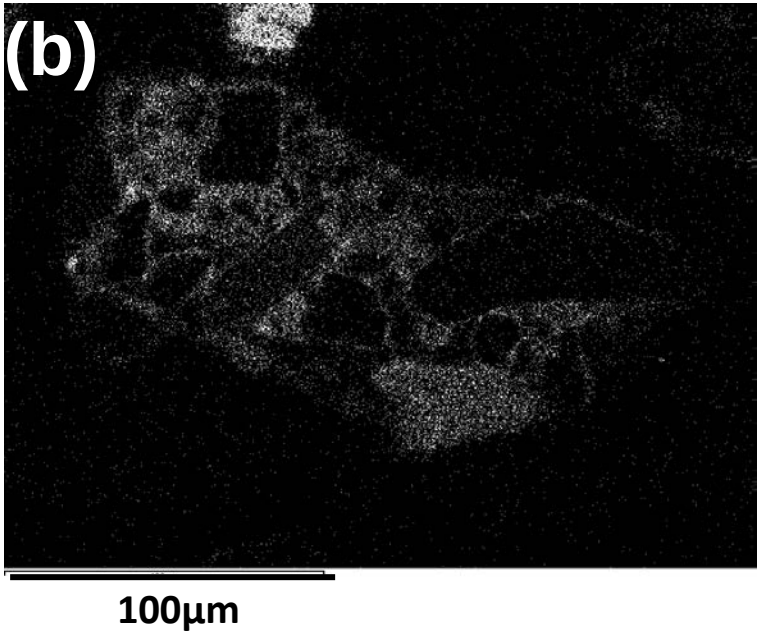
(b)
100µm

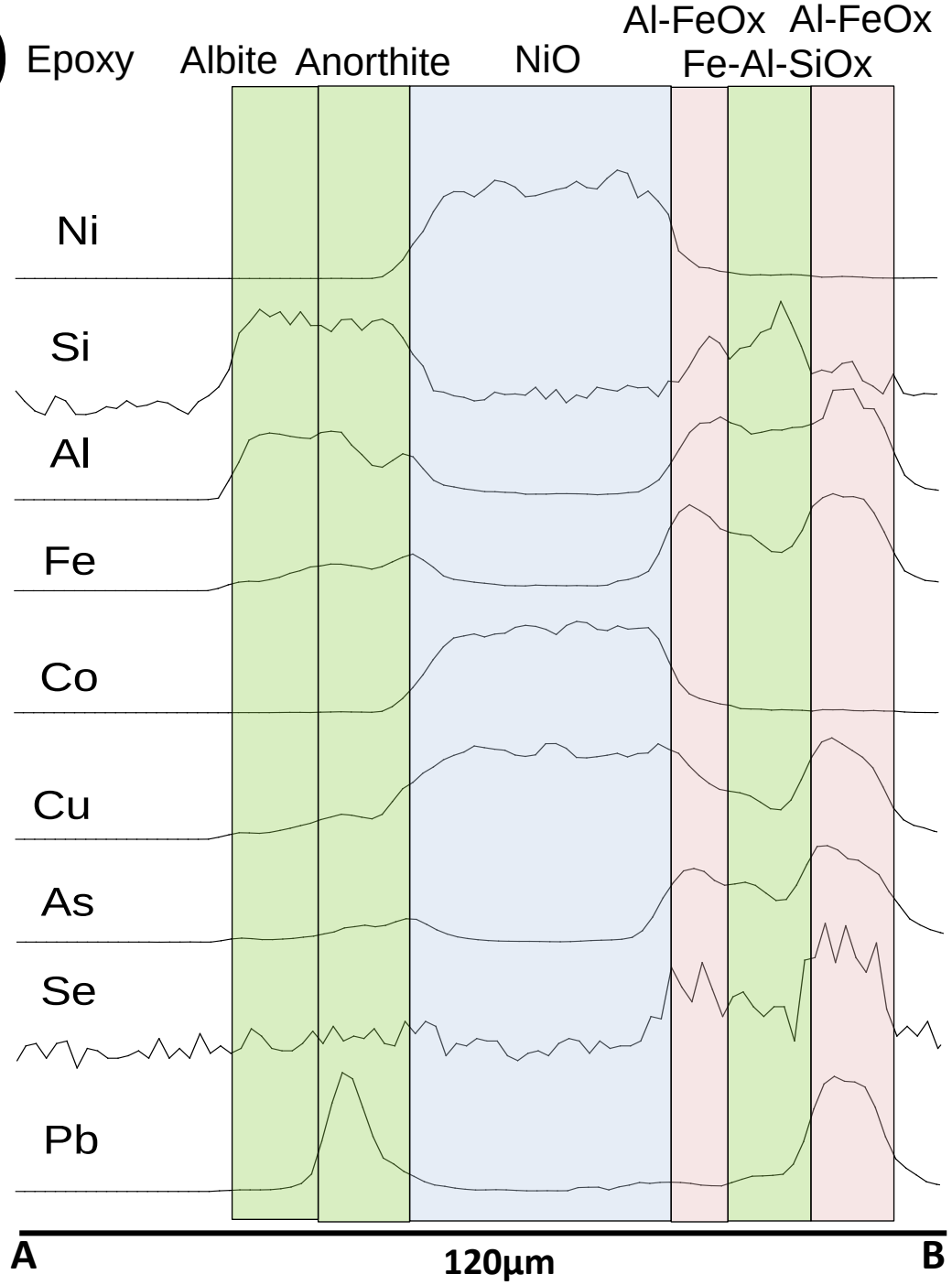
(c)
Epoxy
Albite
Anorthite
NiO
Al-FeOx
Fe-Al-SiOx
Al-FeOx
Ni
Si
Al
Fe
Co
Cu
As
Se
Pb
A
120µm
B

Figure 10

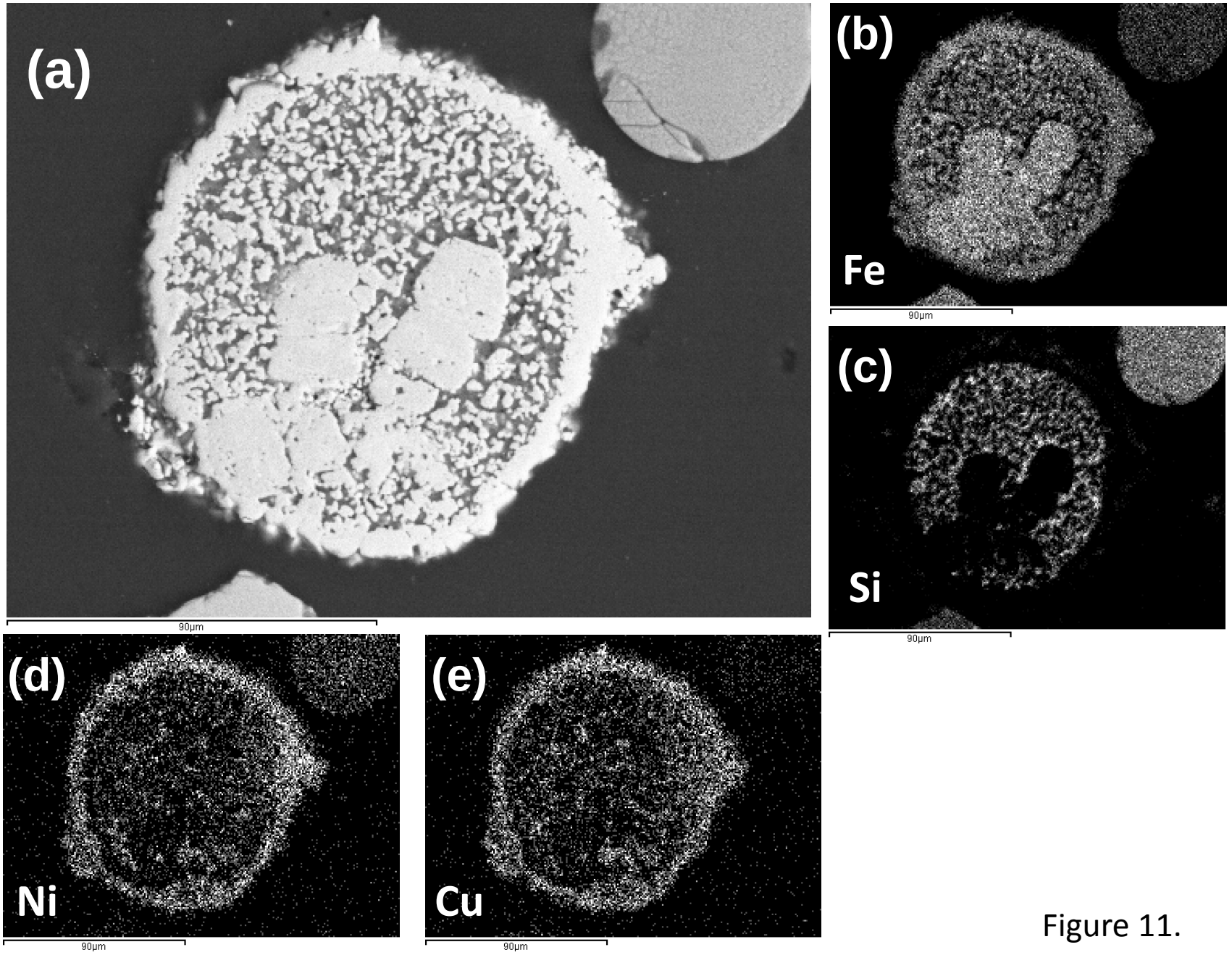

Figure 11.

Attenuation of metal(loid)s by mineral surface coatings in smelter-affected acid soils

Sonia Lanteigne[1], Michael Schindler*[1], Andrew McDonald[1], Frank C. Hawthorne[2]

1. Department of Earth Sciences, Laurentian University, Sudbury, ON, P3E 2C6 Canada.

2. Department of Geological Sciences, University of Manitoba, Winnipeg, MB, R3T 2M9, Canada

*corresponding author

ABSTRACT

The role of mineral surfaces in contaminated acid soils is of critical importance as they influence transport, retention and chemical transformation of metal(loid)s that in turn can directly affect soil and water quality. In order to assess the interaction of mineral surfaces with metal(loid)s in acid soils, samples to a depth of 5 cm were collected from areas around three major smelting centers in the Greater Sudbury area, Ontario, Canada. Nano- to micrometer thick coatings on soil grains were characterized using a combination of scanning electron microscopy, micro-Raman spectroscopy, laser ablation inductively-coupled plasma mass spectroscopy, micro-X-ray fluorescence, and X-ray photoelectron spectroscopy. Many of the minerals (predominantly feldspars and quartz) are coated with Al-rich nanometer-thick layers which can contain elevated concentrations of Cu and S (wt%). Micrometer-thick coatings are predominantly composed of hematite, schwertmannite, ferrihydrite and (amorphous) silica and contain elevated metal(loid) concentrations in the form of metal(loid)-rich sulfate- and phosphate minerals (mainly minerals of the jarosite group). A general model is developed that describes the formation of mineral coatings in acid soils and their important role in the uptake and retention of metal(loids). Here, micrometer-thick Fe-silica coatings form through adsorption, co-precipitation and dehydration processes involving amorphous silica and Fe-hydroxides. Metal(loid)-bearing phases nucleate within a gel-type matrix and are subsequently preserved during dehydration and solidification. Once the pH has been raised sufficiently high (pH~5-6), Al-species start to polymerize on mineral surfaces forming aluminosilicate precursors of clays. The implications of this model are widespread in terms of the attenuation of metal(loid)s in acid soils and their retention or subsequent remobilization in recovered soils with near neutral pH.

1.0 INTRODUCTION

Soil is a vital component in our lives, and with a rapidly increasing global population, shortages of good soil are becoming a reality. Acidified soils (<5.5) are detrimental to crop production and can be found throughout the world, with 30-40% of arable soils having a pH of less than 5.5

(Samac and Tesfaye, 2003). In addition, as pH drops, aluminum (Al) can also be solubilized causing a rise in phytoxic Al ions is the soil solution (Samac and Tesfaye, 2003). Although this free Al can buffer the acidity to a certain extent, it is severely detrimental to plant growth (Samac and Tesfaye, 2003). Acid soils can occur naturally from parent material enriched in silica and depleted in carbonates or alkaline-earth bearing minerals (Samac and Tesfaye, 2003), or they can occur as a result of anthropogenic activities that generate acidic precipitation and contamination. The latter type of acidification occurred and continues to occur in countless localities worldwide such as in southern Italy (Terzano et al, 2007), south-western Spain (Chopin and Alloway, 2007), the Kola Peninsula in Russia (Gregurek et al, 1999;1998), Zlatna, Romania (Williamson et al, 2003), and many locations in the United States of America including Colorado and Montana (Burt et al, 2011; Burt et al, 2003). With the extent of acid soils continuously increasing world-wide, it has become critically important to understand how inorganic and organic pollutants are interacting with the biotic (e.g. plants, bacteria) and abiotic (e.g. pore water, mineral surfaces) components in these acidic environments. Increased emission of metal(loid)s into the atmosphere from industrial processes often results in the severe contamination of the surrounding area (Freedman and Hutchinson, 1980). Metal(loid) contamination is a global concern (Nriagu and Pacnya, 1988), however local examples, such as that of Sudbury, Ontario, clearly show the significant negative effects of major emission sources on the environment (Meadows and Watmough, 2012). Studies on the distribution and mobility of metal(loid)s in soils most often utilized bulk chemical analyses (Wren, 2012; Shaikh, 2006), acid digestions and sequential extractions (Adamo et al, 1996; Ashraf et al, 2012; Dube et al, 2001;Ma and Kao, 1997; Yahaya et al, 2010). Mobility, adsorption and speciation of metal(loids) in acid soils have been studied in laboratory-based environments by doping soils or major components of soils with contaminants (e.g. Al-Hamden and Reddy, 2008; Barabash et al, 2011). These greatly simplify an otherwise complex system in which dissolution-precipitation, co-precipitation and adsorption processes can occur simultaneously (Alloway, 1990). In

comparison, relatively few studies attempted to characterize metal(loid)-bearing phases in soils and sediments using analyses via highly detailed techniques, owing to the nature of the fine grained particles involved. An example of where such studies have been undertaken include that of Motelica-Heino et al. (2001) who identified with LA-ICP-MS Pd-, Pt- and Rh-bearing phases in urban road sediments affected by contamination from catalytic converters and vehicle exhaust. Terzano et al. (2007) applied a combination of μ-XRF, μ-XRD and bulk extraction methods to identify not only the hosts for Cr, Ni, Cu, Zn, Pb, and V in the contaminated soils of southern Italy but also the point sources for these contaminants. McNear et al. (2007) utilized μ-XRF in conjunction with EXAFS, electron microprobe analysis and stirred flow-dissolution experiments to determine the speciation of Ni in soils in the vicinity of a Ni-refinery in Port Colburne, Ontario. A study on the speciation of As in floodplain soils near Muldenstein, Germany with EXAFS and micro-XRF showed that As(V) is preferentially associated with Fe-hydroxides relative to Al/Mn-hydroxides and that plant roots attenuate leached As during high water events (Voegelin et al, 2004). Lastly, five to six different types of Zn species associated with phyllosilicates in clayey soil from terraces surrounding the Ohio River were identified with a combination of μ-XRF, μ-XRD and EXAFS (Manceau et al, 2004).

Despite the rising use of analytical techniques for studying contaminants in soils and sediments, the studies listed above have dealt most often with metal speciation in bulk soil, and therefore little focus has been directed towards the abilities of modified surfaces to sequester metal(loid)s. This study presents a detailed analysis of metal(loid) interaction with altered surfaces and presents results with implications for metal(loid) mobility and transport in soils that have been acidified by anthropogenic sources.

1.1 Objectives

The fate of metal(loid)s in soils is dependent on various transport and transformation processes. These processes are in turn contingent upon the solubility and reactivity of the source materials as well as the properties of mineral surfaces and organic material. The latter

are important as they control the sequestration and release of metal(loid)s at the water-mineral interface in soils (e.g. Schindler et al. 2009, Durocher and Schindler 2011, McNear et al, 2007). Therefore, gaining an understanding of processes at mineral surfaces as well as characterizing metal(loid) bearing hosts and altered surfaces is critical to assessing the behaviour of contaminants. Further, such knowledge is needed to quantify the impact they may have on environmental components such as groundwater, vegetation as well as human health both in the present, as well as in the future (Meadows and Watmough, 2012).

The diversity of solid surfaces in the soil provide capacity for transport, retention (i.e. sorption, incorporation), and chemical transformation of metal(loid)s that affect soil and water quality (Chorover et al, 2007). The mobility of metal(loid)s can slowly decrease during weathering processes through the formation of precipitates and polymeric complexes. When metal(loid)s co-precipitate with elements such as Si, Al, and Fe, their mobility varies as a function of the chemical and mineralogical composition of the secondary mineral including processes such as the solubility and mineral transformation rate (Chorover et al, 2007). Therefore, an understanding of secondary phases is critical in assessing the fate and residence times of metals in acid soils. This study focuses on the identification of secondary metal(loid) bearing phases, and on the chemical and mineralogical characterization of coatings on grains in formerly highly acid soils. In addition these coatings are investigated as a possible sink for attenuating and isolating metal(loid)s from transport. This study also aims to utilize the findings as a proxy for understanding the behaviour of metal(loid) contaminants in soils worldwide that have been acidified by anthropogenic sources. The specific objectives are to determine:

1. Once released from the source (e.g. particulate matter; mineral weathering) what is the fate of metal(loid)s?
2. What possible sinks could be sequestering these metal(loid)s?
3. What is the potential for attenuating free and toxic Al?
4. In which secondary phases are metal(loid)s being held?

5. What is the role of nanometer thick coatings?
6. What are the implications for their possible transport in the future?

2.0 METHODS

2.1 Background information on the Sudbury Area

Sudbury has been one of the largest smelting centers in Canada since the discovery of large deposits of Ni-Cu and other metallic sulfides in the late 1880's (Hutchinson and Whitby, 1974; Whitby, 1976). As a result of processing, the release of metals such as Cu, Ni, Zn, Cd, Co and metalloids such as As, Pb, and Se, in addition to large quantities of sulfur dioxide, has led to the contamination and acidification of local soils. Beginning in 1978, acid soils in the greater Sudbury area were treated with dolomitic limestone, a P-rich fertilizer containing 24 wt% P_2O_5 (Wren, 2012) and a specialized seed mix of five grass species and two legumes. A subsequent major tree planting program (over 8.5 million trees over the period of 1978- 2005) resulted in the decline of barren and semi-barren landscapes by 42 and 28%, respectively (Wren, 2012).

Various studies have examined the distribution and concentrations of metal(loids) in the Sudbury soils. The Sudbury Urban Soil and Sudbury Regional Soil studies focused on metal concentrations in local urban soils, and on the distribution of metal(loid) species in regional soils for the soil depths; 0-5, 5-10, and 10-20 cm (Wren, 2012). In grouping the sampling by depth, this procedure ignored the regional variations of the different soil horizons. These studies showed that metal(loid) concentrations are highest in the top 5 cm of the mineral soil column and undergo a drastic decline with depth (Wren, 2012). A recent study by Meadows and Watmough (2012) focused on assessing metal(loid)s in the Sudbury soils based on a critical-load approach, comparing metal concentrations with the Ministry of the Environment limits for metals in soils, and performing predictive modelling to assess residence times and recovery of the soils. Sequential extraction analyses suggested that Cu is predominantly associated with the organic and clay fractions of the soil (Adamo et al. 1996, Wren et al. 2012). However, the study

by Lanteigne et al. (2012) showed that many acid soils of the Sudbury area contain only a minor clay sized fraction (<1%) composed of mainly quartz and chlorite with some muscovite/illite (confirmed by powder x-ray diffraction in this study). These soils also have a generally poorly developed or non-existent organic (O) horizon in contrast to treated soils. The small proportions of clays and organic material in the O and A horizons thus raises the question as to the potential sinks for metal(loid)s in these horizons of the acid soils.

Smelter-derived particulate matter (PM) in the Sudbury soils consist of spherical particulates in the nano- to millimeter-sized range that exhibit characteristic quench textures (Lanteigne et al, 2012, 2013). The spherical particulates can be classified into two main categories: oxide/silicate, or sulfide-bearing particulate matter. Oxide/silicate particulate matter is composed of magnetite (Fe_3O_4), hematite (Fe_2O_3), Fe-silicates (olivines, pyroxenes), delafossite ($CuFeO_2$), the spinels trevorite ($NiFe_2O_4$), and cuprospinel ($(Cu, Mg)Fe_2O_4$), tenorite (CuO) and cuprite (Cu_2O)(Lanteigne et al. 2012) with only low concentrations of other metal(loid)s (2.35-195.6 ppm) being present. During weathering, the transformation of the spinels into hematite is associated with a concomitant release of Cu, Ni, As and Zn whereas metal(loids) such as Pb are immobile and remain in the hematite rim (Lanteigne et al, 2012, 2013). Sulfide-bearing particular matter contains sulfide inclusions encapsulated by a less soluble rim of Fe-oxides and Fe-silicates. The sulfide inclusions are composed of intergrowths of mainly heazlewoodite (Ni_3S_2), bornite (Cu_5FeS_4) and pyrrhotite ($Fe_{(1-x)}S$) , and contain high concentrations of Pb, As, Zn, Co and Se (Lanteigne et al., 2012, 2013). Weathering of the sulfide-bearing particulate matter begins with the formation of cracks through the Fe-oxide/Fe-silicate rim which facilitate the migration of oxidizing pore water that subsequently leads to the transformation of the sulfides to sulfates, or completely dissolves the former inclusion (depending on the solid/water ratio) thereby releasing the metal(loid)s bound to this core. Subsequently, the silicate matrix dissolves and progressively detaches from the oxidised Fe rim, until the silicate is completely removed and the Fe rim collapses (Lanteigne et al. 2012).

Particular matter composed of sulfides or NiO is another common contaminant in the Sudbury soils. The sulfides consist primarily of chalcopyrite ($CuFeS_2$), pentlandite $(Fe, Ni)_9S_8$ and pyrrhotite ($Fe_{(1-x)}S$). Their origin can be traced back to the composition of Sudbury's major ores which have low concentrations of metal(loid)s. These sulfides are significant sources for Cu and Ni in the soils, but are devoid of any other metal(loids), with the exception of As and Se, the latter having been found in association with alteration layers forming around weathering sulfide grains (Lanteigne et al. 2013).

2.2 Sampling and sample preparation

Soil samples of the upper 0-5 cm were collected in proximity to former smelters located in the towns of Copper Cliff, Coniston and Falconbridge all of which are now incorporated in the City of Greater Sudbury (Figure 1). These were taken in duplicate at three locations surrounding each smelter, from areas that had not been previously treated with lime and fertilizers. The pH of each sample was measured using suspensions containing 1 g of soil and 50 ml ultrapure water. Grains coated with secondary phases were separated from the bulk soil with a metal probe. The bulk soil and coated grains were embedded in epoxy discs in preparation for further microanalyses. Additionally, 62 grains with visible coatings were extracted and mounted on Cu tape for X-ray photoelectron spectroscopic analyses.

2.3 Analytical techniques

2.3.1 Bulk Chemical Analysis

Samples from each location were ground with mortar and pestle and sent to two different labs for chemical analysis. At the GEOLABS laboratory (Sudbury, ON), 0.5 grams of each sample were dissolved in an open vessel using multi-acid digest composed of hydrofluoric, nitric and perchloric acids at T = 140°C until dryness. The samples were completely dissolved in a

mixture of HCl and HNO_3 and spiked with 1.0 mL of a 5 ppm Ru+Re internal standard solution. Element concentrations were measured by ICP-OES and represent the total concentrations of the elements in the sample.

The metal(loid)-concentrations in the more "soluble fraction" of the soil samples (*i.e.* coatings, nanoparticles) were measured at a commercial lab (AGAT labs) using a less aggressive digest. Here, one gram of each sample was digested with Aqua Regia (hydrochloric acid and nitric acid) for one hour at 90ºC. The digests were diluted to 50 mL with de-ionized water and subsequently analysed with ICP-MS. Blanks, sample replicates, duplicates and internal reference materials, both aqueous and geochemical standards are routinely used in both laboratories as part of the quality assurance.

2.3.2 Scanning Electron Microscopy and Powder X-ray Diffraction

Scanning Electron Microscopy (SEM) on cross sections of coatings was conducted with a JEOL 6400 at 20 kV, equipped with both backscattered (BSE) and secondary (SE) electron detectors and an Energy Dispersive X-ray Spectrometer (EDS). Powder X-ray diffraction measurements were done with a Philips PW 1729 X-ray diffractometer operated at a voltage and current of 40 kV and 30 mA using Co Kα (1.79 Å) radiation. Diffraction patterns were collected over a scan range of 5–75° 2θ with a step size of 0.02° 2θ and dwell times of 4–10 s.

2.3.3 Laser Ablation Inductively Coupled Plasma Spectroscopy

Trace element distributions and concentrations in coatings were measured using a laser ablation inductively coupled plasma spectrometer (LA-ICP-MS) consisting of a New WaveNd:YAG 213 nm laser coupled to a quadrupole Thermo X II series. The areas of interest were analysed using both line scans and mapping. The ablation was done in a He atmosphere and Ar was mixed to the carrier gas before it entered the ICP-MS. Spot size varied from 10µm

to 3 µm, depending on the size of the area of interest, and was utilized at a repetition rate of 10 Hz. The energy density was kept constant at 11 J/cm^2. The synthetic glass standard NIST610, which contains a nominal trace element abundance of about 500 mg kg^{-1} was used as the external standard. At the beginning of each analytical run, intermittently during acquisition, and at the end of each sample, the standard was ablated under the same conditions. Detection limits for elements depend on the experimental setting of the laser scan and are listed for a similar experimental setting in Durocher and Schindler (2011). Line scans were designed to traverse the cross-section of coated grains, beginning with the outer epoxy (labeled *A* in Fig. 2) and traveling through the coating towards the underlying mineral (labeled *B*). The selection of integration areas was conducted based on the chemical difference between the coatings and matrix composition obtained through SEM. The breadth of each integration area was determined by monitoring the inflection points of the rise and fall of the Fe and Si peak, and the peaks for Cu, As and Pb which were used to help define the boundary between the coating and the underlying mineral. Laser Ablation ICP-MS data are often quantified by calibrating the counts per second (CPS) with respect to an internal standard as well as an external standard (e.g. NIST glasses). However, the samples analyzed in this study were heterogeneous and partly hydrated, so no single element was suitable as an internal standard and therefore, only the external standards were used. Molar ratios of the elements were calculated from the counts and the known concentrations in the NIST glass and then element concentrations were calculated by normalizing the sum of the moles to 100% assuming that the samples are dominated by Fe, Si, Al, Ca, Na, and K (observed by SEM-EDS). The mole-proportion of H_2O was estimated on the basis of molar ratios between Fe, Si and S and the number of structurally bound H_2O groups in phases identified in the coatings and potential amorphous phases commonly found in acidic systems. This procedure resulted in a semi-quantitative data set based on the uncertainty of the number of structurally bound H_2O groups per mol of Si, Fe or S

(±one H_2O group). This resulted in an estimated error of <10% for the concentration of trace elements in an individual measurement.

2.3.4 *Micro-Raman spectroscopy*

Micro-Raman spectroscopy was performed on cross-sections of coatings with a thickness of at least 10µm. Spectra were obtained over the range of 100 to 4000 cm^{-1} and collected in backscattered mode with a HORIBA Jobin Yvon XPLORA spectrometer interfaced with an Olympus BX 41 microscope, 100x magnification (estimated spot size of 2 µm), a 1200 grating and an excitation radiation of 532 nm. Calibration was made using the 521 cm^{-1} line of a silicon wafer.

2.3.5 *X-ray Photoelectron Spectroscopy*

X-ray photoelectron spectroscopy (XPS) was performed on 62 coated grains from soils at Copper Cliff, Coniston and Falconbridge. The near-surface composition was measured with a Kratos Axis Ultra X-ray Photoelectron Spectrometer (XPS) equipped with a magnetic-confinement charge-compensation system. The advantages of this system for insulators have been described in detail by Schindler et al. (2009). Each spectrum was recorded with a step size of 0.05 eV and an analyzer pass-energy of 20 eV. The lens and aperture were in Hybrid and slot mode, respectively, which allowed the collection of photoelectrons from an area of about 700 x 300 um. Each spectrum was measured using 3 sweeps. The electrostatic sample-charging (which was not completely compensated by the charge neutralizer) was corrected by setting the binding energy of the C 1s electrons of adventitious C-H species on the sample surface equal to 285 eV (Wagner et al.1979). The amount of adventitious species on the surface of each grain was reduced by sputtering the surface with Ar^+ ions. The sputtering was carried out in an angle of 45° relative to the surface and with an acceleration voltage of 4kV. The sputtering removed a layer with a thickness of about 8 nm (measured on an amorphous

silica standard). The inelastic mean free path (IMFP) of the Fe 2p electrons (binding energy 710 eV) was 1.8 nm. Information on the chemical composition of a surface can be gained to a depth three times of the IMFP (so called information depth; Mantha et al 2012a; Hochella, 1988), indicating that the measured intensities of the photoelectrons represents the composition of the upper 3 x 1.8 = 5.4 nm.

2.3.6 Micro-X-ray Fluorescence

Micro X-ray fluorescence (μ-XRF) spectra were collected on cross sections of coatings at the Very Sensitive Elemental and Structural Probe Employing Radiation from a Synchrotron (VESPERS) beam line at the Canadian Light Source, Saskatchewan. Element distribution maps of 350 μm^2 were generated for Fe, Ni, Cu, Co, As and Pb using a beam size of 5μm and a step size of 5μm(dwell time of 1s). The beam was set at a 45º angle with an estimated penetration depth of 100-250μm. Therefore, only grains with thick coatings were selected so as to minimize the interference of fluorescence radiation emitted from underlying minerals.

3.0 RESULTS

The top 5cm of soils surrounding the three smelter locations of Coniston, Falconbridge and Copper Cliff are composed of sandy silts with minor clay (<1%) (Lanteigne et al, 2012). They consist primarily of quartz and plagioclase (abundant anorthite) with minor amphibolite-group minerals, muscovite and chlorite (Table 1). Additionally, a significant proportion (estimated to be 5-10%) of these soils is composed of metal(loid)-bearing particulate matter (Lanteigne et al. 2012, 2013) as well as secondary phases produced through precipitation, oxidation, or weathering among other transformative processes (see below). The occurrence of particulate matter is also reflected by the total metal(loid) concentrations in these soils (Table 2).

The Sudbury soil study previously undertaken, indicated that many soils, especially those around the smelter stacks, were strongly acidified with pH values of <4 (Wren, 2012).

However over the past 20 years, pH levels have raised by one unit throughout the region (Sargent, 1996, Winterhalder, 2002). Improvements are reflected in the pH values of the sampled soils (pH = 4.5 to 6, Table 2), indicating that that most of the acid-producing components (H_2SO_4, HNO_3, H_2S, organic acids, Cu^{2+} and Ni^{2+}) in the soluble fraction of the soils have been either washed out or precipitated in the form of water-insoluble phases.

The depletion in the soluble fraction of acidic components may be reflected in the low S-concentrations (Table 2) and low abundances of sulfide (Lanteigne et al. 2013) and sulfate minerals (this study). The large differences between the total concentrations of metal(loid)s and those in the "soluble" fraction have already been observed by Adamo et al. (1996). This can be explained by the larger proportion of insoluble spinel-type phases deposited as particulate matter relative to secondary metal(loid)-bearing hydroxy-hydrates and sulfates.

The Sudbury soil study also showed that the average concentrations of metal(loids) decrease significantly within the upper 10 cm. For example, concentrations for Cu, Ni, Pb, As and Se decrease at the Copper Cliff sampling sites (Fig. 1) by a factor of 9, 8, 4, 2, 3 from the upper 0-5 cm to a depth at 5-10cm, respectively (Wren, 2012). This steep concentration profile suggests that metal(loids) are subject to very short transport distances before being attenuated. The study by Lanteigne et al. (2012) showed the absence of clay minerals and a poorly developed (if at all present) O horizon, and indicated prior to this study that clays and organic components could therefore not account for the sequestration of Cu, Ni, Pb, As, and Se. Inspection of soils grains with an optical microscope and SEM indicate that the majority of mineral grains in the upper 5 cm are coated by secondary phases (Fig. 3), suggesting that these surface modifiers acted as possible sinks for metal(loid)s in the Sudbury soils. A LA-ICP-MS traverse through an approximately 50 µm thick Fe-Si-rich coating on an albite grain (Fig. 2) shows that this is indeed the case: the coating is highly enriched in the metal(loid)s Co, Ni, Cu, Zn, As and Pb, whereas the albite is enriched in Si and Na relative to the coatings. The occurrence and distribution of metal(loid)s in these modified surfaces can only be understood if

the chemical character and mineralogical composition of the coatings have been characterized. Hence, we will first describe the occurrence, chemical character and mineralogical composition of micrometer-size coatings before inspecting trace-element concentrations and distributions within these coatings. We will additionally describe the occurrence and chemical composition of nanometer-thick coatings, which occur more commonly in soils than their micrometer-size counterparts but which could not be characterized in terms of their mineralogical and trace element composition.

3.1 Micrometer-thick coatings on mineral grains

A ternary diagram depicting the proportion of Fe, Al and Si indicates that the majority of micrometer-thick coatings are enriched in Si and Fe relative to Al (Fig. 4a). Hence, variations in their chemical composition are best visualized when plotting the Fe: Si ratio versus frequency (Fig. 4b). Two distinct populations can be identified in the histogram: coatings with similar element ratios of Fe and Si and those enriched in Si. Doelsch et *al.* (2001) showed that in freshly precipitated mixtures of silica and Fe-hydroxides, Si-O-Si bonds dominate in mixtures with Fe : Si ratios < 1, whereas Fe-O-Si and Fe-O-Fe bonds dominate in mixtures with Fe : Si ratios > 1. Durocher and Schindler (2011) argued that freshly precipitated mixtures of silica and Fe-hydroxide coatings in mine tailings with Fe:Si ratios <1 have properties similar to those of a hydrous silica gel, whereas mixtures with Fe:Si ratios > 1 have properties similar to a Si-rich Fe-hydroxide precipitate. Hence, the authors distinguished between Fe-rich coatings (FeOx) with Fe: Si > 4, Fe-Si-coatings (Fe-SiOx) with Fe: Si between 4 : 1 and 1 : 1 and silica-rich coatings with Fe : Si < 1. Considering the populations in the histogram and the change in properties at equal proportions of Fe and Si, the chemical character of the coatings in the acid soils may be divided into three distinct groups: SiO_x coatings with a Si : Fe element ratio of >7, Fe-SiO_x coatings with ratios between 1 and 7 and FeO_x coatings with ratios smaller than 1. In contrast to those associated with tailings (see Durocher and Schindler, 2011), coatings with Fe>Si are far

less common (15% of the time) than those with Si>Fe (Fe-SiOx+ SiOx = 85% of the time), indicating a silica-rich environment which is characteristic of many acid soils (Hetzel and McColl, 1997).

3.1.1 Mineralogical composition

High-resolution SEM images show that the FeOx coatings are composed of a Fe-silica bearing matrix containing idiomorphic crystals of Fe-(hydr)oxides (Fig. 5a). Data from Raman spectroscopy, chemical composition, and observations made of crystal morphologies suggest that the equi-dimensional crystals are most likely magnetite (bright spots in SEM image), the fibrous crystals are most likely goethite and that a significant proportion of the matrix is composed of hematite.

The Fe-SiOx coatings are characterized by large fragments of SiO_2 within a Fe-Si-matrix (Fig. 3a, b, 6a, 7a). The matrix contains numerous phases on the nanometer scale including 2-line ferrihydrite, schwertmannite, jarosite, hematite, and possible maghemite (Figure 7b, 8a). It should be noted that the occurrence of the latter two phases may be the result of the laser induced transformation of schwertmannite and ferrihydrite (Mazzetti and Thistlethwaite, 2002). Silica-rich SiOx coatings were not examined with Raman spectroscopy but SEM images indicate higher abundances of silica grains and silicate fragments (from the weathering of the underlying grain) relative to Fe-SiOx coatings.

3.1.2 Trace-element composition of the coatings

The differences in the mineralogical and chemical composition of the coatings suggest that trace elements with different crystal-chemical characters (i.e. Cu, Ni, Co, Zn, Pb, As and Se) occur in different proportions within the FeOx, Fe-SiOx and SiOx coatings. The preferred association of a metal(loid) with the different types of coatings may be identified through

inspection of coatings composed of layers with different chemical characters (i.e. Fe-SiOx, FeOx or SiOx).

Multiple coatings occur, for example on a Fe-pyroxene with a composition close to ferrosillite, $FeSiO_3$. The coating is composed of a FeOx layer sandwiched between two Fe-SiOx layers occurring along the grain-coating and coating-atmosphere interfaces (Fig. 9a). Laser-ablation ICP-MS distribution maps indicate higher amounts of As, Cu and Pb in the Fe-SiOx and higher abundances of Ni and Co in the FeOx (Fig.9b). Closer inspection of the Fe-distribution map suggests, however, a lower abundance of Fe in FeOx relative to Fe-SiOx, (Fig. 9b). This apparent disagreement between the LA-ICP-MS maps and EDS can be understood if one considers that intensities measured with LA-ICP-MS also reflect the amount of ablated material. This problem can normally be solved through quantification of the entire map using an internal standard (which is inaccurate for heterogeneous hydrated materials) or through a time-consuming normalization method. For these reasons, and in order to validate the higher abundance of some of the metal(loids) in the Fe-SiOx coatings, µ-XRF chemical distribution maps from the same area were recorded at the Canadian Light Source (see above). Chemical distribution maps for Fe, Cu, Co, Zn and Ni and the corresponding EDS maps for Fe and Si indicate that the µ-XRF distribution maps have lower resolutions as compared to the LA-ICP-MS maps due to the incident angle and higher penetration depth of the synchrotron radiation although both used similar spot sizes (3, 5 µm)(Fig. 9 *vs.* 10). Nevertheless, the µ-XRF distribution maps clearly show higher abundances of Fe, Co and Ni in the FeOx and of Cu and Zn in the Fe-SiOx layer along the coating-atmosphere interface (note that the Fe-SiOx on the grain-coating interface is not resolved). The micro-XRF and LA-ICP-MS maps also indicate that Ni occurs in the form of discrete particles, whereas Cu, Zn, Pb and As are closely associated in the Fe-SiO_x layers (Figs. 9 and 10). The higher resolution LA-ICP-MS maps also reveal higher concentrations of metal(loids) in the outer relative to the inner Fe-SiOx coating, an important observation that later be used to develop a model for coating formation.

An SiOx layer along the grain-coating interface can also be observed in association with an Fe-SiOx layer at the coating-atmosphere interface (Fig. 11). Similar to the coatings on the Fe-pyroxene, the layer at the coating-atmosphere interface, in this case a Fe-SiOx layer, is enriched in metal(loids) relative to the SiOx on the K-feldspar-coating interface. Important to note is that the latter layer is enriched in K, which was most likely derived from the weathering of the underlying feldspar (Figure 11).

Coatings of FeOx without underlying Si-rich layer only occur on Fe-hydroxide grains. These types of FeOx coatings have the highest trace elements compositions of all coatings observed in the soils, especially with respect to As and Pb (Figure 6a-c).High concentrations of metal(loid)s within the Fe-hydroxide matrix coincide with phosphorus-rich areas. A close examination of the corresponding backscatter image (Fig 6b) indicates the occurrence of bright inclusions most likely representing metal-bearing arsenates or phosphates.

Coatings composed of layers with different chemical characters (FeOx, Fe-SiOx, and SiOx) are rare. Most commonly, only one type of coatings is observed on mineral grains. For example, Figure 3 shows the occurrence of a Fe-SiOx coating on albite whereas Figure 6 depicts the occurrence of a Si-bearing FeOx coating on a Fe-hydroxide grain without significant proportions of Si.

The relationship between the abundance of a metal(loid) and the chemical composition of coatings on exclusively silicate minerals can also be investigated through plotting metal(loid) concentrations of the coatings as a function of their Si : Fe element ratio (Fig. 12).These plots indicate that maximum concentrations for Cu, As, Pb and Se occur in Fe-SiOx coatings with Si : Fe ratios between 1 : 1 and 7 : 1. These plots also show that SiOx coatings generally have the lowest metal(loid) concentrations, and that these concentrations increase with the Fe-content in the coatings.

3.2 Nanometer thick coatings

Almost all grains in the Sudbury soils are coated. Many of these coatings are, however, very thin (on the nanometer scale) and so their chemical compositions could not be investigated by SEM and LA-ICP-MS. As such, the near surface compositions (top 5.4 nm) of 62 grains were examined with XPS. The chemical composition of these upper surface coatings can be visualized in a ternary diagram depicting the proportions of Si, Fe and Al (Fig. 13a). All grains were subsequently mounted in epoxy and the average proportions of Si, Fe and Al in the underlying mineral phases (silicates, quartz and Fe-hydroxides) were determined with EDS and plotted in the same ternary diagram as their surface composition (Fig. 13a). Closer inspection of the diagram shows that in general, the surface coatings have a higher proportion of Al relative to their underlying minerals. The enrichment of Al on the surface may be expressed with an enrichment factor, which can be calculated by dividing the Al : Si ratio of the surface with the corresponding average ratio in the underlying minerals. A semi-logarithmic plot containing the Al enrichment factors for all 62 grains indicates that the factor significantly varies between 1 and 250 (average 23) and that none of the examined coatings is depleted in Al with respect to the underlying mineral. A comparison between surface composition and type of minerals in the underlying grain suggests that the proportions for Si and Al on the surface are independent of the mineralogical composition of the underlying grain. For example, a surface with a high and low proportion of Si (21 at%) and Al (12 at%) occurs on a chlorite group mineral grain with Al > Si whereas a surface with low and high proportions of Si (3 at%) and Al (33 at%) occurs on a grain containing quartz and K-feldspar with Si : Al > 3 : 1.

The detection limit of an element in XPS depends among other factors on the sensitivity factor of the element. For example, elements with a high sensitivity factor such as U can be detected down to 1000 $mgkg^{-1}$ at the Kratos Ultra instrument at the University of Manitoba (Michael Schindler, personal communication). Measurements of the Cu 2p and S 2s electrons indicate that only 2 out of 62 surfaces contain detectable amounts of Cu and that the surfaces of 27 grains have detectable amounts of S. In the latter case, 85 % of the surfaces have, however,

less than 1.0 at% S. The two surfaces with detectable amounts of Cu contain 3 and 20 at% Cu^{2+}, overlie feldspar grains, and are characterized by Si : Al element ratios of > 1 (Fig. 14).

4.0 DISCUSSION

The results above show that Fe-rich coatings on Fe-hydroxide grains and Fe-Si-bearing coatings on silicate minerals with elemental Fe : Si ratios from 1 : 1 to 1: 7 contain the highest metal(loid) concentrations of all examined coatings. Due to the absence of organic material, clays and large proportions of Fe-hydroxides, these observations suggest that nano-to micrometer thick Fe-silica coatings on siliceous grains are the most important sink for metal(loid)s in the acid soils of the Sudbury area. The incorporation of metal(loid)s in these coatings can be understood if one considers the stability and structure of the observed minerals and the formation mechanism of the coatings. Inspection of correlations between different element concentrations will demonstrate that many metal(loid)s likely co-precipitated with the minerals present in these coatings. Finally, the formation and structure of the nanometer thick coatings will be discussed in reference to current soil conditions and high-resolution XPS spectra of Si and Al 2p electrons.

4.1 Mineralogical composition

Studies of Fe-oxy-hydroxides and sulfates common in acid mine drainage (AMD) and acid soil systems have demonstrated that the stability of these minerals depends on their bulk and surface composition (i.e. type of adsorbed species) and on the composition, pH and redox potential of the solution (Blowes and Ptacek, 2003). Hence, we will focus first on the composition and stability of these minerals before discussing the role of silica in these coatings.

4.1.1 Iron-sulfate, hydroxides and oxides

Coatings from all sample locations contain various combinations of schwertmannite, jarosite-group minerals, 2-line ferrihydrite, goethite, magnetite, maghemite, hematite and silica modifications (amorphous or crystalline).

Minerals of the jarosite group have the general formula ($D[M_3(TO_4)_2(OH,H_2O)_6]$) and their crystal structures can accommodate mono-, di- and tri-valent cations at different crystallographic sites (*D*, *M* and *T*) (Dutrizac and Jambor 2000). Trace elements in the coatings such as Cu^{2+}, Ni and Zn commonly occupy the crystallographic site *M*, Pb, Na and K the crystallographic site *D* and S, P, As and Se occur at the crystallographic site *T* (see below for more details on substitution mechanisms).

Jarosite-group minerals are common constituents of acid soils (pH <4), especially those which have developed in marine sediments containing pyrite (Dutrizac and Jambor, 2000). Alkali-ions needed for jarosite formation are liberated during the weathering of silicate minerals, particularly tri-octrahedral micas (Jambor and Blowes, 2000).The release of alkali ions and Pb during the weathering of silicate minerals is also the reason for the occurrence of jarosite-group minerals in rock coatings observed in mine tailings facilities and in proximity to volcanoes (Durocher and Schindler, 2011, Schiffman *e*t al, 2006). Here, the jarosite group minerals are embedded within a silica-rich matrix, which was formed during weathering of the underlying siliceous rocks by acidic solutions.

Review articles by Dutrizac and Jambor (2000) and Bigham and Nordstrom (2000) indicate that jarosite-group minerals are commonly stable under acidic conditions with pH values < 4. The pH value in many acid soils of the Sudbury area has increased one unit from pH 4-5 in recent years (Table 2), suggesting that pore waters in these soils would not be expected to be in equilibrium with the earlier-formed jarosite-group minerals.

Similarly, schwertmannite [$Fe_8O_8(OH)_{4.4}(SO_4)_{1.8}(H_2O)_{8.4}$] and ferrihydrite, $Fe_{10}O_{14}(OH)_2$ may exist metastably in the silica-rich coatings, transforming with time into the more crystalline and thermodynamically stable goethite and hematite (Mayer and Jarrell, 1996;Schwertmann

and Thalmann, 1976; Jones *et al.,* 2009). The precipitation of schwertmannite and ferrihydrite is often kinetically favoured, even when the pH of the aqueous solution is below the pH range of its maximum stability (pH = 2.5-4.5; Bigham and Nordstrom, 2000). While schwertmannite controls the concentration of As in tailings water (Acero et al, 2006), it's transformation into goethite (FeOOH) can lead to the release of adsorbed oxyanions such as $(SO_4)^{2-}$ and $(AsO_4)^{3-}$ (Acero et al. 2006).

Ferrihydrite commonly forms under oxidizing conditions in solutions with pH values above 5 (Bigham and Nordstrom, 2000). It is often associated with silica as a result of the high affinity of silica aqueous-species towards its surface, a key property that will later be utilized to explain the formation of silica-rich coatings at the coating-atmosphere interface.

Hematite likely represents the stable end-product of the transformation and oxidation of ferrihydrite, goethite, schwertmannite, jarosite and magnetite (Durocher and Schindler, 2011; Jones et al., 2009; Mayer and Jarrell, 1996; Schwertmann and Thiemann, 1976). However, hematite can also be produced through the transformation of Fe-hydroxides when exposed to Micro-Raman laser beams (Mazzetti and Thistlethwaite, 2002). Detection of multiple phases and crowding of peaks in the Raman spectra indeed confirms that an unknown portion of the hematite in coatings was produced during the recording of the Raman spectra (Mazzetti and Thistlethwaite, 2002).

The common occurrence of jarosite-group minerals, schwertmannite and ferrihydrite with goethite and hematite in Fe-SiOx coatings may reflect different generations of Fe-hydroxides, variations in pH over time (Majzlan and Myneni, 2005) or slow transformation processes of the former to the latter minerals (see below for more details).

4.1.2 Sources of silica

Two sources of silica for the formation of silica-rich coatings have to be considered: silica produced through the non-stoichiometric dissolution of the minerals in the underlying siliceous grains and aqueous silica species mobilized by acidic pore waters.

Amorphous silica layers have been identified on the surface of numerous silicate minerals after dissolution experiments under acidic conditions. Dissolution experiments on labradorite (*e.g.* Casey *et al.*, 1989), glasses (*e.g.* Hamilton *et al.* 2001), inoslicates (*e.g.* Casey *et al.* 1993) and phyllosilicates (Kalinowski and Schweda, 1996) have demonstrated that these layers even form when the solution is under-saturated with respect to amorphous silica. The formation of these silica-rich layers has been explained by a leaching-proton-exchange process on the surface of dissolving silicates (*e.g.* Schweda *et al.*, 1997), where Na, K, Ca and Al are replaced by hydronium ions. However, TEM observations indicate a sharp interface (on the atomic scale) between an amorphous silica-rich layer and the underlying mineral (Hellmann *et al.*, 2003, 2012), which one would not expect to form during a process that involved the gradual leaching of cations from a crystal structure. Given this, Hellmann *et al.* (2003, 2012) proposed an alternative process involving interfacial dissolution-reprecipitation process, where all elements of the feldspar structure are removed and amorphous silica re-precipitates on the surface of the underlying mineral. Chemical profiles measured with Secondary Ion Mass Spectroscopy (SIMS) showed that the elements Al, Na, Ca and K are continually removed from the dissolving minerals below and subsequently diffuse through an earlier formed silica-rich alteration layer (Schindler and Ilton, 2013). Dissolution experiments have also shown that the thickness of the alteration layer on feldspar increases with decreasing pH and decreasing flow rate of the solution above (Teng et al. 2001). Long duration dissolution-experiments on feldspar showed that the rate of diffusion of the leached cations Na, Ca and Al through an altered Si-rich surface layer becomes equal to the rate of silica-release from the exterior of the altered layer (Stillings and Brantley, 1995). Hence, the initial non-stoichiometric dissolution of feldspar becomes stoichiometric, limiting the thickness of the alteration layer to hundreds of nanometers

(*e.g.* Hellmann *et al.* 2003, 2012). Note that the change between a non-stoichiometric and stoichiometric dissolution process is independent of whether the former process is based on an interfacial dissolution-precipitation process or a leaching-proton-exchange process.

Silica-rich coatings on mineral grains within aquifers and acidic soils commonly occur on the nanometer scale (Nugent *et al*. 1998, Zhu *et al.* 2006). Micro- to millimeter thick silica coatings occur in environments characterized by either low precipitation rates (e.g. deserts, Schindler *et al.,* 2010 and Antarctica, Giorgetti and Baroni, 2007), highly acidic precipitation (*i.e.* rain and fog in proximity to volcanoes and smelters, Tosca *et al.,* 2004; Minitti *e*t al*.,* 2007, Mantha et al. 2012a,b) and on siliceous rocks in more or less permanent contact with acidic tailings ponds (Schindler *et al.*, 2009, Durocher and Schindler, 2011). The accretion of silica to form these coatings can be a result of the weathering of the underlying rock (Minitti *et al.,* 2007, Schindler *et al.*, 2009, Manta et al. 2012a, b) or from dissolution of Aeolian particles deposited on the rock surface (Thiagarajan and Lee, 2004; Giorgetti and Baroni, 2007, Curtiss *et al.* 1985, Schindler *et al.* 2010).

These observations and the fact that soils around the smelters of the Sudbury area had pH values of < 4 suggest that silica present in SiOx and Fe-SiOx along grain-coating interfaces likely originated from the non-stoichiometric dissolution of siliceous minerals in the underlying grains. At the same time, silica in FeOx and Fe-SiOx layers overlaying Fe-hydroxide grains (Fig. 6) and FeOx layers (Figs. 9 and 10) could not have originated from the dissolution of the underlying mineral/layer as these units contain traces of silica (Fig. 6a) or significantly less silica than the overlaying silica-rich layer (Fig. 10), respectively. The silica in these types of coatings may have originated from the interaction of pore waters with the underlying Fe-hydroxides as aqueous silica species show a high affinity to sorb to the surface of the latter minerals (e.g.Sigg and Stumm, 1981, see above). In this regard, Dyer *et al.* (2010) and Swedlund *et al.* (2009) proposed that ferrihydrite surfaces trigger the polymerization of adsorbed silicic-acid species and Davies *et al.* (2002) and Swedlund *et al.,* (2009) showed that Fe-hydroxide surfaces with

high silica content (up to 0.4 mol SiO_2 per mol Fe) contain adsorbed oligomeric silica species rather than layers of $H_{2x}SiO_{2+x}$. Furthermore, X-ray photoelectron spectroscopy (XPS) and TEM studies indicated that Si-rich ferrihydrite samples (with Si : Fe ratios up to 1 : 1) are composed of ferrihydrite nanoparticles with a silica-rich surface (Cornell and Schwertmann, 1996).

4.2 Models for coating formation

Discussions and observations made with respect to the origin of silica in the coatings provide a basis with which a model for the formation of micrometer-thick coatings on siliceous grains in the acid soils of the Sudbury area can be developed. A summary of the facts and findings are as follows. First, coatings along the grain-coating interface were formed through the non-stoichiometric dissolution of the underlying silicate minerals. The formation of silica gel-type layers (Durocher and Schindler, 2011, Mantha et al. 2012a, b) on the grain-coating interface promoted the nucleation of jarosite-group minerals on or within the silica-rich matrix. Continuous weathering of the soil grain required a mass exchange between the grain-coating interface and pore water which in turn involved the diffusion of alkaline cations and Pb^{2+} from the interface to the bulk soil and of $(H_3O)^+$, $Fe^{2+,3+}$,Cu^{2+}, Ni^{2+}, Zn^{2+}, $(SO_4)^{2-}$, $(AsO_4)^{3-}$ and $(PO_4)^{3-}$ from the bulk soil to the interface (Fig. 15a, b). The mixing of these components resulted in the precipitation of metal(loid)-bearing jarosite-group minerals in pores within or near the surface of the silica-rich alteration layers. Subsequent continuous weathering of the underlying silicate minerals may have diluted surface layers enriched in jarosite-group minerals with silicic acid producing silica-rich Si-FeOx layers.

Changes in the pH of pore waters resulted in the transformation of jarosite into schwertmannite or ferrihydrite, which subsequently transformed *via* dehydration into goethite and hematite. The kinetics of the latter transformation processes may have been affected by adsorbed silica-species, which are known to inhibit the transformation of ferrihydrite to goethite (Cornell and Schwertmann, 1996).The common occurrence of jarosite-group minerals,

schwertmannite, ferrihydrite, goethite and hematite can also be explained with the hardening of the silica gel into an opaline matrix. This process commonly entombs and preserves soluble minerals (Schindler et al. 2010, Mantha et al. 2012a, b), and most likely inhibited the complete transformation of the former to the latter minerals in soil coatings. Hence, the role of amorphous silica is of great importance in these coatings as the stability of Fe-hydroxides and minerals of the jarosite group (and thus the release of metal(loids)) are controlled by the presence of adsorbed silica species and the hardening of the silica gel.

Alternatively, FeOx coatings on siliceous grains may have developed through the precipitation of Fe-hydroxides on the surface of silica-enriched alteration layers (Fig. 9, 10, 15a, b). Silica-rich layers overlying FeOx formed through the adsorption of aqueous silica species onto the surface of FeOx and their subsequent polymerization to a silica-rich matrix (as proposed by Dyer et al. 2010 and Swedlund et al. 2009). Minerals of the jarosite-group in the overlying Fe-SiOx layers developed from components originating from the underlying FeOx (mainly Fe) and the bulk soil (alkaline cations, Pb, $(AsO_4)^{3-}$, $(PO_4)^{3-}$, $(SO_4)^{2-}$. Nucleation and preservation of these minerals were once again largely controlled by the properties of the silica gel-type matrix and adsorbed silica species.

The two models for the formation of Fe-SiOx (non-stoichiometric dissolution and adsorption of silica species) may be evaluated through the inspection of the distribution of P in coatings as

I. The P content in the bulk soil ranges from 500 to 1000 $mgkg^{-1}$ (Table 2) and can be considered as the predominant source for P in these coatings (Fig. 15b).
II. Aqueous $(PO_4)^3$ species have a higher affinity to sorb on positively charged Fe-O than on negatively-charged Si-O surface terminations (Stumm, 1992); i.e. FeOx layers should always contain higher concentrations of $(PO_4)^{3-}$ than Si-FeOx layers if both types of layers were formed *via* the same mechanism (e.g. precipitation).

Inspection of the distribution map for P (Fig.15a) in coatings composed of two Fe-SiOx interlayered by an FeOx layer (Figs. 9, 10 and 15a) indicates a higher abundance of P in the Fe-SiOx relative to the FeOx layer (note that the underlying $FeSiO_3$ grain contains only 260 $mgkg^{-1}$ P). This distribution suggest that

I. The two Fe-SiOx must have formed via different mechanisms than FeOx and that the incorporation of $(PO_4)^{3-}$ into Si-FeOx must have occurred *via* precipitation rather than adsorption (see also below);
II. $(PO_4)^{3-}$ species entered the Fe-SiOx along the grain-coating interface prior to the formation of FeOx;
III. $(PO_4)^{3-}$ species entered the Fe-SiOx along the coating-atmosphere interface after the formation of FeOx and during or after the formation of the Fe-SiOx;

One interesting observation is the development of FeOx coatings on the less abundant Fe-hydroxide grains (Fig. 6a). The coatings are enriched in Pb, As and silica and depleted in divalent cations and $(PO_4)^{3-}$ with respect to the underlying mineral (Fig. 6b). Chemical distribution maps for Fe and Si and LA-ICP-MS traverses suggest that the coatings were formed through adsorption of aqueous silica species onto the Fe-hydroxide surface and their subsequent polymerization towards an iron-silica gel-type material. This gel subsequently promoted the mixing of pore solutions originating from the bulk soil (alkaline ions, Pb^{2+}, $(AsO_4)^{3-}$ and $(SO4)^{2-}$), the grain-coating interface (Cu^{2+}, Ni^{2+}, Zn^{2+} and $(PO_4)^{3-}$), and the nucleation of jarosite-group minerals within the coating matrix.

4.3 Metal(loid)-rich coatings: products of co-precipitation or adsorption?

The models for the formation of coatings on siliceous grains can be used to explain the enrichment of metal(loid)s in Fe-SiOx relative to SiOx and FeOx coatings (Fig. 12) as (1)

jarosite-group minerals and Fe-hydroxides are the major hosts of metal(loid)s and (2) a silica-rich matrix is required to promote mixing of fluids, nucleation, and preservation of Fe-bearing phases. Correlations between different trace-elements can be now used to identify whether the majority of metal(loid)s in the coatings co-precipitated with jarosite-group minerals or adsorbed to the surface of Fe-hydroxide minerals.

The incorporation of divalent trace elements into jarosite-group minerals (JGM), requires charge balance via coupled substitution (e.g. $K^{+} + S^{6+} \rightarrow Pb^{2+} + As^{5+}$ or $K^{+} + Fe^{3+} \rightarrow Pb^{2+} + Cu^{2+}$) or protonation of the $(OH)^{-}$ groups (e.g. $Fe^{3+} + OH \rightarrow Cu^{2+} + H_2O$).The crystal structure of JGM is sufficiently flexible so as to permit rather extensive substitution (Dutrizac and Jambor, 2000). For example, a large fraction of Cu in the coating could substitute for Fe^{3+} on the *M* site, creating a solid-solution between jarosite and Cu-jarosite, $K[(Fe^{3+}, Cu^{2+})(SO_4)_3(OH, H_2O)_6]$ or beaverite, $Pb[Fe, Cu)_3(SO_4)_2(OH)_6]$ (Dutrizac and Jambor, 2000). Furthermore the coatings contain similar (P + As) to S-concentrations, suggesting significant substitutions of these elements on the *T* site. For example, corkite $Pb[Fe_3(PO_4)(SO_4)(OH)_6]$, kintoreite, $Pb[Fe_3(PO_4)_2(OH)_6]$ and beudanite, $Pb[Fe_3((As, S)O_4)_2(OH,H_2O)_6]$ are examples of phosphorous and arsenic bearing jarosite minerals (Dutrizac and Jambor, 2000).

The type of occurrence of metal(loid)s in the coatings (incorporated into jarosite or adsorbed to Fe-hydroxides) can be identified from plots of the concentrations of elements forming oxy-anions (P + As) versus the concentrations of the cationsFe^{3+}, Zn^{2+}, Pb^{2+} and Cu^{2+}.Oxy-anions such as $(PO_4)^{3-}$ and $(AsO_4)^{3-}$show a higher affinity towards the positively-charged surface of Fe-hydroxides under acidic conditions than do the divalent cations Zn^{2+}, Pb^{2+} and Cu^{2+} (Stumm, 1992). On this basis there should not be a correlation between the concentrations of P + As and the latter divalent cations if the majority of all elements are sorbed to the surface of Fe-hydroxides. Rather, correlations between the concentrations of these elements should exist if they are predominantly incorporated via coupled substitutions into the structure of Fe-minerals present in the coatings.

These considerations do not, however, consider the chemical variability of the coating layers as well as their occurrence within the coatings (e.g. at the grain coating or coating-atmosphere interface). For example, a plot with the concentrations of As+P versus Fe^{3+} indicate multiple trends (Fig. 16a). Each trend can be assigned to a certain type of coating, which is shown as a sketch in Figure 15:

(1) coatings with high Fe and low P concentration occur when FeOx coatings are sandwiched by two Fe-SiOx layers (labelled as *c* in Figs. 15 and 16a);

(2) coatings with high Fe and P contents occur when FeOx coatings occur on Fe-hydroxides or siliceous grains (labelled *f* and *g* in Figs. 15 and 16a);

(3) coatings with lower Fe but high P contents occur in Fe-SiOx coatings (labelled *d* in Figs. 15 and 16a);

(4) coatings with low Fe and P content occur in SiOx coatings (labelled *e* in Figs. 15 and 16a).

Instead, the plot of the concentrations of P+ As versus Zn effectively demonstrated only one trend (Fig. 16b), suggesting that the majority of P, As and Zn are structurally incorporated into the same mineral phase. The plot of the concentrations of As + P versus Pb shows two distinct linear correlations (Fig. 16c) which mainly involve data from Fe-SiOx and FeOx coatings. These correlations may depict two different types of coupled substitution mechanisms for Pb, $(AsO_4)^{3-}$ and $(PO_4)^{3-}$ into the structure of jarosite or perhaps another (unidentified) Fe-bearing mineral. The plot of the concentrations of As + P versus Cu also depict two different trends, with that involving Cu exhibiting and almost exponential character (Fig. 16d).The latter type of correlation may indicate the presence of Cu-bearing nano- to micro-size particles as these and Ni-bearing particles were observed in LA-ICP-MS and µ-XRF maps (Fig. 9 and 10).

To summarize, correlations between (As + P) and Zn^{2+}, Cu^{2+}, and Pb^{2+}, suggest that the majority of trace-elements are structurally incorporated into Fe-bearing minerals, particularly into JGM. The extent of incorporation depends, however, on the abundance of the element in the

underlying mineral grain (*e.g.* FeOx on Fe-hydroxide), the type of the coating (*e.g.* SiOx without a large proportion of Fe-bearing minerals) or the location of the coatings (*e.g.* FeOx sandwiched between two Fe-SiOx).

4.4 Nanometer-thick coatings: formation and possible mineralogical composition

The above results show that the upper 5.4 nm of the coatings are enriched in Al with respect to the underlying grain (Fig. 13a, b). These Al-enriched coatings can be either explained by a non-stoichiometric dissolution process under weak acidic condition, at which Al is considered to be immobile relative to Si, (Faure, 1998) or with the adsorption of formerly free Al species on the surface of Fe-silica coatings.

The fact that surfaces of high Al content occur, for example, on soil grains dominated by quartz, suggests that the majority of Al in the upper surface layers have been adsorbed by altered mineral surfaces. The absence of Al-rich micrometer-thick coatings (Fig. 4a) further suggests that the nanometer-thick Al-rich coatings have formed more recently than their micrometer-size counterparts. This also leads to the conclusion that the increase in soil pH from below 4 to 4.5-6 in the last twenty years may have triggered the formation of Al-enriched surfaces, as the stability of Al-bearing minerals commonly increases with increasing pH.

Aluminum-hydroxide species are common weathering products of soil, forming from minerals such as feldspars and micas and are generally incorporated into clay minerals under weak acidic to basic conditions and moderate precipitation rates (Vazquez Martinez, 2011). In acid soils, protonation impedes Al adsorption onto surfaces, forcing it to remain in solution and causing aluminum toxicity (Sumner et al, 1991, see also above). Free Al-species in soils include Al^{3+}, Al-organic complexes, and Al-fluoride complexes (David and Driscoll, 1984; Haynes and Mokolobate, 2001).These free Al species tend to form polymerized Al-hydroxy-polyhedral chains with increasing Al activity and can show a high affinity to sorb on Fe-hydroxide surfaces (Farmer, 1980), thus leading to the formation of clay precursors. These precursors are Al-rich

clays such as imogolite ($Al_2SiO_3(OH)_4$) and allophane ($(Al_2O_3)(SiO_2)_{1.3\text{-}2}2.5\text{-}3(H_2O)$), which commonly form under weakly acidic to near neutral conditions (pH 5 - 6.5)(Farmer, 1980; Sumner, 1991). Higher ordered Al-rich phyllosilicates such as kaolinite, $Al_2Si_2O_5(OH)_4$ and halloysite $Al_2Si_2O_5(OH)_4\ (H_2O)_2$ commonly form at higher pH (maximum stability between pH 5 and 8) than imogolite and allophane (Huang and Keller, 1973).

Most surfaces on the examined soil grains have (Al + Fe) : Si and Al : Si ratios above one, suggesting either the occurrence of adsorbed polymerized Al-hydroxy species on Fe-silica surfaces or the presence of imogolite and allophane on Fe-hydroxy surfaces. An identification of the exact nature of the Al-species on the soil grains is only possible with High-resolution TEM. However, inspection of the binding energy of the Si 2p and Al 2p electrons may yield information on the change in the coordination environment of Si and Al with the content of both elements in the surface coatings.

Schindler et al. (2010) showed that a shift of the Si peak in an XPS spectrum is related either to the proportion of Si-O-Si bridges (i.e. to the polymerization degree of the silicate tetrahedra) or $Si\text{-}OH_2$ terminations. For example, the Si 2p spectra of quartz and silicic acid, H_4SiO_4 occur at higher binding energy than the spectra for an olivine or a pyroxene (Schindler et al. 2010).

Inspection of the binding energies for Si 2p electrons of surfaces with high and low Si-content indicate that the binding energy increases with increasing Si-content (Fig. 17). Similarly, the binding energy of the Al 2p electron increase with increasing Al content on the surface (Fig. 17). There has been no systematic study of the change in Al 2p binding energy with the coordination environment around Al, but it can be noted that reported Al 2p binding energies for Al-hydroxides and Al-rich silicates such as imogolite and allophane are in the range of 74±0.3 eV. This binding energy range overlaps with binding energies for surfaces with high Al content. The correlation between binding energies for Si 2p and Al 2p electrons and Si and Al content

suggest that the proportion of Si-O-Si and Al-O-Al bridges on the surface increases with increasing Si and Al content, respectively.

This conclusion combined with the observed Al : Si ratio range of 1 to 3 suggests that with increasing Al content on the surface, the proportions of phyllosilicates such as imogolite or allophane increases. Hence, the nanometer-thick Al-enriched coatings may indicate a change in surface geochemical processes with increasing soil pH, and may represent the beginning stage of clay formation.

4.5 Significance of this study with respect to the fate of metal(loid)s and free Al in acid soils

The results above show that the role of surface coatings in contaminated acidic soils is an important factor in controlling the transport, retention and chemical transformation of hazardous metal(loid)s in acid soils. The incorporation of metal(loid)s during the formation of jarosite group minerals promoted by Si-rich Fe-hydroxide micro-coatings, and subsequent entombment of these minerals in a hardened silica-matrix control the retention and thereby the potential for release of metal(loid)s over time. In addition, the formation of Al-rich silicates due to a rise in pH over the last few decades has sequestered free Al and incorporated them into proto-clays. Hence, the mobility and phytotoxicity of Al in the current soils has been significantly reduced due to the formation of nanometer-thick coatings on soil grains. Therefore, this study has shown the significance of soil coatings with respect to the fate of metal(loid)s and free aluminum in acid soils, and so altered surfaces should be considered as a possible sink for metal(loid)s in contaminated acid soils worldwide.

5.0 CONCLUSIONS

Analysis of micrometer-thick coatings on mineral surfaces in contact with acid soils revealed the occurrence of Si rich (S I :Fe > 7), Fe-Si rich (Fe : Si = 1-7) and Fe rich coatings (Fe : Si <1). A comparative study of the metal(loid) distributions in these coatings indicated that

Fe-Si coatings on siliceous soil grains have higher trace-element concentrations than their Fe- and Si-enriched counterparts. This observation was explained with the incorporation of metal(loid)s and P in jarosite-group minerals during their formation in a silica gel-type matrix. The presence of jarosite-group minerals, schwertmannite, ferrihydrite, magnetite, goethite and hematite in coatings indicated that the transformation of the former to the latter minerals was inhibited by adsorbed silica species or by the entombment of these minerals in a hardened silica-matrix. Therefore, Si-rich Fe-hydroxide micro-coatings are not only effective in promoting the formation of jarosite-group minerals, they also preserve metal(loid)-bearing phases over a longer time period (and thus control the release of metal(loid)s). Characterization of nanometer-thick surfaces with XPS indicated that the upper 5.4 nm of surfaces on soil grains were enriched in Al with respect to the underlying minerals and micrometer thick coatings, and that the proportion of higher polymerized Al-phases (e.g. imogolite or allophane) increased with the Al content in these coatings. These observations suggested that Al-rich surfaces in the Sudbury soils were the result of an increase in soil pH during the last 20 years and might represent precursors for high Al first order clays. To summarize, this study showed that coatings on soil grains are effective sequestering agents for metal(loid)s and free Al in acid soils and that coatings in general may have a more significant effect on the behaviour and transport of metal(loid)s in soils than previously assumed.

6.0 REFERENCES

Acero P., Ayora C., Torrentó C., Nieto J-M. (2006). *The behavior of trace elements during schwertmannite precipitation and subsequent transformation into goethite and jarosite*, Geochimica et Cosmochimica Acta, 70:16, 4130‑4139.

Adamo P., Dudka S., Wilson M. J., McHardy W. J. (1996). *Chemical and mineralogical forms of Cu and Ni in contaminated soils from the Sudbury mining and smelting region, Canada*. Environ. Pollut. 91, 11–19.

Al-Hamden A.Z., Reddy K.R. (2008).*Transport and Speciation of Heavy Metals in Soils during Electrokinetic Remediation: Influence of Soil Type and Electric Potential*, Geocongress 2008.

Alloway B.J. (1990). *Soil processes and the behaviour of metals*. In B.J. Alloway (Ed.), Heavy metals in soils. New York: Wiley, 339. p.7-28.

Ashraf M.A., Maah M.J., Yusoff I. (2012).*Chemical Speciation and Potential Mobility of Heavy Metals in the Soil of Former Tin Mining Catchment*, The Scientific World Journal, 1-11.

Barabash S.J., Evans L.J., Gauthier J. (2011). *Development and Application of Adsorption Models for Arsenic, Copper and Nickel in Sudbury Area Soils*, Submitted to the Ontario Ministry of the Environment (Final Report).

Bigham J.M., Nordstrom D.K. (2000).*Iron and aluminum hydroxysulfates from acid sulfate waters.* Reviews in Mineralogy and Geochemistry, 40, (D.K. Nordstrom, Ed). Mineralogical Society of America, Washington DC. 351-402.

Blowes, D.W., Ptacek, C.J., 2003. Mill tailings hydrogeology and geochemistry. In: Jambor, J.L., Blowes, D.W., Ritchie, A.I.M. (Eds), Environmental Aspects of Mine Wastes. Mineralogical Association of Canada short Course Series 31, 95-116.

Burt R., Weber T., Park S., Yochum S.C., Ferguson R. (2011). *Trace Element Concentration and Speciation in Selected Mining-Contaminated Soils and Water in Willow Creek Floodplain, Colorado*, Applied and Environmental Soil Science, 1-20.

Burt R., Wilson M.A., Keck T.J., Dougherty B.D., Strom D.E., Lindahl J.A. (2003).*Trace element speciation in selected smelter-contaminated soils in Anaconda and Deer Lodge Valley, Montana, USA*, Advances in Environmental Research. 8, 51-67.

Casey W.H., Westrich H.R., Arnold G.W., Banfield J.F. (1989).*The surface chemistry of dissolving labradorite feldspar*, Geochim.Cosmochim.Acta. 53, 821–832.

Casey W.H., Westrich H.R., Banfield J.F., Ferruzzi G., Arnold G.W. (1993). *Leaching and reconstruction at the surface of dissolving chain-silicate minerals*. Nature, 366, 253–256

Chopin E.I.B., Alloway B.J. (2007). *Trace element partitioning and soil particle characterisation around mining and smelting areas at Tharsis, Ríotinto and Huelva, SW Spain*, Science of the Total Environment. 373, 488-500.

Chorover J., Kretzschmar R., Garcia-Pichel F., Sparks D.L. (2007). *Soil Biogeochemical Processes within the Critical Zone*, Elements, 3, 321-326.

Cornell R.M., Schwertmann U. (1996). *The Iron Oxides: Structure, Properties, Reactions, Occurences and Uses*, 13.2.7-Formation: Effect of Foreign Compounds.

Curtiss B., Adams J. B., Ghiorso M. S. (1985).*Origin, development and chemistry of silica-alumina rock coatings from the semiarid regions of the island of Hawaii*. Geochemica et Cosmochimica Acta, Vol. 49, 49-56.

David M.B., Driscoll C.T. (1984). *Aluminum speciation and equilibria in soil solutions of a Haplorthod in the Adirondack Mountains (New York, U.S.A.)*, Geotherma, 33:4, 297-318.

Davies, B. E. (1983). *Heavy metal contamination from base metal mining and smelting: Implications for man and his environment*. Appl. Environ. Geochem., 1, 425–462.

Doelsch E., Stone W. E. E., Petit S., Masion A., Rose J., Bottero J.Y., Nahon D. (2001). *Speciation and crystal chemistry of Fe(III) chloride hydrolyzed in the presence of SiO4 ligands. 2.Characterization of Si–Fe aggregates by FTIR and ^{29}Si solid state NMR*. Langmuir 17, 1399–1405.

Dube A., Zbytniewski R., Kowalkowski T., Cukrowska E., Buszewski B. (2001). *Adsorption and Migration of Heavy Metals in Soil*, Polish Journal of Environmental Studies. 10;1, 1-10.

Durocher J., Schindler M. (2011). *Iron-hydroxide, iron-sulfate and hydrous-silica coatings in acid-mine tailings facilities: A comparative study of their trace-element composition*, Applied Geochemistry. 26, 1337-1352.

Dutrizac J.E., JamborJ.L. (2000). *Jarosites and their Application in Hydrometallurgy,* Reviews in Mineralogy & Geochemistry. 40, 405-452.

Dyer L., Fawell P. D., Newman O. M. G., Richmond W. R.(2010).*Synthesis and characterization of ferrihydrite/silica coprecipitates.*J. Colloid Interface Sci. 348, 65–70.

Farmer V.C. Russell J.D., Berrow M.L. (1980). *Imogolite and proto-imogolite allophane in spodic horizons: evidence for a mobile aluminium silicate complex in podzol formation*. J. Soil Sci. 31, 673-684.

Faure G. (1998). *Principles and applications of geochemistry: a comprehensive textbook for geology students*. Prentice Hall, 2nd Ed.

Freedman B., Hutchinson T. C. (1980).*Pollutant inputs from the atmosphere and accumulations in soils and vegetation near a nickel–copper smelter at Sudbury, Ontario, Canada*, Canadian Journal of Botany. 58, 108–132.

Giorgetti G., Baroni C. (2007). *High-resolution analysis of silica and sulphate-rich rock varnishes from Victoria Land (Antarctica)*. European Journal of Mineralogy, 19, 381-389.

Gregurek D., Reimann C., Stumplf E. F. (1998). *Mineralogical fingerprints of industrial emissions—an example from Ni mining and smelting on the Kola Peninsula, NW Russia*, Science Total Environ. 221, 189–200.

Gregurek D., Melcher F., Pavlov V. A., Reimann C., Stumpfl E. F. (1999). *Mineralogy and mineral chemistry of snow filter residues in the vicinity of the nickel–copper processing industry, Kola Peninsula, NW Russia*. Mineralogy and Petrology, 65, 87–111.

Hamilton J.P., Brantley S.L., Pantano C.G., Criscenti L.J., Kubicki J.D. (2001). *Dissolution of nepheline, jadeite and albite glasses: Toward better models for aluminosilicate dissolution*, Geochimica et Cosmochimica Acta, Vol. 65:21, 3683–3702.

Haynes R.J., Mokolobate M.S. (2001). *Amelioration of Al toxicity and P deficiency in acid soils by additions of organic residues: a critical review of the phenomenon and the mechanisms involved*, Nutrient Cycling in Agroecosystems, 59:1, 47-63.

Hellman R., Wirth R., Daval D., Barnes J-P., Penisson J-M., Tisserand D., Epicier T., Florin B., Hervig R.L. (2012). *Unifying natural and laboratory chemical weathering with interfacial dissolution–reprecipitation: A study based on the nanometer-scale chemistry of fluid–silicate interfaces,* Chemical Geology, 280:1-2.

Hellman R., Penisson J-M., Hervig R.L., Thomassin J-H., Abrioux M-F. (2003). *An EFTEM/HRTEM high-resolution study of the near surface of labradorite feldspar altered at acid pH: evidence for interfacial dissolution-reprecipitation*, Phys Chem Minerals, 30: 192–197.

Hetzel F., McColl J.G. (1997).*Silicon, aluminum, and oxalic acid interactions in two California forest soils,* Communications in Soil Science and Plant Analysis. 28;13-14.

Hochella M.F.Jr., Eggleston C.M., Lindsay J.R., Mossotti M.G. (1988). *Sputter depth profiling in mineral-surface analysis*, American Mineralogist, 73:11-12, 1449-1456.

Huang W. H., Keller W.D. (1973). *New stability diagrams of some phyllosilicates in the SiO_2-Al_20_3-K_20-H_20 system*. Clays & Clay Minerals, 21, 331-336.

Hutchinson T. C., Whitby L. M. (1974).*Heavy-metal pollution in the Sudbury mining and smelting region of Canada, I. Soil and vegetation contamination by nickel, copper, and other metals*, Environmental Conservation. 1, 123–131

Isambert T., De Resseguier A., Gloter B., Reynard F., Guyot J., Valet P. (2006). *Magnetite-like nanocrystals formed by laser-driven shocks in siderite*, Earth and Planetary Science Letters, 243:3–4, pp.820-827.

Jambor J.L., Blowes D.W. (2000). *Mineralogy of mine wastes and strategies for remediation,* Vaughan D.J., Wogelius R.A (Eds*),* Environmental Mineralogy, EMU (European Mineralogical Union) Notes Mineral, 2, 255-290.

Jones A.M., Collins R.N., Rose J., Waite T.D. (2009). *The effect of silica and natural organic matter on the Fe(II)-catalysed transformation and reactivity of Fe(III)minerals*. Geochim.Cosmochim.Acta 73, 4409–4422.

Kalinowski B.E., Schweda P. (1996). *Kinetics of muscovite, phlogopite and biotite dissolution and alteration at pH 1-4, room temperature*. Geochim.Cosmochim. Acta 60, 367–385.

Lanteigne S., Schindler M., McDonald A.M., Skeries K., Abdu Y., Mantha M., Murayama M., Hawthorne F.C., Hochella M.F.Jr. (2012).*Mineralogy and Weathering of Smelter-Derived Spherical Particles in Soils: Implications for the Mobility of Ni and Cu in the Surficial Environment*. Journal of Water, Air and Soil Pollution, 223:7, 3619-3641.

Lanteigne S., Schindler M., McDonald A.M. (2013). *Distribution of Metals and Metalloids in Particulate Matter in Soils,* Part 1 of this thesis.

Ma L.Q., Rao G.N. (1997). *Chemical Fractionation of Cadmium, Copper, Nickel, and Zinc in Contaminated Soils*, Journal of Environmental Quality.26;1, 259-264.

Majzlan J., Myneni S.C.B. (2005).*Speciation of iron and sulfate in acid waters: Aqueous clusters to mineral precipitates*. Environmental Science and Technology, 39, 188-194.

Manceau A., Marcus M.A., Tamura N., Proux O., Geoffroy N., Lanson B. (2004). *Natural speciation of Zn at the micrometer scale in a clayey soil using X-ray fluorescence, absorption, and diffraction*, Geochimica and Cosmogeochimica Acta, 68(11), 2467-2483.

Mantha N.M., Schindler M., Murayama M. and Hochella M.F.Jr. (2012a).*Silica- and sulfate-bearing rock coatings in smelter areas: Products of chemical weathering and atmospheric pollution I. Formation and mineralogical composition.*Geochimica et Cosmochimica Acta, 85, 254-274.

Mantha N.M., Schindler M.,Kyser T.K. (2012b) *Silica- and sulfate-bearing rock coatings insmelter areas: Part II. Forensic tools for atmospheric metal(loid)- and sulfur-isotope compositions*, Geochimica et Cosmochimica Acta, 90:1, 221‑241.

Mayer T.D., Jarrell W.M. (1996). *Formation and stability of iron(II) oxidation products under natural concentrations of dissolved silica*. Water Res. 30, 1208–1214.

Mazzetti L., Thistlethwaite P.J. (2002). *Raman spectra and thermal transformations of ferrihydrite and schwertmannite*, Journal of Raman Spectroscopy.33,104-111.

McNear D. H. Jr., Chaney R. L., & Sparks D. L. (2007). *The effects of soil type and chemical treatment on nickel speciation in refinery enriched soils: A multi-technique investigation*, Geochim. Cosmochim.Acta. 71, 2190–2208

Meadows M., Watmough S.A. (2012).*An Assessment of Long-term Risks of Metals in Sudbury: A Critical Loads Approach,* Journal of Water, Air, and Soil Pollution. 223:7, 4343-4354.

Minitti M. E., Weitz C. M., Lane M. D., and Bishop J. L. (2007).*Morphology, chemistry, and spectral properties of Hawaiian rock coatings and implications for Mars*. Journal of Geophysical Research, 112.

Motelica-Heino M., Rauch S., Morrison G.M., Donard O.F.X. (2001).*Determination of palladium, platinum and rhodium concentrations in urban road sediments by laser ablation-ICP-MS*, Analytica Chimica Acta, 436, 233-244.

Nriagu J.O., Pacnya J.M. (1988). *Quantitative Assessment of Worldwide Contamination of Air, Water and Soils by Trace Metals,* Nature. 338, 47-49.

Nugent M.A., Brantley S.L., Pantano C.G., Maurice P.A. (1998). *The influence of natural mineral coatings on feldspar weathering,* Nature, 395:588-591.

Samac D.A., Tesfaye M. (2003). *Plant improvement for tolerance to aluminium in acid soils—a review.* Plant Cell Tissue Organ Cult 75: 189–207

Sargent D.G. (1996). *The response of the terrestrial ecosystem at Sudbury, Ontario to 20 years of reduced smelter pollution*, M.Sc. thesis, Trent University, Peterborough, Ont.

Schiffman P., Zierenberg R., Marks N., Bishop J.L., Dyar M.D. (2006). *Acid-fog deposition at Kilauea volcano: A possible mechanism for the formation of siliceous-sulfate rock coatings on Mars*, Geology,34(11), 921– 924.

Schindler M., Ilton E.S. (2013).*Uranium mineralogy and geochemistry on the nano-to micrometer scale: redox, dissolution and precipitation processes at the mineral water interface*. Uranium - Cradle to Grave, MAC Short Course 43 Eds. Burns P.C., Sigmon G.E. Mineralogical Association of Canada (in press).

Schindler M., Fayek M., Hawthorne F.C. (2010).*Uranium-rich opal from the Nopal I uranium deposit, Pena Blanca, Mexico: Evidence for the uptake and retardation of radionuclides*, Geochimica et Cosmochimica Acta, 74,187-202.

Schindler M., Durocher J., Abdu Y., Hawthorne F.C. (2009). *Hydrous Silica Coatings: Occurrence, Speciation of Metals, and Environmental Significance*, Environ. Sci. Technol., 43 :23, 8775–8780.

Schweda P.,Sjöberg L.,Södervall U. (1997). *Near-surface composition of acid-leached labradorite investigated by SIMS*, Geochimica et Cosmochimica Acta, 61:10,1985‑1994.

Schwertmann U., Thalmann H. (1976). *The influence of Fe(II) and Si and pH on the formation of lepidocrocite and ferrihydrite during the oxidation of aqueous $FeCl_2$ solutions*. Clay Mineral. 11, 189–200.

Shaikh M., Moleele N., Ekosse G.I.E., Totolo O., Atlhopheng J. (2006). *Soil Heavy Metal Concentration Patterns at Two Speed Zones along the Gaborone-Tlokweng Border* Post Highway, Southeast Botswana, J. Appl. Sci. Environ. Mgt, 10 (2) 135 – 143.

Sigg L., Stumm W. (1981). *The interaction of anions and weak acids with the hydrous goethite (a-FeOOH) surface*, Colloid Surf. 2, 101–117.

Stillings L.L., Brantley S.L. (1995). *Feldspar dissolution at 25ºC and pH 3: reaction stoichiometry and the effect of cations*. Geochimica and Cosmogeochimica Acta, 59, 1483-1496.

Stumm W. (1992).*Chemistry of the solid-water interface.* John Wiley & Sons, Inc. New York.

Sumner M.E., Fey M.V., Noble A.D. (1991). *Nutrient status and toxicity problems in acid soils*, Soil Acidity, p.149-182.

Swedlund P. J., Miskelly G. M. McQuillan A. J. (2009).*An attenuated total reflectance IR study of silicic acid adsorbed onto a ferric oxyhydroxide surface*. Geochim.Cosmochim.Acta, 73, 4199–4214

Teng H.H., Fenter P., Cheng L.,Sturchio N.C. (2001).*Resolving orthoclase dissolution processes with atomic force microscopy and X-ray reflectivity*, Geochimica et Cosmochimica Acta, 65:20,3459‑3474.

Terzano R., Spagnuolo M., Vekemans B., De Nolf W., Janssens K., Falkenberg G., Fiore S., & Ruggiero P. (2007). *Assessing the Origin and Fate of Cr, Ni, Cu, Zn, Pb, and V in Industrial Polluted Soil by Combined Micro-spectroscopic Techniques and Bulk Extraction Methods*, Environ. Sci. and Technol. 41, 6762-6769.

Thiagarajan N., and Lee C.A. (2004). *Trace-element evidence for the origin of desert varnish by direct aqueous atmospheric deposition*. Earth and Planetary Science Letters, 224, 131-141.

Tosca, N.J., McLennan, S.M., Lindsley, D.H., and Schoonen, M.A., 2004, *Acid-sulfate weathering of synthetic Martian basalt: The acid fog model revisited,* Journal of Geophysical Research, 109.

Vazquez Martinez O.C. (2011). *Effects of Acid Mine Drainage on the Release of Aluminum from Clay Minerals*, PhD Dissertation.

Voegelin A., Weber F.A., Kretzschmar R. (2004). *Distribution and speciation of arsenic around roots in a contaminated riparian floodplain soil: Micro-XRF element mapping and EXAFS spectroscopy*, Geochimica and Cosmochimica Acta, 71, 5804–5820.

Wagner C.D., Riggs W.M., Davis L.E., Moulder J. (1979). *Handbook of X-ray Photoelectron Spectroscopy*, Physical Electronics, G. E. Muilenberg, Perkin Elmer Corporation, 1st edition.

Whitby L. M., Stokes P. M., Hutchinson T. C., Myslik G. (1976). *Ecological consequence of acidic and heavy-metal discharges from the Sudbury smelters*, The Canadian Mineralogist. 14, 47–57.

Williamson B.J., Har N., Purvis W.O., Rusu A.M. (2003). *Preliminary Studies of Airborne Particulate Emissions from the Ampellum S.A Copper Smelter, Zlatna, Romania*, Studia UBB, Geologia. 48;1, 67-76.

Winterhalder, K. (2002). *The effects of the mining and smelting industry on Sudbury's landscape (chapter 7),* The physical environment of the City of Greater Sudbury, D.H. Rousell and K.J. Jansons (eds*),* OGS special Vol 6.

Wren C. (2012*). Risk assessment and environmental management: A case study in Sudbury, Ontario, Canada,* Progress in Environmental Science, Technology and Management. 1, 1–450.

Yahaya M.I., Ezeh G.C., Musa Y.F., Mohammad S.Y. (2010).*Analysis of heavy metals concentration in road sides soil in Yauri, Nigeria*, African Journal of Pure and Applied Chemistry. 4;3, 22-30.

Zhu C., Veblen D.R., Blum A.E., Chipera S.J. (2006). *Naturally weathered feldspar surfaces in the Navajo Sandstone aquifer, black mesa, Arizona: electron microscopic characterization*. Geochim.Cosmochim.Acta 70, 4600–4616.

Table 1.Major phases and their modal abundances (vol %) in the soils of the Falconbridge (Fal), Coniston (Co) and Copper Cliff (CC) areas.

Phase	Fal	Co	CC
Quartz	56.2	64.7	50.7
Feldspar mainly Plagioclase	39.4	26.9	39.4
Actinolite	1.9	2.4	5.3
Muscovite	0.7	4.6	3.5
Chlorite	1.9	1.4	1.1

Table 2.Trace element composition of the soil samples in [$mgkg^{-1}$], concentrations measured after complete dissolution of the samples (full digest) are labelled *total* and concentrations measured after aqua regia digest are labelled *soluble*.

sample	CO2A	CO5A	CO8A	FB1A	FB3A	FB5A	CC1A	CC2A	CC3A
pH		5.8			5.3			4.5	
$S^*_{soluble}$	300	200	300	300	100	800	300	200	1200
$P_{soluble}$	655	224	479	466	248	976	522	523	462
$Mn_{soluble}$	299	100	309	125	378	344	222	307	266
Co_{total}	50	293	48	30	74	30	50	770	42
$Co_{soluble}$	11	5	47	17	9	16	18	7	32
Ni_{total}	878	5149	769	132	288	420	640	1969	313
$Ni_{soluble}$	103	91	88	60	31	66	265	39	269
Cu_{total}	1192	3326	989	89	196	182	787	1595	448
$Cu_{soluble}$	80	89	87	81	92	46	384	66	372
Zn_{total}	63	287	66	105	146	44	51	134	49
$Zn_{soluble}$	42	13	44	41	36	39	49	34	47
$As_{soluble}$	5	3	6	4	7	24	21	3	12
$Se_{soluble}$	0.4	0.5	0.6	0.5	0.3	1.2	5.1	0.3	2.6
$Cd_{soluble}$	0.3	0.1	0.3	0.5	0.2	0.9	0.5	0.2	0.3
Pb_{total}	50	154	37	12	3	17	32	99	36
$Pb_{soluble}$	15	4	13	8	16	14	24	6	23

*estimated uncertainty ±100 $mgkg^{-1}$

Table 3. Range in chemical composition of the micrometer-thick coatings

Element	SiOx [wt%]	Fe-SiOx [wt%]	FeOx [wt%]
Na	0.06 – 4.16	0.1 - 4.71	0.2 – 0.79
Mg	0.14 – 1.29	0.24 - 2.56	0.13 – 0.47
Al	9.3 – 32.2	5.71 - 13.2	3.75 – 7.62
Si	9.35 – 25.3	13.0 - 27.8	3.89 – 18.3
P	0.05 – 0.51	0.05 - 0.74	0.18 – 1.65
S	0.14 – 1.15	0.05 – 0.51	0.053 – 0.073
K	0 – 1.71	0.56 – 1.84	0.11 – 1.84
Ca	0.19- 1.12	0.54 – 3.50	0.93 – 1.49
Fe	0.49 – 11.4	4.26 – 18.96	24.52- 45.6
	SiOx [$mgkg^{-1}$]	Fe-SiOx [$mgkg^{-1}$]	FeOx [$mgkg^{-1}$]
Cr	43.3 – 179.04	70 - 329.2	195.8 – 317.3
Mn	47.3 – 2983.4	208.1 – 3690	208.1 – 27112.0
Co	0.59 – 33.6	21.7 – 364.8	45.8 – 364.8
Ni	7.3 – 1019.5	49.8 – 6208.8	549.2 – 1194.5
Cu	67.4 – 396.6	311.7 – 15948.9	638.6 – 1035.8
Zn	20.2 – 271.3	44.8 – 388.4	135.9 – 552.0
As	9.04 – 412.6	10.3 – 911.9	114.0 – 2544.4
Se	0.53 – 24.4	7.1 – 44.7	7.5 – 12.02
Cd	0 – 1.46	0.13 – 9.15	0.76 – 61.6
Pb	8.21 – 102.8	20.5 – 381.5	65.9 – 831.4

7.0 FIGURE CAPTIONS

Figure 1. Map of the Sudbury area, depicting the locations of smelters, and soil sample sites (Modified from Lanteigne et al, 2012).

Figure 2. SEM backscatter image (a) showing the location of a laser ablation transect (A-B) and the distribution of Fe and Si (b). Also shown are laser ablation line scans showing element distributions for Si, Na, Fe, Co, Ni, Cu, Zn, As, and Pb in an Fe-SiOx coating overlying an albite grain.

Figure 3. A-Optical image showing secondary phases on a mineral grain; B-SEM image showing and altered surface with visible particles within.

Figure 4. Diagram showing: A-Ternary diagram showing Si, Fe, Al distribution of micrometer thick coatings, and B-A graph showing the abundance of FeOx, Fe-SiOx and SiOx coatings based on their Si:Fe ratios.

Figure 5. A-An SEM Backscatter image of magnetite and goethite particles in an FeOx coating and B-Raman spectrum of an FeOx coating compared to a magnetite reference material (Isambert et al, 2006).

Figure 6. a) An SEM element map showing the distribution of Si (red) and Fe (green) in an FeOx coatings on an Fe-hydroxide, b) A high resolution image of alteration in the Fe-hydroxide matrix showing bright inclusions and c) Element distribution in a laser-ablation traverse (A-B).

Figure 7. A- SEM element map showing the distribution of Si (red) and Fe (green) in an Fe-SiOx coating on a silicate, B-Raman spectrum for an Fe-SiOx coating, and C+D-Reference spectra for Schwertmannite and Hematite+Maghemite respectively (Mazzetti and Thistlethwaite, 2002).

Figure 8. A- Raman spectrum of an Fe-SiOx coating compared to B-A reference spectrum for jarosite (Wang et al, 1998).

Figure 9. a) SEM backscatter image of an Fe-silicate with multiple coatings and b) corresponding laser ablation ICP-MS element distribution maps for Fe, Co, Ni, Cu, As and Pb.

Figure 10. µXRF element distribution maps for Fe, Cu, Co, Zn and Ni in 1-an Fe-silicate, 2-An FeOx coating, 3-An Fe-SiOx coating and 4-Epoxy. Also shown is an SEM-EDS image showing the distribution of Fe and Si in the 4 zones.

Figure 11. A-Optical image of a K-feldspar grain coated with secondary phases showing the location of a laser ablation transect (A-B) and b) Corresponding laser ablation line scans showing element distributions for Si, K, Fe, Co, Ni, Cu, Zn, As, and Pb in Fe-SiOx and SiOx coatings overlying an orthoclase grain.

Figure 12. a)-d): Plots of As, Se, Pb, and Cu in function of Si:Fe ratios.

Figure 13. a) Ternary diagram showing Si, Fe and Al distribution in nanometer surface coatings and underlying grains and b) A plot showing Al enrichment in surface coatings with respect to the underlying minerals.

Figure 14. a) XPS map for Si of a grain associated with surface Cu and b) corresponding XPS spectrum of Cu 2p doublet.

Figure 15. a) Laser ablation element distribution map showing for phosphorous, b) Diagram showing origin of elements found within coatings, and c-h) models showing different observed scenarios for coatings on mineral grains.

Figure 16.a)-d) Plots of Fe, Zn, Pb, and Cu in function of As+P.

Figure 17. a) Ternary plot showing Si, Fe and Al concentrations for nanometer thick coatings and b) corresponding XPS spectra for Si 2p (1-2) and Al 2p (3-4).

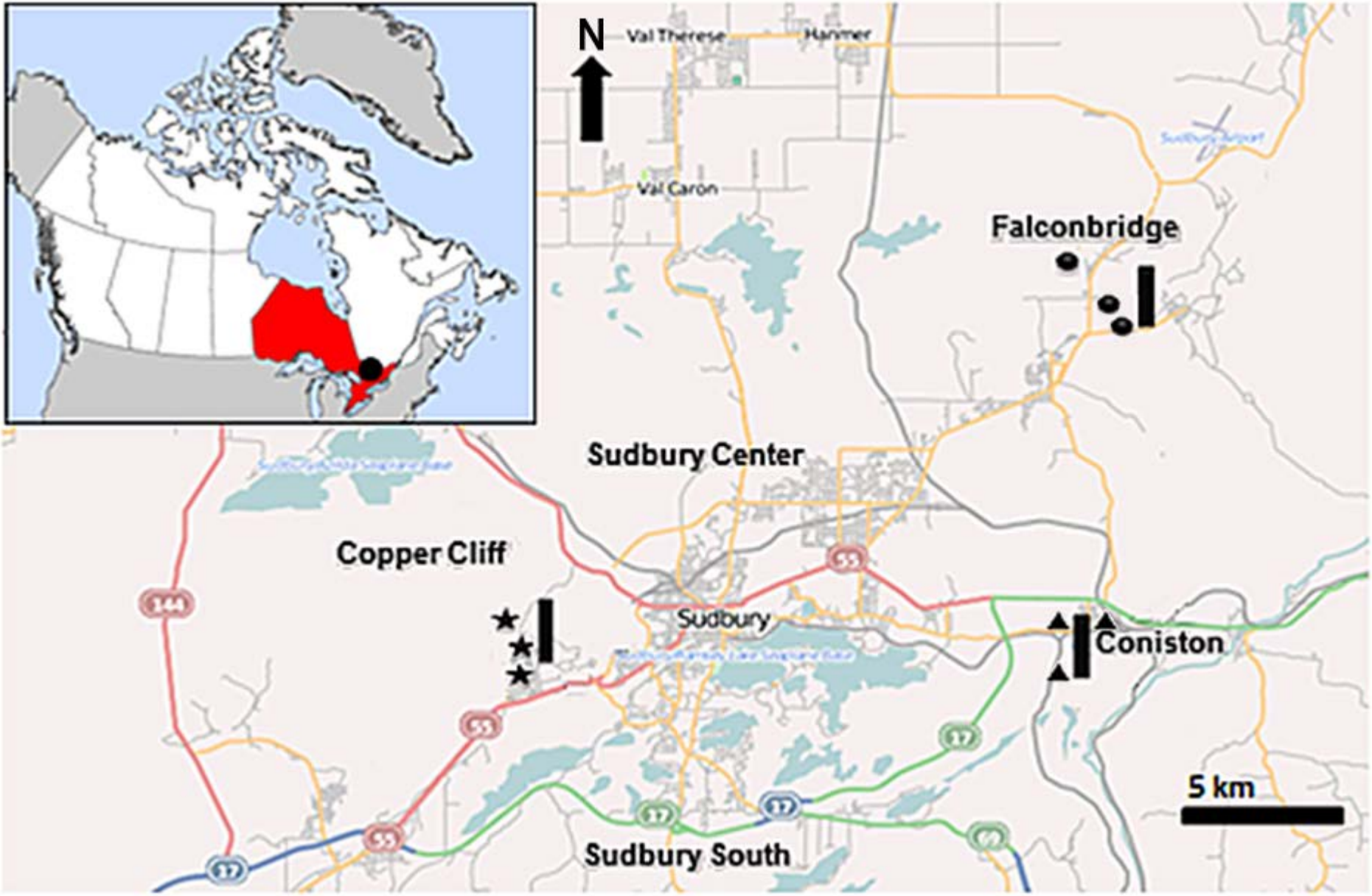
N
Val Therese
Hanmer
Val Caron
Falconbridge
Sudbury Center
Copper Cliff
Sudbury
Coniston
Sudbury South
5 km

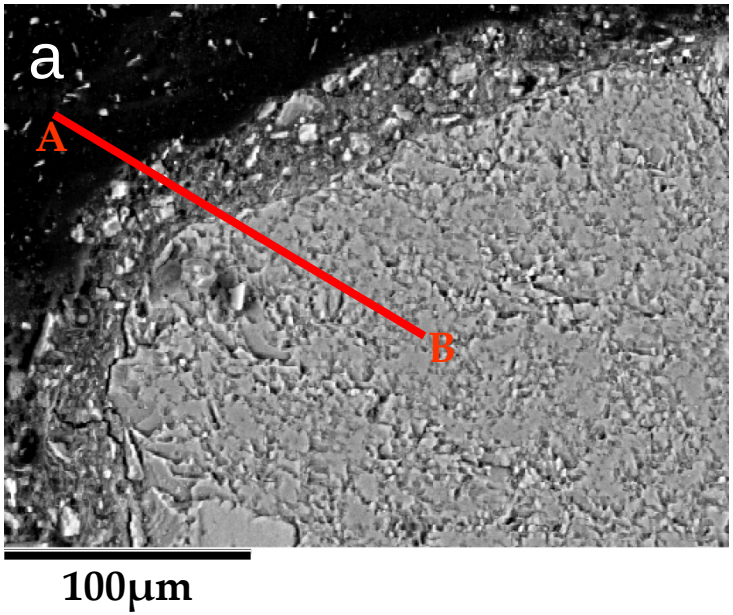
a
A
B
100µm

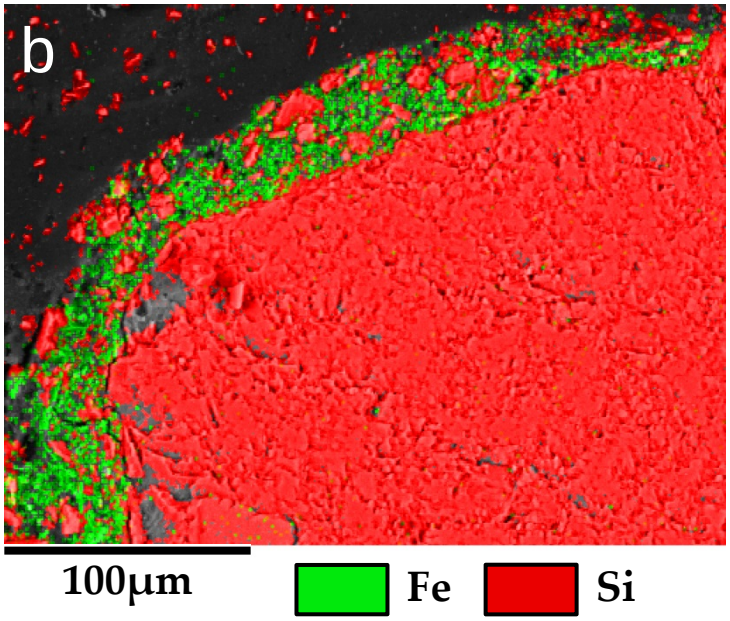
b
100µm
Fe
Si

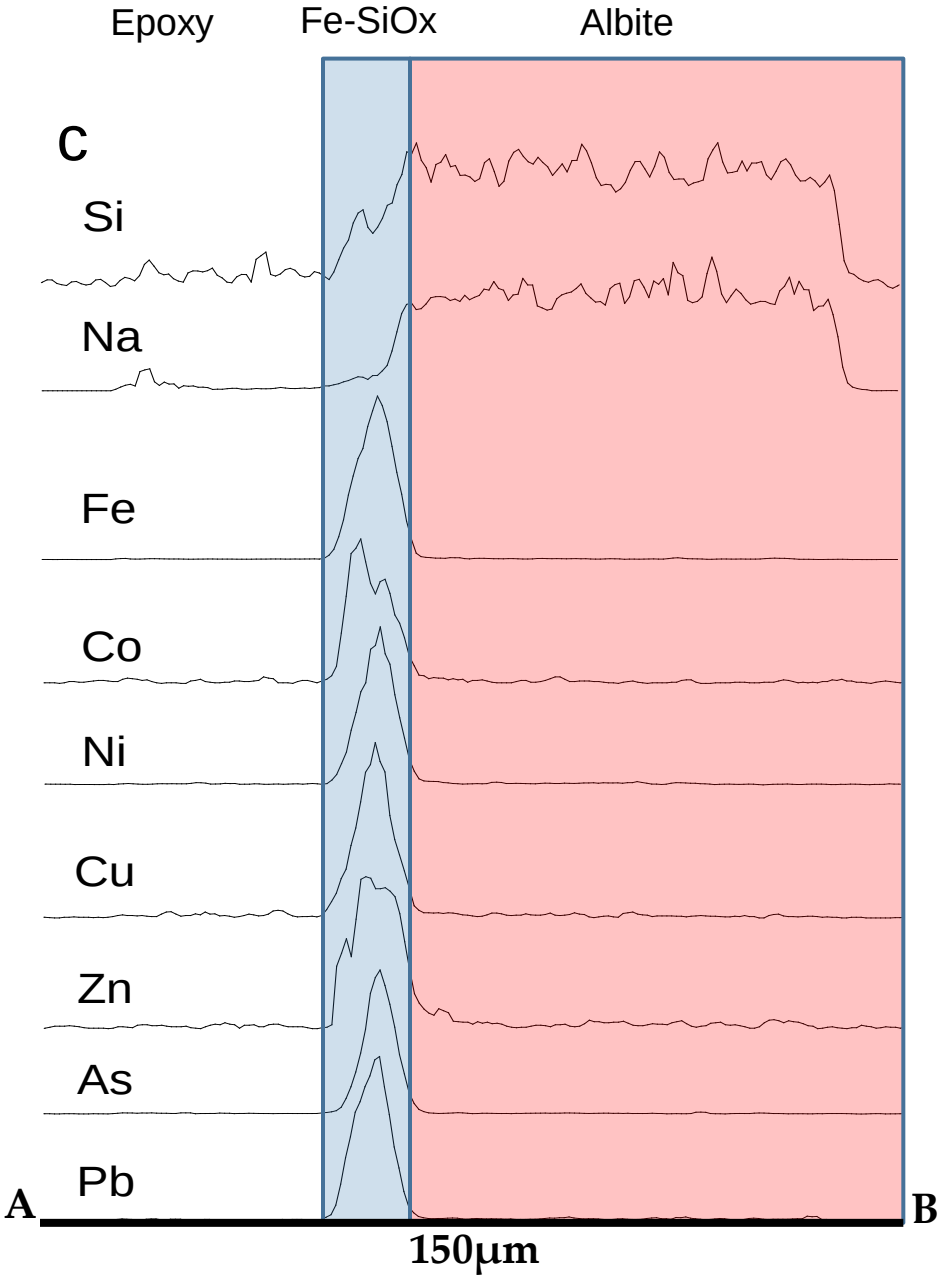
Epoxy
Fe-SiOx
Albite
c
Si
Na
Fe
Co
Ni
Cu
Zn
As
Pb
A
B
150µm

A

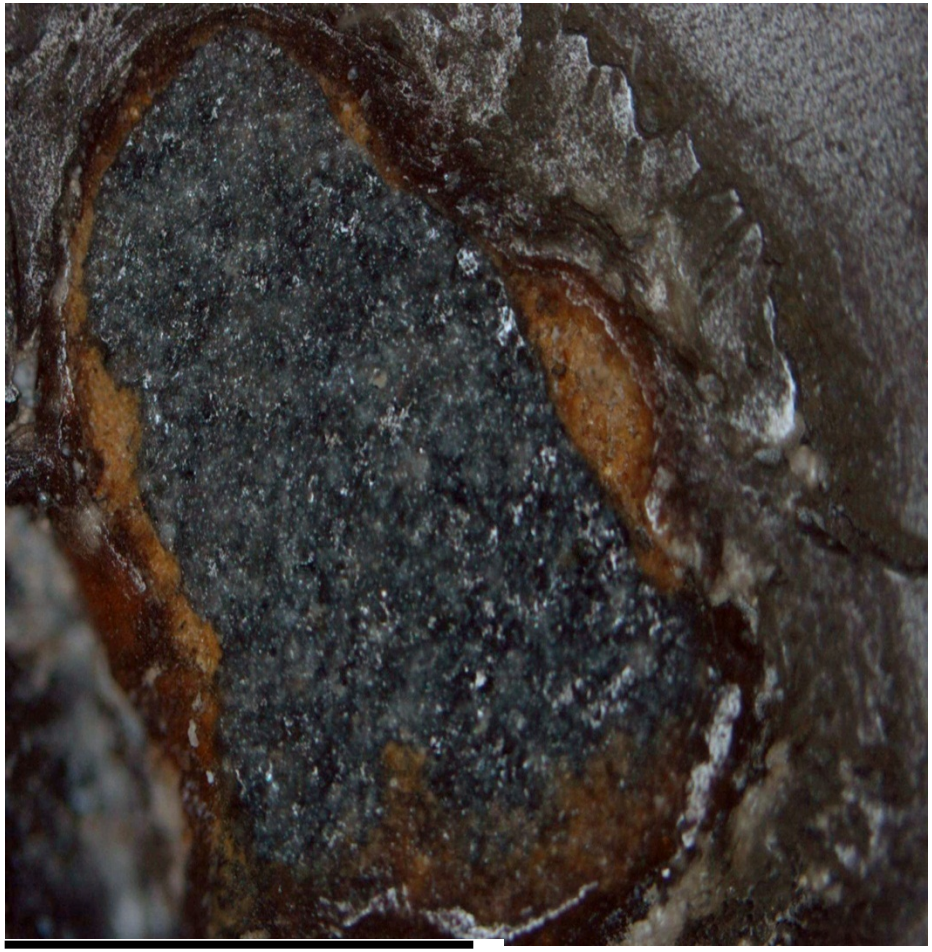

1mm

B

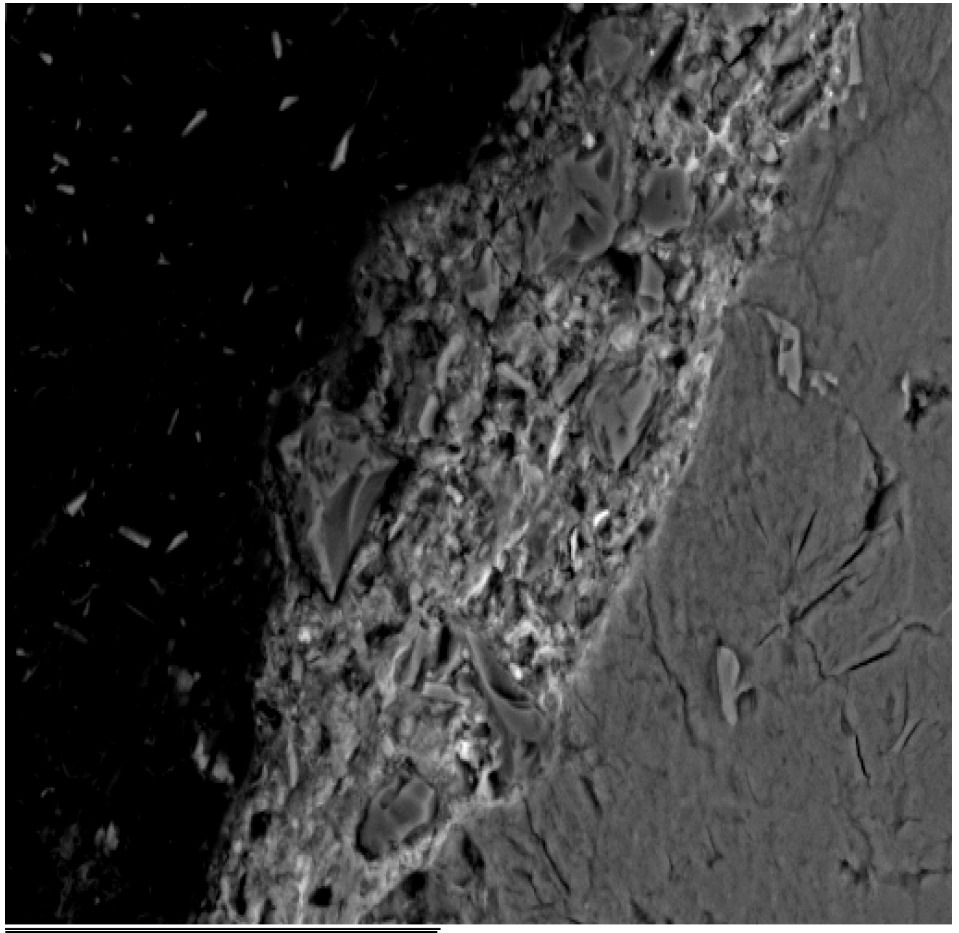

90µm

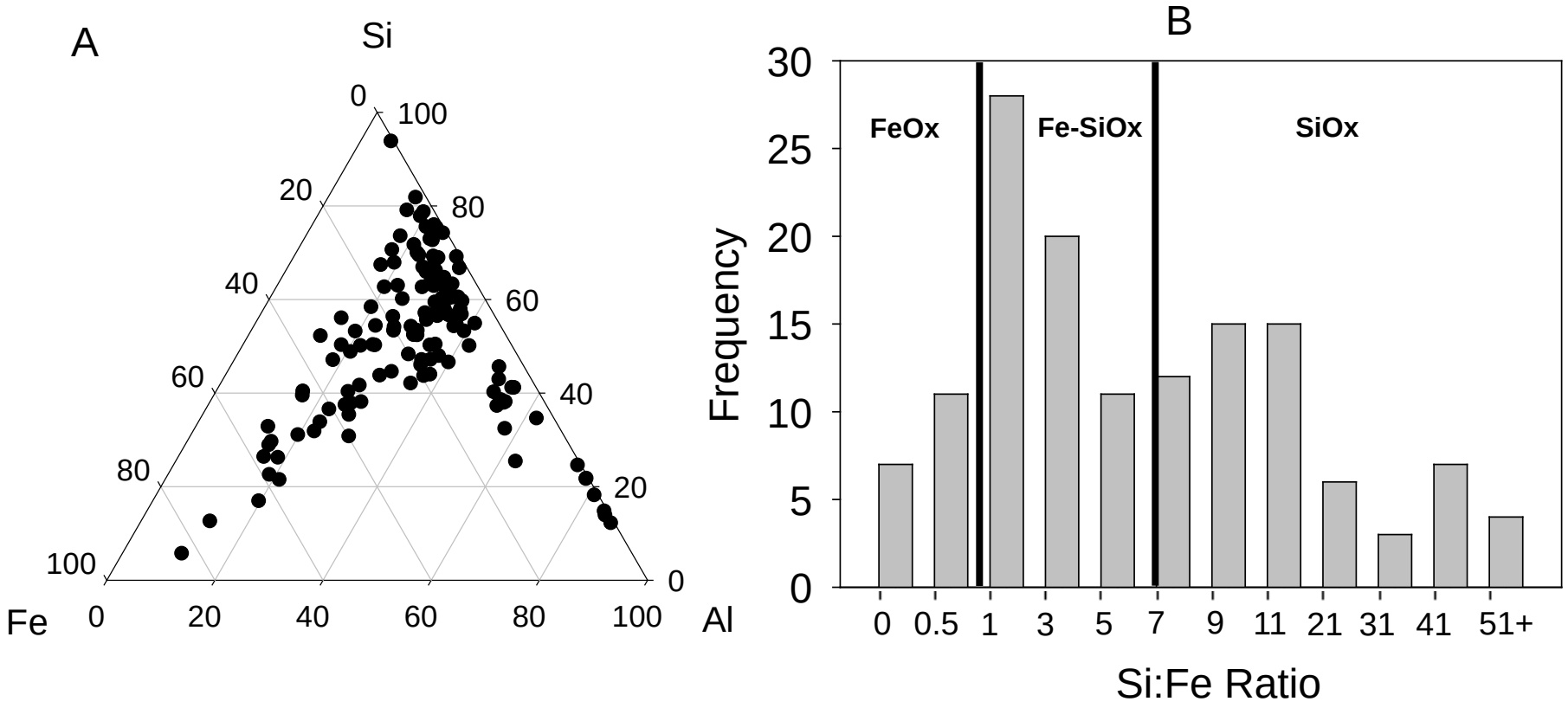
A
Si
0
100
20
80
40
60
60
40
80
20
100
0
Fe
0
20
40
60
80
100
Al
B
Frequency
30
25
20
15
10
5
0
FeOx
Fe-SiOx
SiOx
0
0.5
1
3
5
7
9
11
21
31
41
51+
Si:Fe Ratio

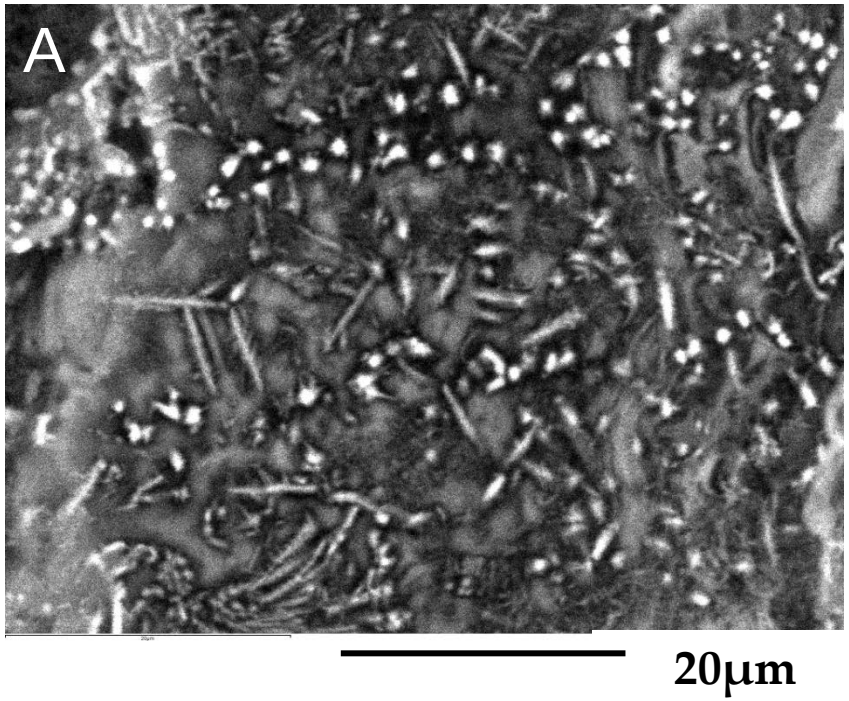
A
20μm
B
FeOx
Coating
Magnetite
1600
1400
1200
1000
800
600
400
200

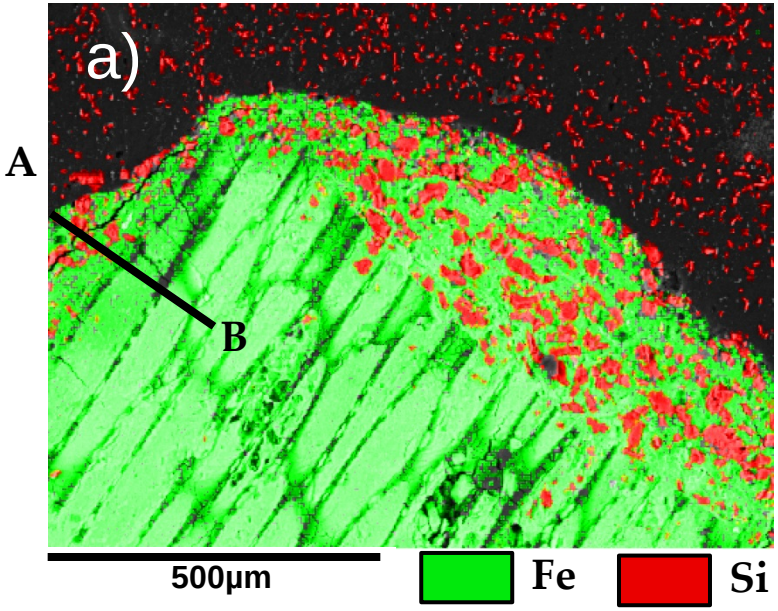
a)
A
B
500µm
Fe
Si

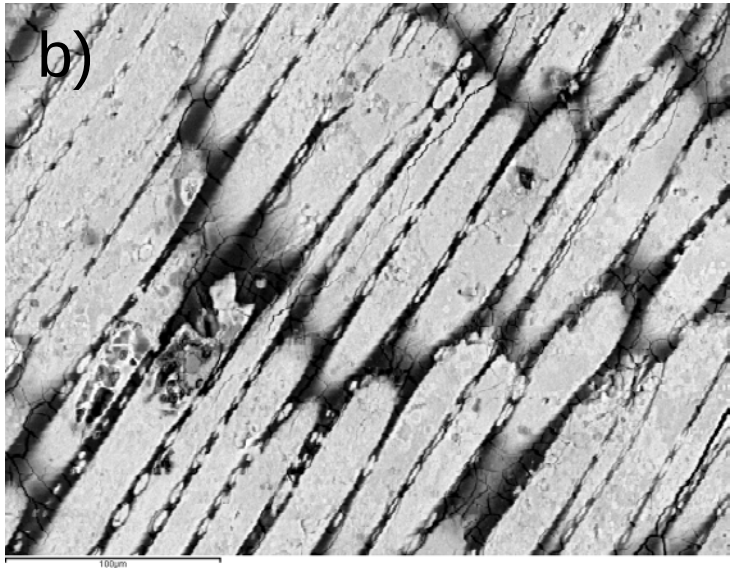
b)

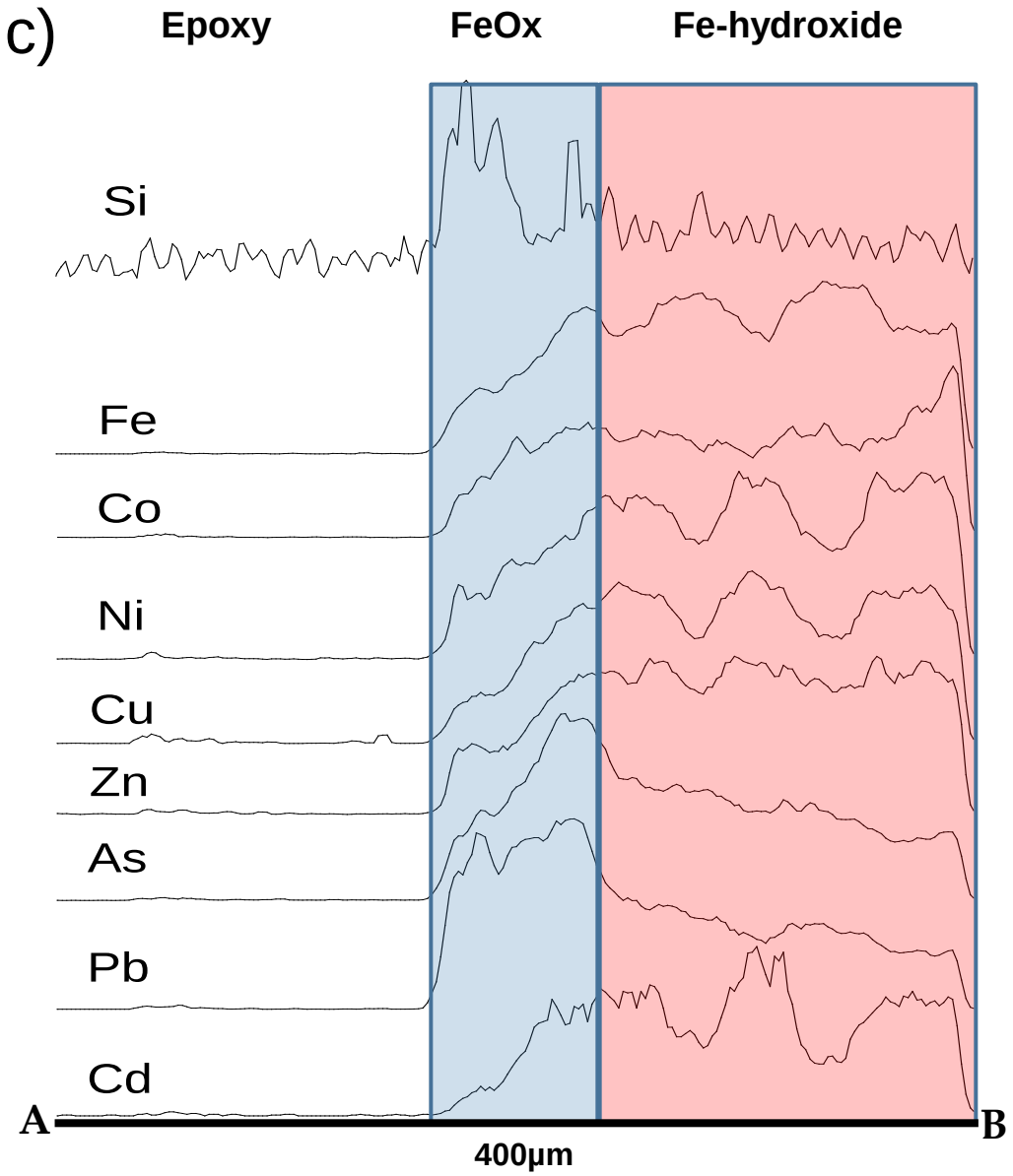
c)
Epoxy
FeOx
Fe-hydroxide
Si
Fe
Co
Ni
Cu
Zn
As
Pb
Cd
A
B
400µm

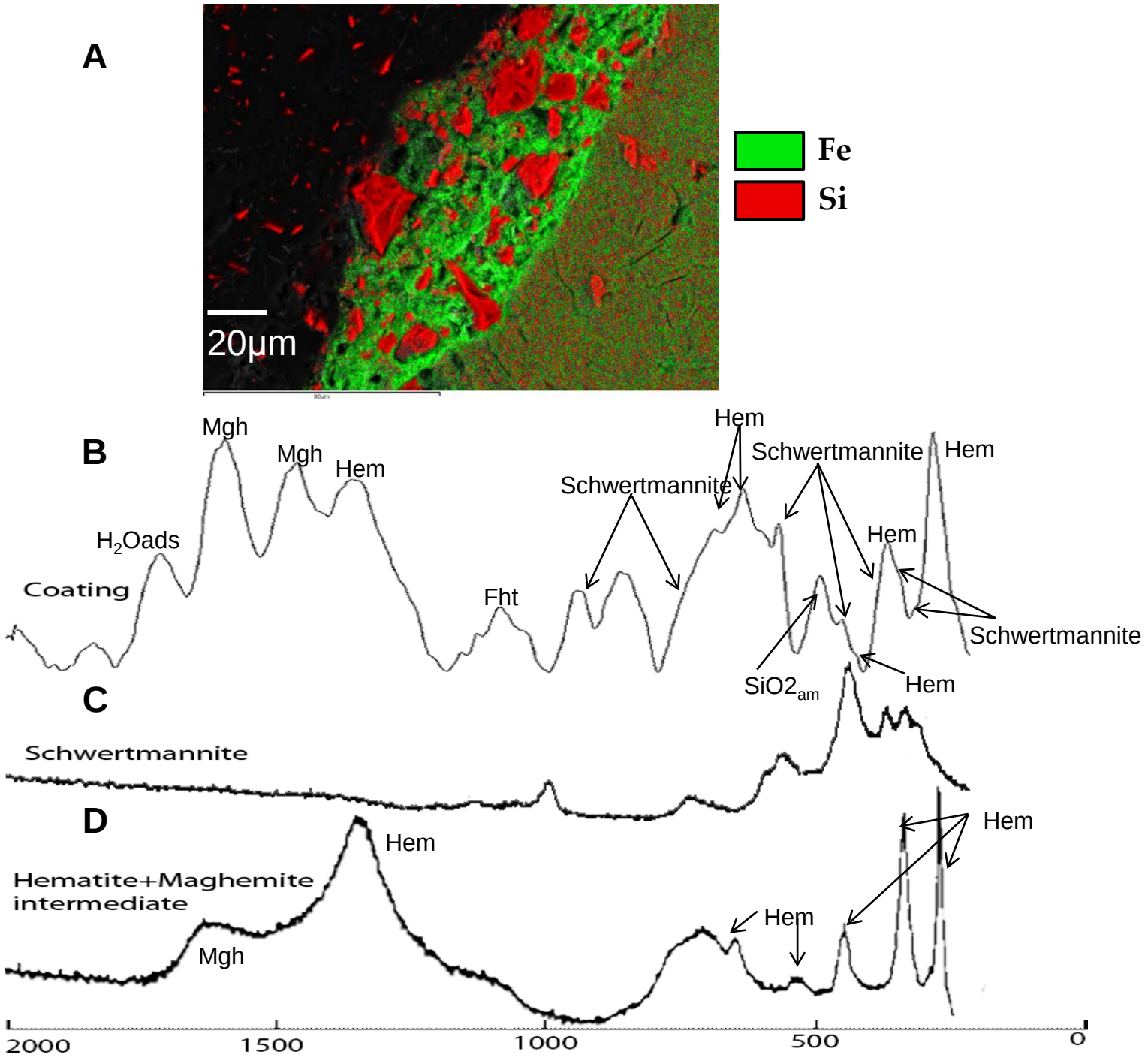
A
20µm
Fe
Si
B
Mgh
Mgh
Hem
Hem
Schwertmannite
Schwertmannite
Hem
H2Oads
Coating
Fht
Hem
Schwertmannite
SiO2am
Hem
C
Schwertmannite
D
Hem
Hematite+Maghemite
intermediate
Mgh
Hem
Hem
2000
1500
1000
500
0

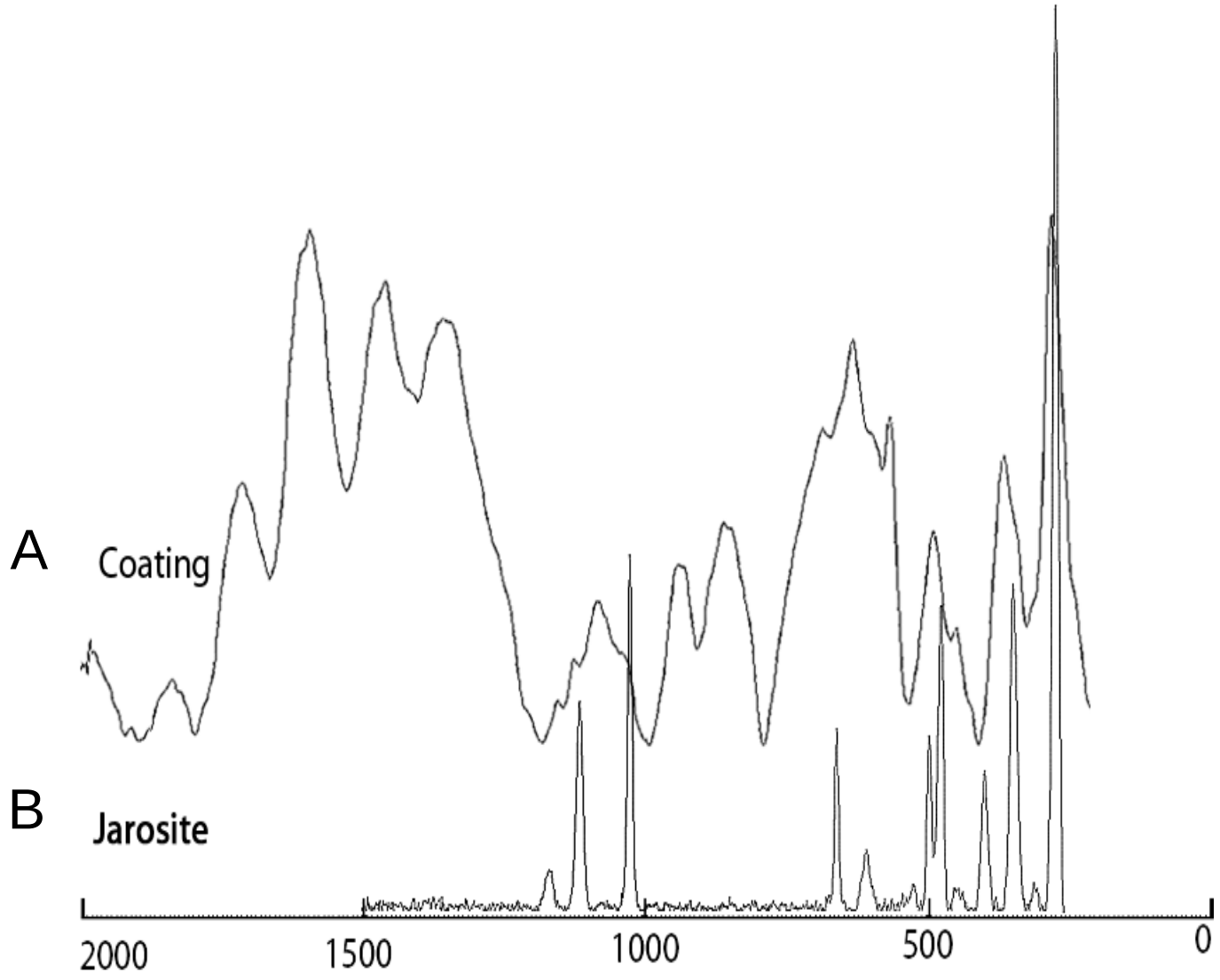
A
Coating
B
Jarosite
2000
1500
1000
500
0

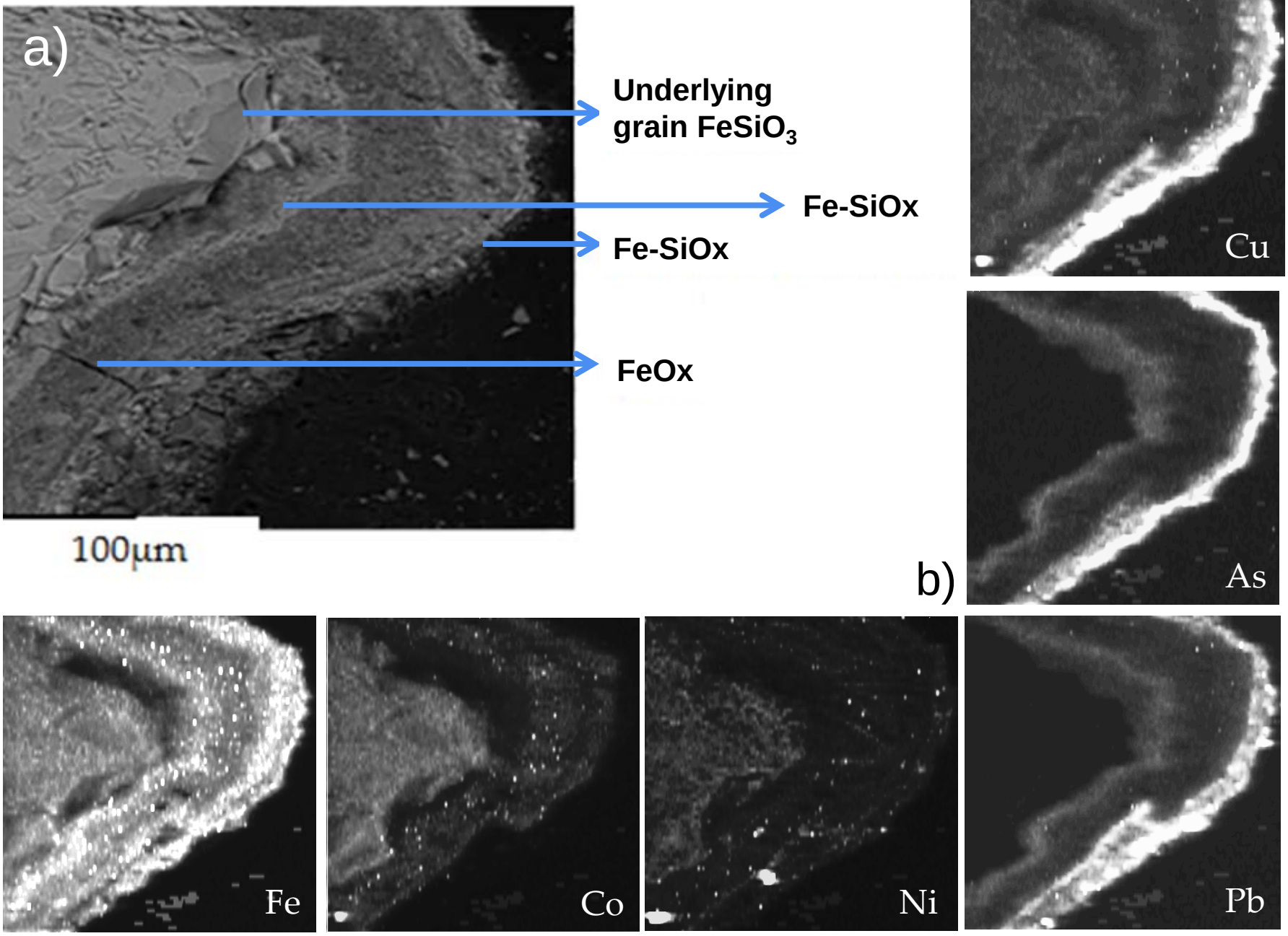
a)
Underlying grain $FeSiO_3$
Fe-SiOx
Fe-SiOx
FeOx
100µm
b)
Cu
As
Fe
Co
Ni
Pb

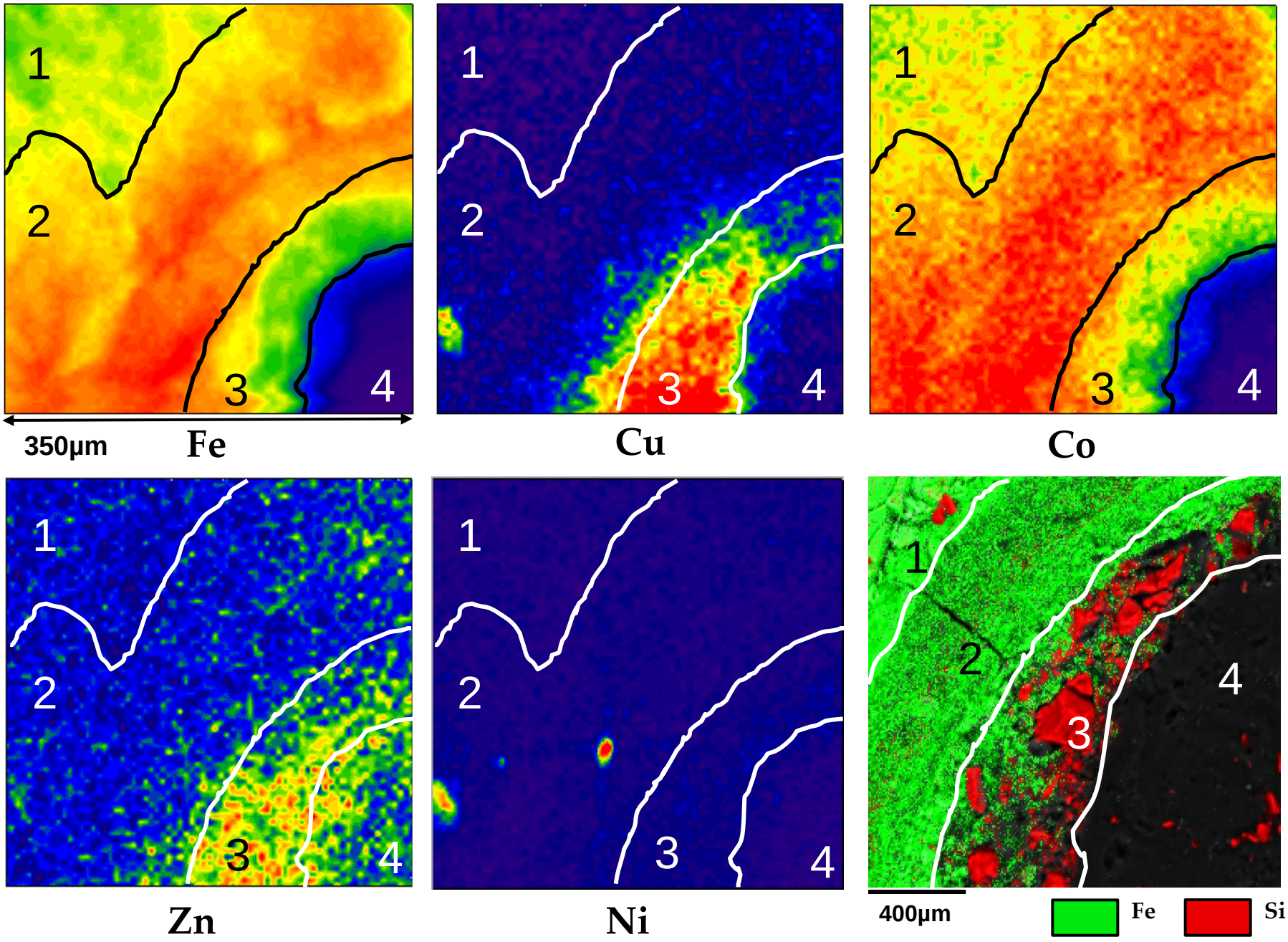
1
2
3
4
350μm
Fe
Cu
Co
Zn
Ni
400μm
Fe
Si

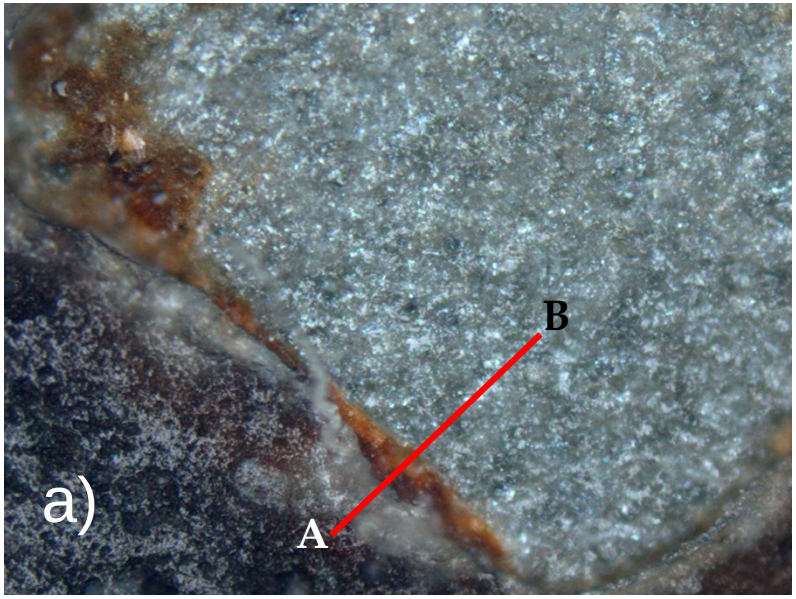
a)
B
A
400µm

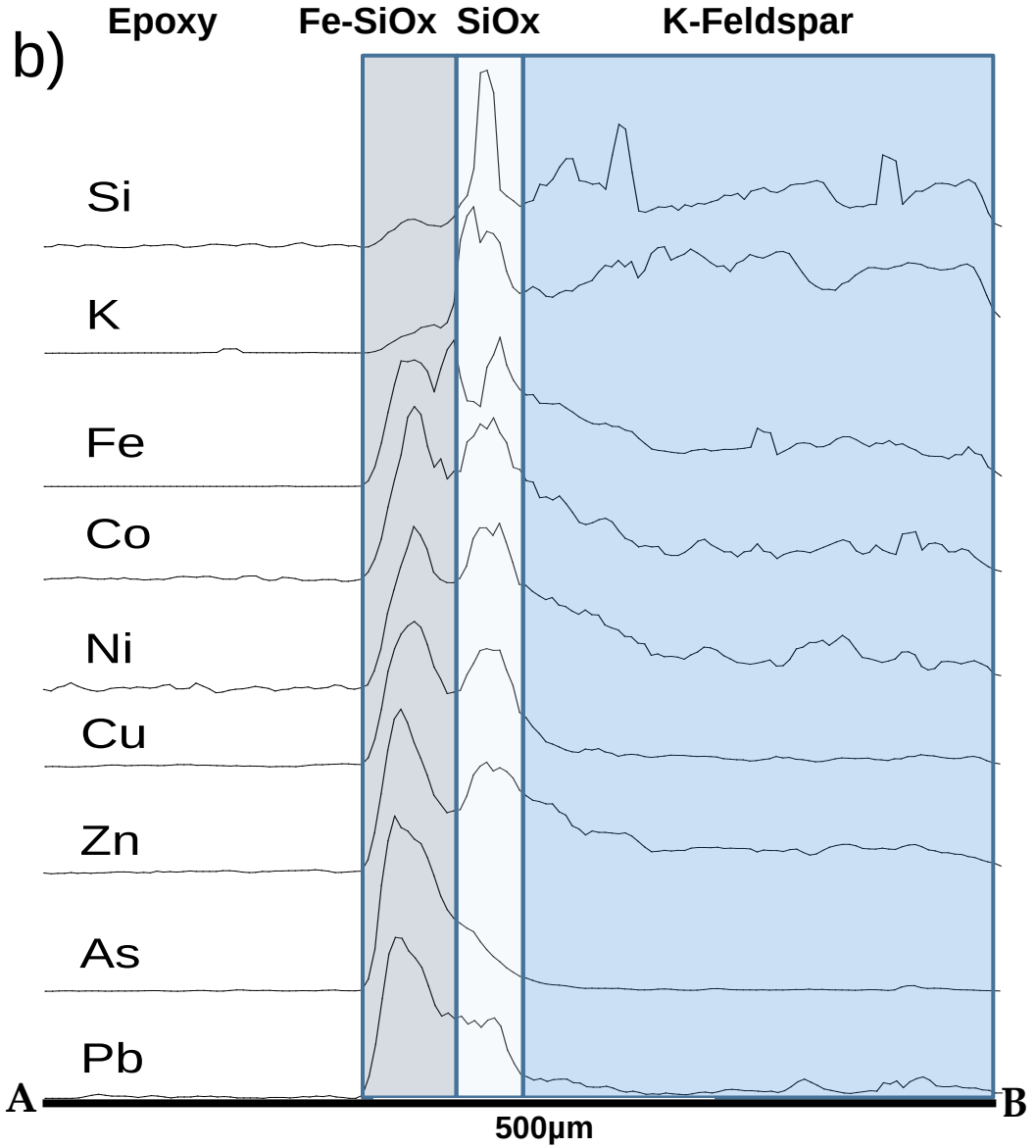
b)
Epoxy
Fe-SiOx
SiOx
K-Feldspar
Si
K
Fe
Co
Ni
Cu
Zn
As
Pb
A
B
500µm

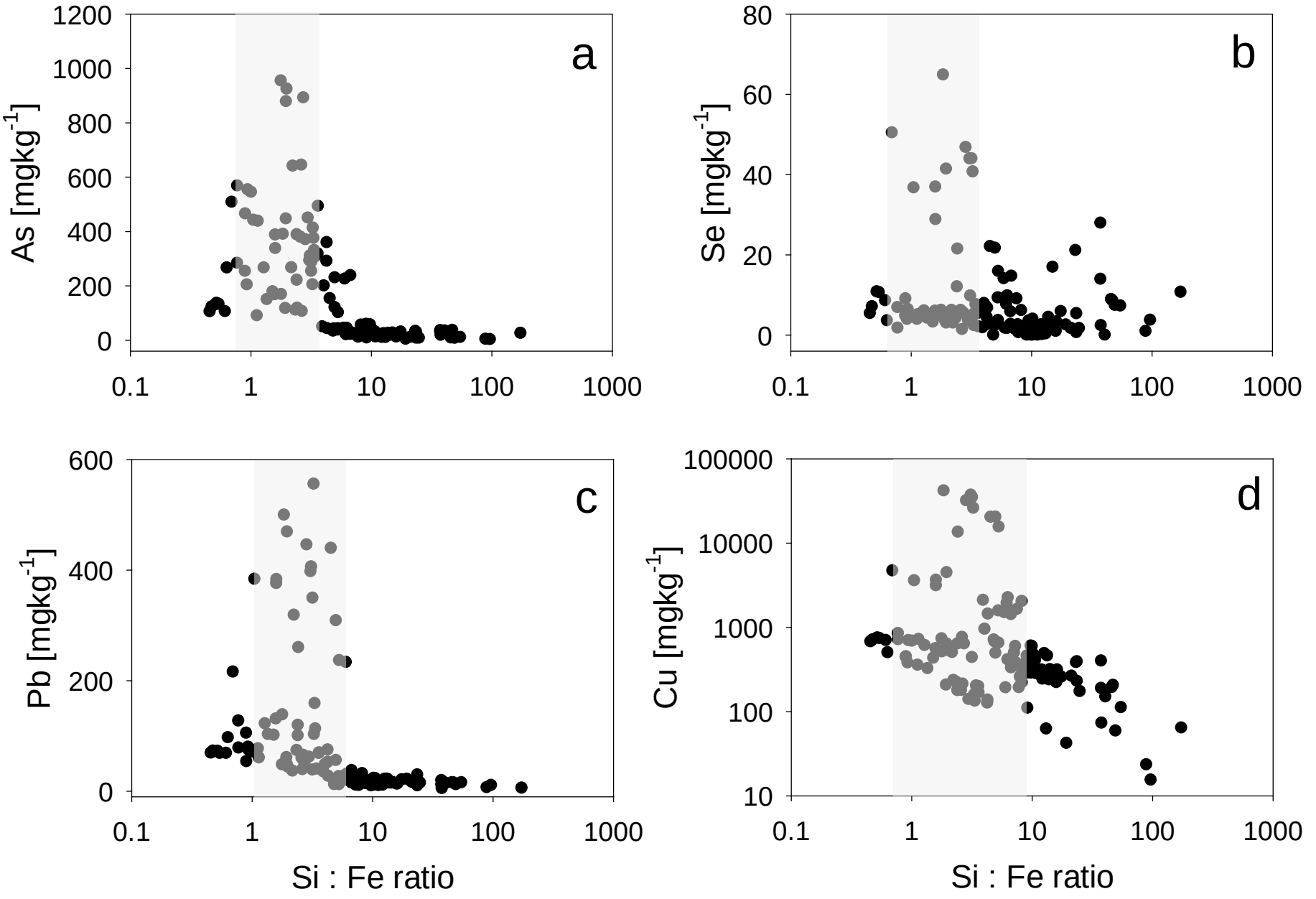
a
b
c
d
As [mgkg-1]
Se [mgkg-1]
Pb [mgkg-1]
Cu [mgkg-1]
Si : Fe ratio
Si : Fe ratio
0
200
400
600
800
1000
1200
0
20
40
60
80
10
100
1000
10000
100000
0.1
1
10
100
1000

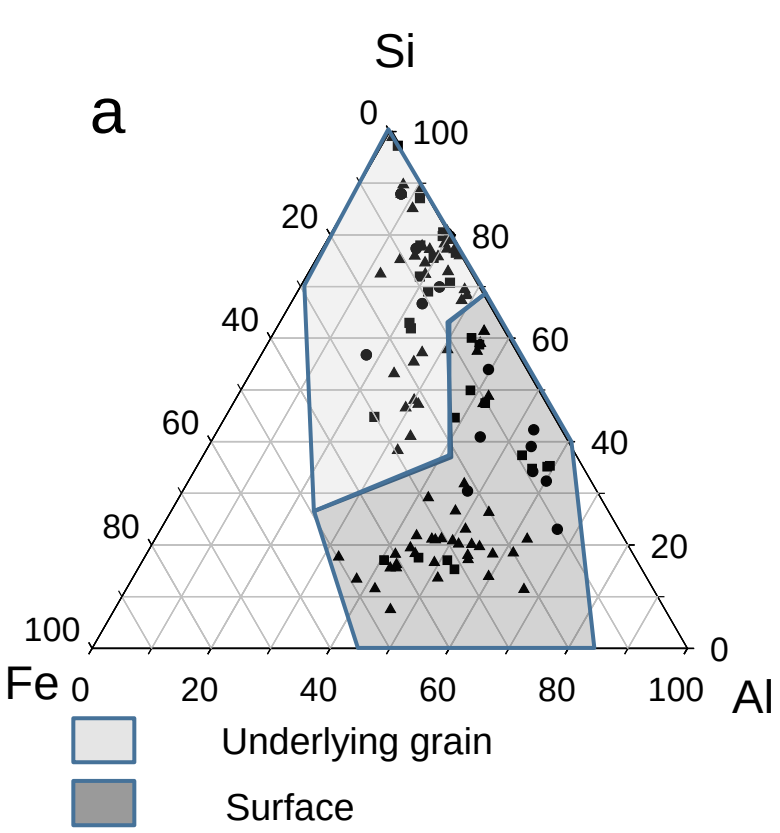
a
Si
0
100
20
80
40
60
60
40
80
20
100
0
Fe
0
20
40
60
80
100
Al
Underlying grain
Surface

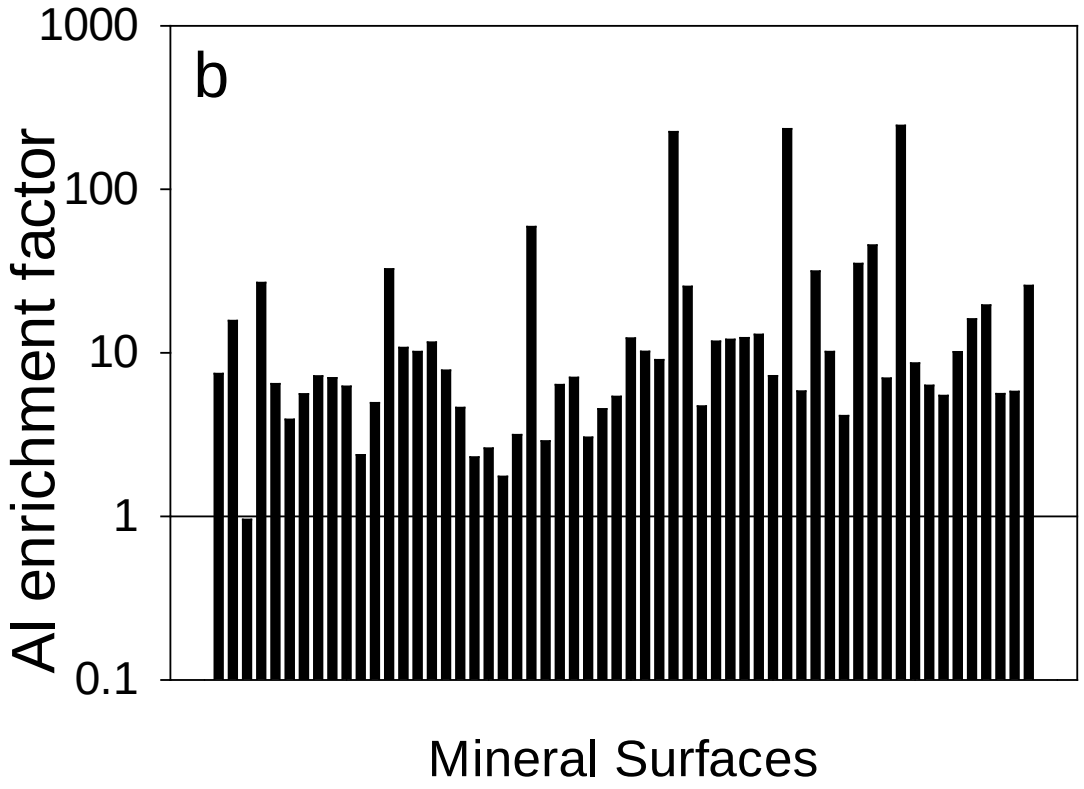
b
1000
100
10
1
0.1
Al enrichment factor
Mineral Surfaces

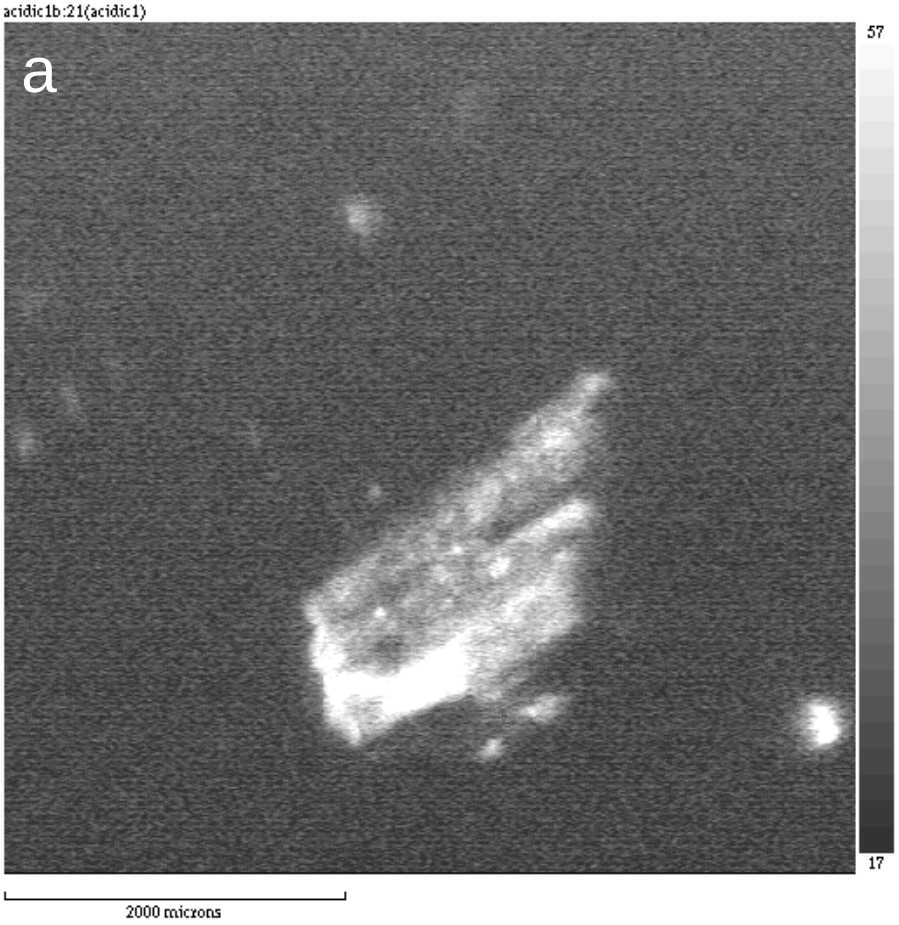
acidic1b:21(acidic1)
a
57
17
2000 microns

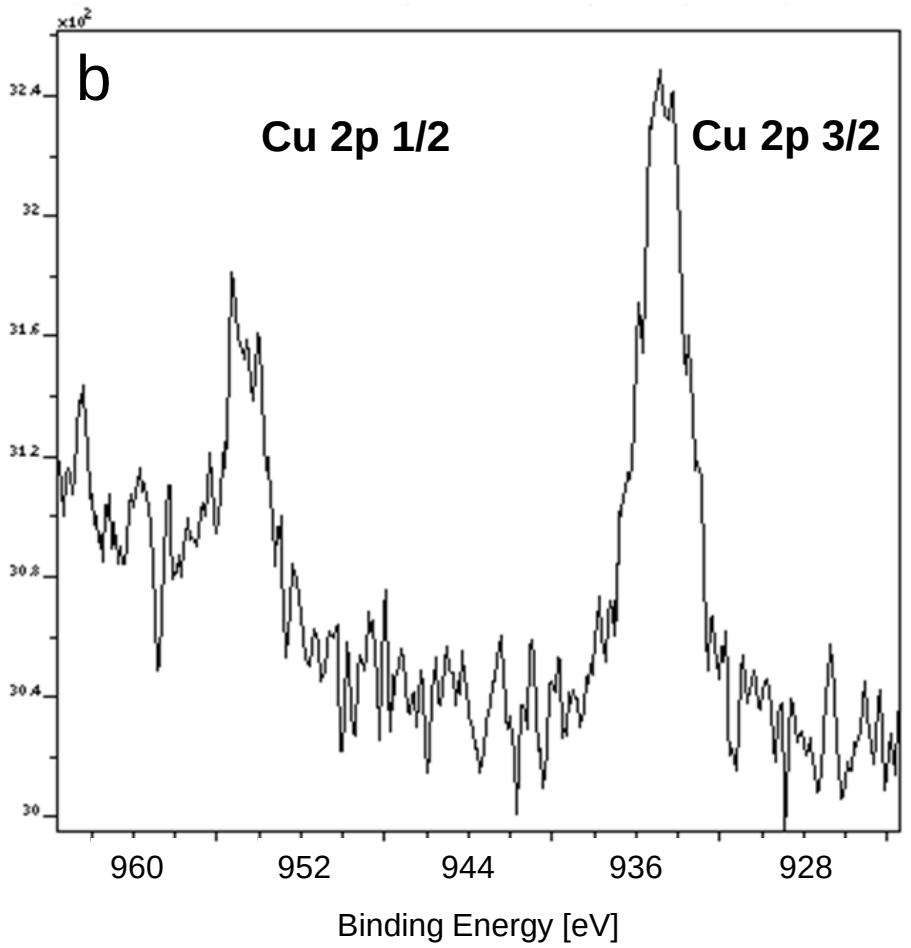
b
Cu 2p 1/2
Cu 2p 3/2
x10²
32.4
32
31.6
31.2
30.8
30.4
30
960
952
944
936
928
Binding Energy [eV]

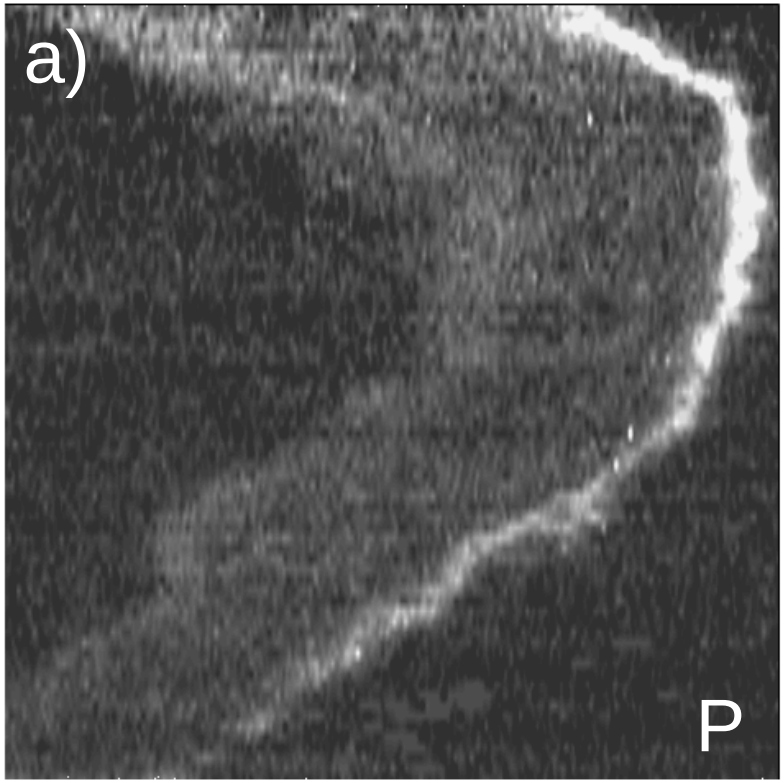
a)
P

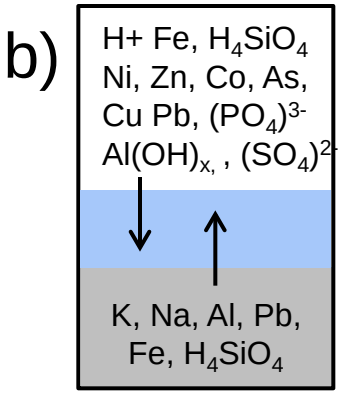
b)
H+ Fe, H_4SiO_4
Ni, Zn, Co, As,
Cu Pb, $(PO_4)^{3-}$
$Al(OH)_{x,}$, $(SO_4)^{2-}$
K, Na, Al, Pb,
Fe, H_4SiO_4

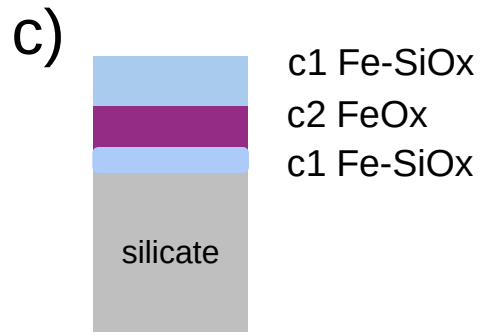
c)
c1 Fe-SiOx
c2 FeOx
c1 Fe-SiOx
silicate

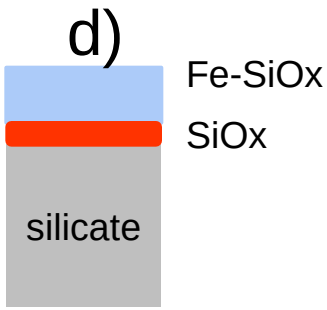
d)
Fe-SiOx
SiOx
silicate

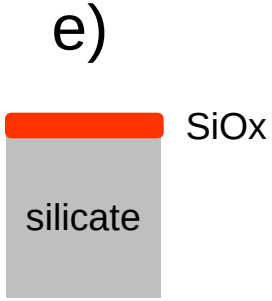
e)
SiOx
silicate

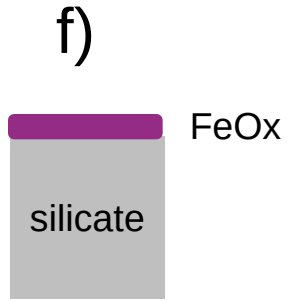
f)
FeOx
silicate

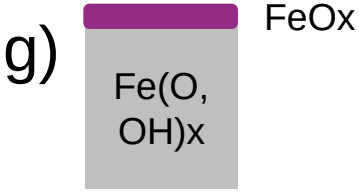
g)
FeOx
Fe(O,
OH)x

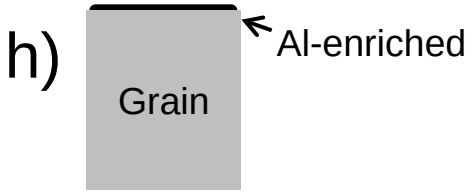
h)
Al-enriched
Grain

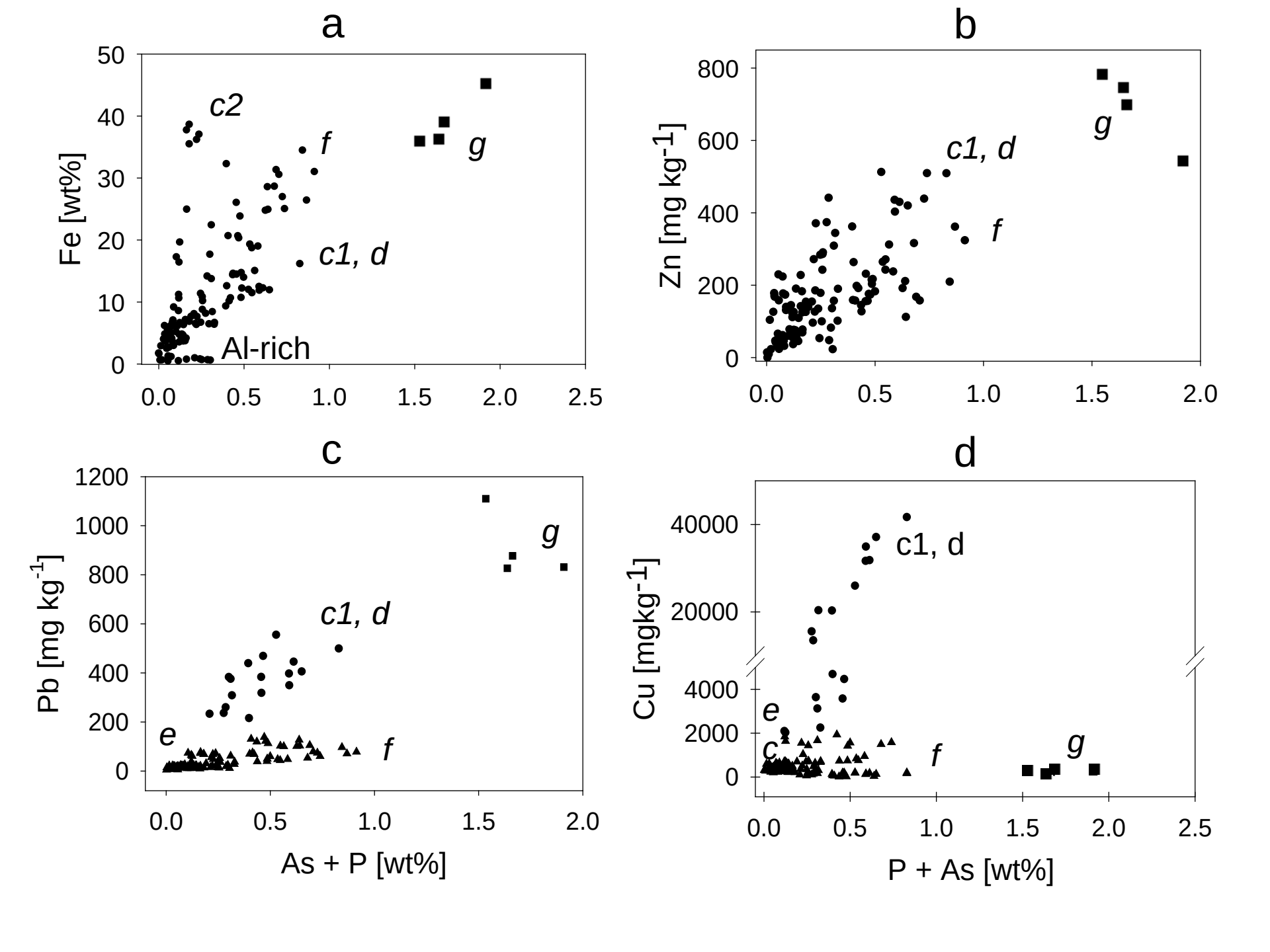
a
Fe [wt%]
c2
f
g
c1, d
Al-rich
b
Zn [mg kg-1]
g
c1, d
f
c
Pb [mg kg-1]
g
c1, d
e
f
As + P [wt%]
d
Cu [mgkg-1]
c1, d
e
c
f
g
P + As [wt%]

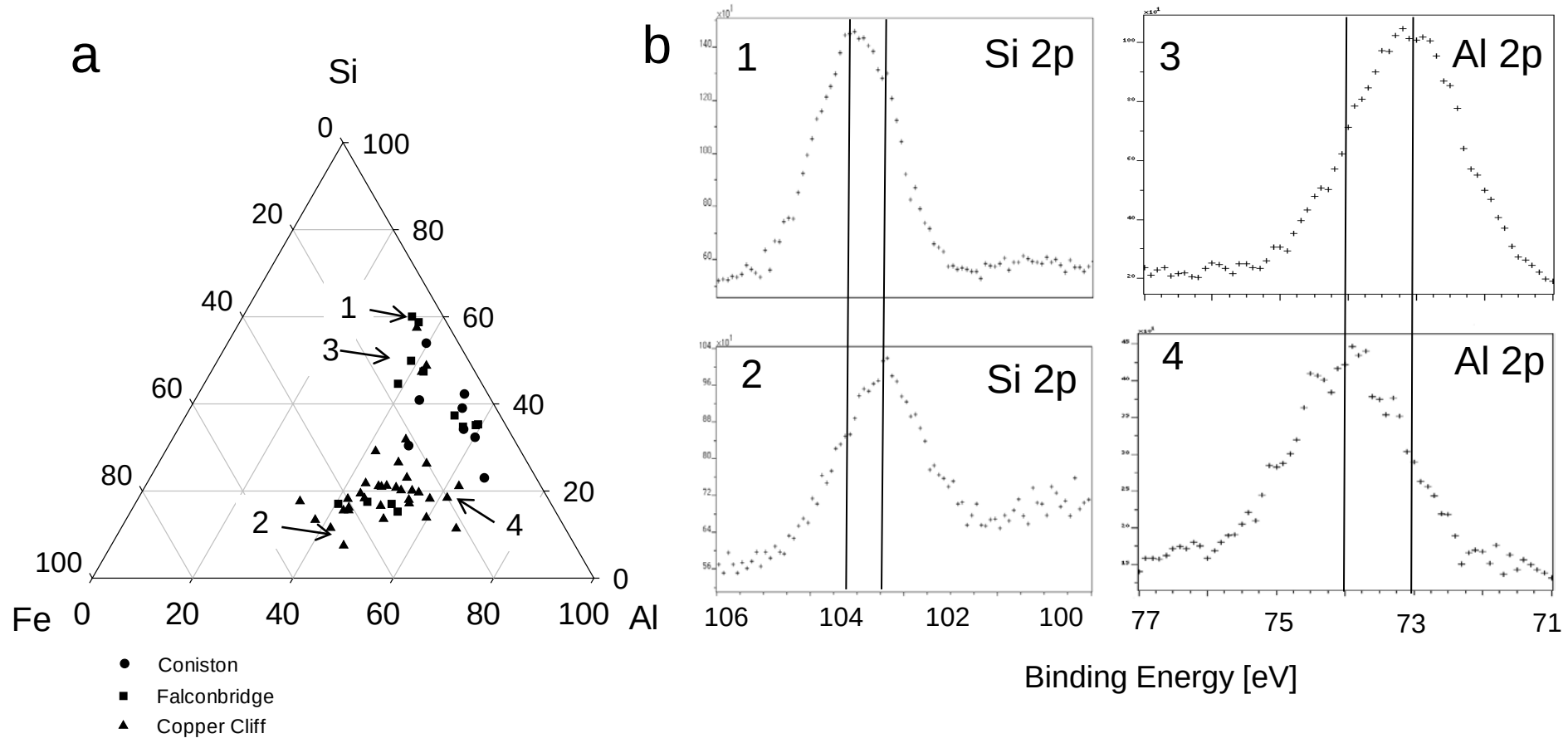
a
Si
0
100
20
80
40
60
60
40
80
20
100
0
Fe
0
20
40
60
80
100
Al
1
2
3
4
Coniston
Falconbridge
Copper Cliff
b
1
Si 2p
2
Si 2p
3
Al 2p
4
Al 2p
106
104
102
100
77
75
73
71
Binding Energy [eV]

APPENDIX A

Copper Cliff Sample Site 1 (46°28'45.09"N, 81° 3'43.51"W)-Site image (left) and soil image (right).

Copper Cliff Sample Site 2 (46°28'49.35"N, 81° 4'5.58"W)-Site image (left) and soil image (right).

Copper Cliff Sample Site 3 (46°28'57.88"N, 81° 3'31.74"W)-Site image (left) and soil image (right).

Coniston Sample Site 2 (46°28'37.47"N, 80°51'10.27"W)-Site image (left) and soil image (right).


Coniston Sample Site 5 (46°29'6.34"N, 80°50'54.26"W)-Site image (left) and soil image (right).


Coniston Sample Site 8 (46°28'43.40"N, 80°50'58.54"W)-Site image (left) and soil image (right).

Falconbridge Sample Site 1 (46°34'35.89"N, 80°48'27.87"W)-Site image (left) and soil image (right).

Falconbridge Sample Site 3 (46°34'45.88"N, 80°48'55.89"W)-Site image (left) and soil image (right).

Falconbridge Sample Site 5 (46°34'40.60"N, 80°48'31.66"W)-Site image (left) and soil image (right).